QUANTITATIVE ASSESSMENT OF INHALABLE PARTICULATE MATTER POLLUTION RESULTING FROM QUARRY ACTIVITIES

BY

OKUNADE IBRAHIM OLUSOLA

A thesis submitted to the Postgraduate School of Ahmadu Bello University, Zaria, Nigeria, in fulfillment of the requirements for the award of the degree of Doctor of Philosophy in Physics.

Department of Physics,

Faculty of Science,

Ahmadu Bello University,

Zaria, Nigeria.

AUGUST, 2000

DECLARATION

I hereby declare that:

(1) The report presented in this thesis is the result of my original research.

(2) This thesis has not been submitted to any other Institution, Organization or body for any award other than to Ahmadu Bello University; and

(3) All inclusions from other authors have been dully acknowledged.

Okunade Ibrahim Olusola

12/9/2000

Date

CERTIFICATION

This thesis entitled "QUANTITATIVE ASSESSMENT OF INHALABLE PARTICULATE MATTER POLLUTION RESULTING FROM QUARRY ACTIVITIES" by Okunade Ibrahim Olusola meets the regulations governing the award of the degree of Doctor of Philosophy (Physics) of Ahmadu Bello University, Zaria, Nigeria and is approved for its contribution to knowledge and literary presentation.

Dr. I. M. Umar
(chairman, Supervisory Committee) — Date: 24/11/2000

Dr. B. W. Jimba
(Member, Supervisory Committee) — Date: 8/11/2000

Prof. I. B. Osazuwa
(Head, Department of Physics) — Date: 30-11-2000

(Dean, Postgraduate School) — Date: 24/09/01

DIGITIZED

ACKNOWLEDGEMENT

My profound gratitude goes to Almighty Allah for granting me good health, resources, wisdom, knowledge, and perseverance in carrying out this research and making its completion a reality.

I wish to acknowledge the contribution of my supervisor, Dr. I. M. Umar for his guidance, encouragement and assistance throughout this work. I am also grateful to my second supervisor Dr. B. W. Jimba for his critical review and evaluation of this work and his useful suggestions, which had contributed immensely in enhancing its overall quality.

I remain indebted to Professor Willy Maenhaut of University of Gent, Belgium with whom I worked for one year. My collaboration with him greatly expanded my knowledge in the field of environmental Research using nuclear analytical techniques. I'm particularly grateful to him for releasing his patented design of the PM10 aerosol inlet used in this work. My sincere appreciation also goes to my Research colleagues and friends in Belgium who also assisted me while I was there. They are Jan Cafmeyer, Stijn Van Lierde, Phillip Francois, and Professor Franc De Corte.

My sincere appreciation also goes to Professor S. B. Elegba who was formerly the chairman of the supervisory committee and Director of CERT with whom the project was conceived but who had to leave the services of the university in the middle of the programme. My colleagues here in CERT cannot definitely be left

KASHIM IBRAHIM LIBRARY

out as they all contributed in various ways to the successful completion of this work. I am particularly grateful to Dr. H. B. Garba and Alhaji Gammawa for their assistance during the analysis. I am also grateful to Drs G. I. Balogun, S. A. Jonah, P. Egun, I. G. E. Ibeanu and Mr. P.O. Ogunleye for their support and encouragement. Furthermore, My appreciation goes to the Centre for Energy Research and Training for providing research grant and the facilities used in this work. The cooperation and assistance of the Postgraduate programme coordinator, Professor N. Harriharan and the head of department of physics, Professor I. B. Osasuwa is also acknowledged.

Finally, my sincere appreciation goes to my parents, Mr. R. O. Okunade and Alhaja A. A. Okunade, my brothers Alhaji Ianre Okunade, and Dr. W. G. Okunade and all my other brothers and sisters, and also to my friends Dr. A. I. Raji and Mr. F. O. Amole for their assistance, love, concern and encouragement during the difficult period in the course of this research. My wife, Aisha and my son Adulrahman Olawale have been an immense source of determination and encouragement. To them I am most grateful.

ABSTRACT

Quantitative assessment of pollution from the quarry industry was based on sampling and analysis of PM10 component of the particulate matter released into the atmosphere during rock crushing activities at the Quarry industry. The investigation was restricted to PM10 particulate matter because of their ability to be transported over long distances and their lung penetration and deposition characteristics. Thus a low volume air sampler was modified and converted to a i stacked filter unit (SFU) aerosol sampler capable of collecting PM10 particulate matter and further fractionating it to coarse (2-1 Opm) and fine (< 2pm) components. The accuracy of the sampler was tested by evaluating its characteristics in relation to criteria for accurate sampling established by Davies and Agarwal & Liu. The performance of the sampler was in agreement with these criteria. As a result of the small sample loading of the SFU, Total Reflection X-ray Fluorescence capable of analyzing nanogram amount of elements in a sample was used for analysis. The analysis was preceded by such initial steps as emphasizing grazing incidence angle through proper adjustment of the principal components of the TXRF, energy and sensitivity calibration of the TXRF spectrometer, simple extraction of PM10 particulate matter greatly aided by the surface deposition property of membrane filters and internal standardization. Thus up to 12 elements were measured simultaneously in the PM10 samples collected from various quarry activities. The multi-element multi-sample data showed that PM10 emission from the quarry industry is dominated by coarse fractions and application of wetting agents greatly reduced PM10 emission. The health impact of PM10 particulate matter on workers at the quarry industry was also assessed

by calculating the regional deposition of the measured constituent elements in the human respiratory tract using EPA models. The results obtained suggests deposition fraction ranging from 0.37 to 0.68 for elements Pb, Zn, Cu, Fe, Ca, K, Si, Al. Furthermore, the level of air pollution in the neigbouring environment of the quarry industry was investigated by calculating the source strengths of the various mechanized crushing plants using the multi-sample data along with meteorological factors as input in the Gaussian plume dispersion model. The various source strengths calculated were used in conjunction with the dose response values from the literature to determine the mortality and morbidity estimates for PM10 particulate matter using the uniform world model and hence determine the health impact of quarry industry on the environment.

TABLE OF CONTENTS

CHAPTER		PAGE
	Title Page	i
	Declaration	ii
	Certification	iii
	Acknowledgement	iv
	Abstract	vi
	Table of Contents	viii
	List of Tables	xii
	List of figures	xv
	List of Appendices	xviii
	Abbreviations	xix
1	**INTRODUCTION AND PURPOSE**	1
1.1	The Hygenic Significance of Mineral Dust	4
1.2	Quarry Operations	6
1.3	Project Planning.....	9
2	**PARTICULATE MATTER CHARACTERISTICS, AERODYNAMIC BEHAVIOUR AND SAMPLING TECHNIQUES .....**	14
2.1	Introduction.....	14
2.2	Physical Properties	15
2.2.1	Viscosity	15
2.2.2	Reynold's Number	17

2.2.3	Relaxation Time	18
2.3	Analysis of Particle Motion in The Gravitational Field	19
2.4	Behaviour Of Pollutants in the Atmosphere	25
2.4.1	Gas to Particle Conversion	26
2.4.2	Particle Growth by Coagulation.....	27
2.5	The Multimodal Character of Aerosols.....	28
2.6	Aerosol Removal Mechanisms from the Atmosphere.....	29
2.6.1	Dry Deposition.....	31
2.6.2	Wet Deposition.....	32
2.7	Sampling Techniques.....	34
2.7.1	Principles of Air Sampling.....	34
2.7.2	Sampling Efficiency.....	36
2.7.3	Particulate Samplers	38
2.7.4	Filters.....	42
2.7.5	Deposition Samplers.....	44
3	**X-RAY FLUORESCENCE ANALYTICAL TECHNIQUE**.....	45
3.1	Introduction.....	45
3.2	Physics of X-Ray Emission Spectra.....	46
3.3	X-Ray Tube Excitation Systems.....	50
3.4	Semiconductor X-Ray Spectrometer.....	53
3.4.1	Physical Processes in Semiconductor Detectors.....	54
3.4.2	Performance Characteristics of Semiconductor Detector.....	57

3.4.3	X-Ray Spectrum	66
3.5	Total Reflection X-Ray Fluorescence	66
3.5.1	Introduction	66
3.5.2	Physics of TXRF	68
3.5.3	Basic Experimental Arrangement	69
4	**METHODOLOGY OF PM10 SAMPLING AND LABORATORY ANALYSIS**	72
4.1	Methodology of PM10 Sampling	72
4.1.1	Sampling Equipment	74
4.1.2	Evaluation Of Stacked Filter Unit Aerosol Sampler	83
4.1.3	Criteria for Accurate Sampling	84
4.1.4	Sampling Programme	89
4.2	Analytical Procedures	101
4.2.1	Description of the Principal Components of TXRF	102
4.2.2	Practical Adjustment Procedures for the TXRF Set-Up	102
4.2.3	Elemental Analysis Procedures	105
4.2.4	Results and Discussion	118
5	**HEALTH IMPACT OF PM10 PARTICULATE MATTER FROM THE QUARRY INDUSTRY**	129
5.1	Introduction	129
5.2	The Human Respiratory System	130
5.3	Theory of Particle Deposition in Human Respiratory Tract	132

5.4	Quantitative Determination of Deposition in Human Respiratory Tract	134
5.4.1	Determination Of Fractional Deposition Estimates	134
5.4.2	Determination Of Regional Deposition	138
5.5	Clearance of Particles from the Respiratory System.....	140
6	**IMPACT ASSESSMENT OF PM10 PARTICULATE MATTER POLLUTION.....**	143
6.1	Theory of Impact Pathway Methodology.....	143
6.2	Dispersion Theory	146
6.2.2	Meteorological Effects.....	148
6.2.3	The Gaussian Plume Model.....	154
6.3	Application of Gaussian Model to Quarry Industry Emissions.....	160
6.4	Dose Response Functions.....	163
6.4.1	Introduction.....	163
6.4.2	The Nature of the Dose-Response Function.....	164
6.4.3	Problems of the Dose Response Function.....	165
6.5	Methodology of Estimating Impacts of PM10 Particulate Matter	
6.6	from the Quarry Industry.....	169
7	**CONCLUSIONS AND RECOMMENDATIONS**.....	174
	REFRENCES.....	181
	APPENDIX.....	189

LIST OF TABLES

1.1	Samples Collected Based on Various Quarry Operations	13
4.1	Calibration of Low Volume Air Sampler	77
4.2	Impaction Design Parameters	81
4.3	Characteristics of Stacked Filter Unit Aerosol Sampler	89
4.4	Aerodynamic Characteristics of Aerosol Particles	91
4.5	Sampling Data for PM10 Particulate Matter (Coarse Fraction).	97
4.6	Sampling Data for PM10 Particulate Matter (Fine Fraction)	98
4.7	Summary of the Emission Data for the Workplace and Ambient PM10 Particulate Matter for Various Quarry Operations	99
4.8	Comparison of Measured Concentration of a Multi-Element Standard with Actual Values Using TXRF	116
4.9	Analytical Detection Limit of TXRF Spectrometer	118
4.10	Mean Elemental Concentration of Background PM10 Particulate Matter for Zaria and FCT	121
4.11	Mean Elemental Concentration of Workplace PM10 Particulate Matter (Coarse Fraction) for various Quarry Operations	122

4.12 Mean Elemental Concentration of Workplace PM10 Particulate Matter (Fine Fraction) for Various Quarry Operations 123

4.13 Comparison of Measured Workplace PM10 Concentration with Threshold Limit Values for some Elements 124

4.14 Elemental Concentration of Ambient PM10 Particulate Matter (Coarse Fraction) for Various Quarry Operations 126

4.15 Elemental Concentration of Ambient PM10 Particulate Matter (Fine Fraction) for Various Quarry Operations 127

5.1 Fractional Deposition Estimates for Fine and Coarse Fraction of PM10 Particulate Matter from the Quarry Industry 138

5.2 Regional Deposition Fraction for N-P, T-B And P Compartments of Human Respiratory System for Various Elements 140

6.1 Key to Pasquill Stability Categories (from Turner, 1969) 152

6.2 Values of Constants in Equation 6.16 And 6.17 158

6.3 Coefficients 'a' and 'b' for Equation 6.4 159

6.4 Relation Between Gustiness Category and the Pasquill Class (Gifford, 1966) 159

6.5	The Briggs Sigma Functions for Urban Conditions (from Panosky and Dutton, 1984)	160
6.6	The Briggs Sigma Functions for Rural Conditions (Panosky and Dutton, 1984)	161
6.7	Atmospheric Stability Conditions During Sampling from the Quarry Operations	162
6.8	Vertical and Horizontal Dispersion Parameters for Quarry Operations	162
6.9	Calculated Source Strengths for Various Quarry Operations	163
6.10	Morbidity and Mortality Dose Response Functions for PM10 Particulate Matter (Effect per 10µg/m^3 Change in PM10 (from Rowe Et Al, 1995; Calthtrop and Maddison, 1996).	170
6.11	Calculated Morbidity and Mortality Values for Various Quarry Operations	172

LIST OF FIGURES

Fig. 1.1	Schematic Representation of a Rock Crushing Plant.	8
Fig. 2.1	Velocity Versus Time for an Accelerating Particle.	23
Fig 2.2	Multi-Modal Character of a Typical Pollution Aerosol and the Interactions that Modify it.	30
Fig. 3.1	Schematic Diagram of an X-Ray Tube.	51
Fig. 3.2	Block Diagram of a Typical Energy Dispersive X-Ray Fluorescence Spectrometer.	55
Fig. 3.3	Full Energy Detection versus X-ray Energy	61
Fig. 3.4	Basic Instrumental Arrangement for TXRF Set Up.	70
Fig. 4.1	Schematic Diagram of a Low Volume Air Sampler.	75
Fig. 4.2	Schematic Representation of Impaction Phenomenon.	78
Fig. 4.3	Typical Impactor Efficiency Curve.	80
Fig. 4.4	PM10 Aerosol Inlet Consisting of Polyethylene Container and the Stacked Filter Cassette.	82
Fig. 4.5	Aerosol Collection Efficiency Curves for the Naso-Pharynx and Nuclepore Filters Of 8 and 0.4μm Pore-Size Arranged in Series (Cahill, 1977).	85

Fig. 4.6	Criteria for Accurate Sampling in Calm Air as Applied to SFU.	90
Fig 4.7	Schematic Representation of SFU Sampling Line.	93
Fig 4.8	Technical Drawing of TXRF Components.	103
Fig. 4.9	TXRF Calibration Curve for K	108
Fig. 4.10	TXRF Calibration Curve for Fe	108
Fig. 4.11	TXRF Calibration Curve for Cu	109
Fig. 4.12	TXRF Calibration Curve for Zn	109
Fig. 4.13	TXRF Calibration Curve for Co	110
Fig. 4.14	TXRF Calibration Curve for Sr	110
Fig. 4.15	TXRF Calibration Curve for Ba	111
Fig. 4.16	TXRF Calibration Curve for Pb	111
Fig. 4.17	Typical TXRF Spectrum for Coarse PM10 Sample.	113
Fig. 4.18	Typical TXRF Spectrum for Fine PM10 Sample	113
Fig. 4.19	Variability of Selected Elements in Workplace PM10 Samples from (a) Manual Quarrying (WP-MAN) (b) Semi-Mechanized Quarry (MECH1) (c) Packing and Loading (WP-P&L) and (d) Fully Mechanized Quarry (WP-MECH3).	120

Fig. 4.20	Mean Fine/Coarse Concentration Ratios for Selected Elements in PM10 Samples Collected near Mechanized Quarries.	126
Fig. 5.1	The Human Respiratory System.	131
Fig. 5.2	Deposition Curves for the Naso-Pharyngeal (N-P) Region.	135
Fig. 5.3	Deposition Curves for tracheo-Bronchial (T-P) Region	136
Fig. 5.4	Deposition Curves for the Pulmonary (P) Region.	137
Fig. 6.1	Co-Ordinate Representation of the Gaussian Distribution as Applied to a Point Source.	156
Fig. 6.2	Graphical Representation of the Dose-Response Function	166

LIST OF APPENDICES

Appendix 1	Summary of Analytical Procedure for PM10 particulate Matter (Coarse Fraction)	189
Appendix 2	Summary of Analytical Procedure for PM10 particulate Matter (Fine Fraction)	190

ABBREVIATION

AED	Aerodynamic Equivalent Diameter.
AMB-DRILL	Ambient aerosol from Sample from Drilling of Rock Deposit
AMB-MECH1	Ambient Aerosol Sample in the vicinity of MECH1 Crusher
AMB-MECH2	Ambient Aerosol Sample in the Vicinity of MECH2 Crusher Assembly.
AMB-MECH3	Ambient Aerosol sample in the Vicinity of MECH3 Crusher Assembly.
AMB-MECH2-W	Ambient Aerosol Sample in the Vicinity of MECH3 crusher Assembly Using Wet Rocks
AMB-FCTBG	Background Aerosol Samples from the Federal Capital Territory
AMB-ZBG	Background Aerosol Samples from Zaria.
AXIL	Analysis of X-Ray Spectra by Iterative Least Squares
CRM	Certified Reference Material
d_{50}	Cut-off Aerodynamic diameter corresponding to 50% Sampling Efficiency.
ED-XRF	Energy Dispersive X- Ray Fluorescence

ET-AAS	Electrothermal Atomic Absorption spectrometry
FCT	Federal Capital Territory
FEPA	Federal Environmental Protection Agency
FWHM	Full Width at Half Maximum
IAEA	International Atomic Energy Agency
ICP-MS	Inductively Coupled Plasma Mass Spectrometry
ICRP	International Committee on Radiation Protection
INAA	Instrumental Neutron Activation Analysis
IPM	Inhalable Particulate Matter
IRRD	Increase in Relative Risk of Death
KD ROAD	Kaduna Road
KN ROAD	Kano Road
LRI	Lower Respiratory Illness
MCA	Multi-Channel Analyzer
MECH1	Mechanized Rock Crushing Plant Using One Crusher
MECH2	Mechanized Rock Crushing Plant Using Two Crushers

MECH3	Mechanized Rock Crushing Plant Using Three Crushers
NBS	National Bureau of Standards
N-P	Naso-Pharygeal Region
P	Pulmonary Region
PM10	Particulate Matter with Aerodynamic Equivalent Diameter greater than or less than 10μm.
QXAS	Quantitative X-ray Analysis Software
RAD	Restricted Activity Days
SFU	Stacked Filter Unit
Si(Li)	Lithium Drifted Silicon Detector
SRM	Standard Reference Material
Stk_{50}	Stokes Number for particles corresponding to 50% collection Efficiency
T-B	Tracheo-Bronchial Region
TLV	Threshold Limit Value
TSP	Total Suspended Particulate Matter
TXRF	Total Reflection X-Ray Fluorescence

USEPA	United State Environmental Protection Agency
WD-XRF	Wavelength Dispersive X- Ray Fluorescence
WP-MAN	Work Place Aerosol Sample from Manual Quarry
WP-MECH1	Work Place Aerosol Sample from MECH1 Quarry
WP-MECH2	Work Place Aerosol Sample from MECH2 Quarry
WP-MECH3	Work Place Aerosol Sample from MECH3 Quarry
WP-P&L	Work Place Aerosol Sample from Packing and Loading of Crushed Rocks.
XRF	X-Ray Fluorescence
ZNS	Zinc Sulphide Screen

CHAPTER 1

INTRODUCTION AND PURPOSE

The increasing demand for crushed rock aggregates in building and road construction had necessitated the establishment of several quarry operations in the country where there is a large number of rock deposits. Quarrying is a process of crushing rock deposits in order to obtain rock samples of different size aggregates. In the process of crushing, dust particles of various sizes are released into the atmosphere. Since the crushing activities takes place by mechanical action, one would expect the dust generated to consist of only large sized particles which will be rapidly deposited close to the source. However, preliminary studies conducted showed that significant amount of fine particles in form of PM10 particulate matter is also generated. PM10 particulate matter consists of particles with aerodynamic equivalent diameter (AED) of less than or equal to 10μm AED. Aerodynamic equivalent diameter is the diameter of a particle with unit density, which has the same settling speed as the particle under consideration. PM10 particulate matter has significant resident time range in the atmosphere and is thus transported over long distances by the winds. This may lead to continual accumulation of toxic element at locations far from the source and hence increases the relative risk of illness or even death.

The toxic nature of PM10 particulate matter mediated by the surrounding air confront the analyst with an important task of assessing the particulate matter qualitatively and quantitatively as an environmental contaminant in ambient air or workplace air. Such an assessment will require collection and analysis of aerosol

samples that are representative of the surrounding air. In addition, the sampling process must ensure compatibility between the sampling device, collection substrate and the chosen analytical technique. The latter requirement is difficult to attain in reality, as there are always mutually incompatible combinations of sampling device, filter media and analytical methodology. However, it is necessary that these factors be taken into consideration in the design of sampling and analysis program bearing in mind the ultimate use of the data generated in order to meet the program objectives. In the design of sampling and analysis protocol for the Quarry Industry, consideration was given to such factors as the type and mode of quarry operation and capacity of the equipment used. Other factors considered were nature of the rock (dry or wet) before crushing, available analytical technique, meteorological factors, transport of pollutants, and potential health effects.

In the present study, PM10 particulate matter samples were collected within the workplace and at a fixed distance from the source. While the samples collected within the workplace provides information on the exposure levels of Quarry workers, the samples collected at a distance from the source provides the basic input required in the dispersion model used to determine the source strengths of the various quarry operations.

PM10 particulate matter sampling requires a special device, which allows the air stream to be processed on its way to the filter so that only particles with upper size cut-off of 10μm AED are allowed to reach the filter. Initial designs of PM10 inlets were based on 50% collection efficiency at 10μm (Wedding and McFarland, 1985). These inlets eliminate most of the wind speed and direction problems usually

encountered with conventional aerosol samplers. They also prevent passive loading on the filters when there is strong wind. However, the inlets operate on the principle of impaction on a plate, a situation that may lead to particle bounce-off. Such problems are corrected by coating the impaction plate with grease or using the principle of virtual impaction (Dzubay and Stevens, 1975) whereby the particles are deposited within a separate volume of air within the inlet. The major limitation of PM10 inlets is that they do not permit high flow-rate especially when membrane filters, which are suitable for analysis by sensitive nuclear and related analytical techniques, are used.

The restriction on flow-rate and particle size caused by inclusion of PM10 aerosol inlet in the sampling line implies small sample loading on the filters, and hence requirement of very sensitive analytical techniques for analysis of such filters. X-ray Fluorescence (XRF) is a very sensitive and tried analytical technique for the determination of trace elements in the particulate matter (Rhodes et al, 1972) both in the natural environment and occupational workplace. All the various modes of XRF based on the source of X-rays such as Radioisotope XRF, Tube XRF, Total Reflection XRF and synchrotron radiation XRF may be used. This however depends on the concentration levels of elements of interest, intensity of X-rays produced, sensitivity and availability. In this work, Total Reflection XRF was used because it provides sensitivities of several orders of magnitude better than radioisotope XRF and Tube XRF. Synchrotron radiation XRF, which offers better sensitivity than TXRF, was not available. Because XRF is multi-elemental, an enormous amount of information can be generated from a relatively small number of samples.

At the beginning of this campaign a six point objectives were set based on project planning, sampling, laboratory analysis, and data analysis. These objectives include:

(i) Development of sampling device for collection of inhalable and fractionated PM10 particulate matter.

(ii) Development of analytical procedure for analysis of PM10 particulate matter using Total Reflection X-ray fluorescence (TXRF).

(iii) Sampling within the workplace and at a specified distance from the quarry Industry and subsequent analysis of the samples by TXRF.

(iv) Study of the deposition patterns of various elements in the human respiratory tract, thereby assessing the health impact of quarry dust.

(v) Determination of source strengths for different mechanized quarry operations using the Gaussian plume dispersion model and meteorological factors.

(vi) Impact assessment of emissions from various quarry operations.

The above mentioned objectives can be better appreciated if there is adequate knowledge of the hygienic significance of mineral dust. Therefore, Considerable treatment will be given to this aspect in the following subsection. This will be followed by description of the various quarry operations and sampling areas. Finally, the strategy adopted in the project planning will be discussed.

1.1 The Hygienic Significance of Mineral Dust

Quarry dust is a type of mineral dust, which is regarded as a non-fibrogenic, biologically inert or "nuisance" dust. These designations had however been criticized on the ground that inhalation of such mineral dusts induces at least a

microphage reaction. Irritations of the upper respiratory tract and subsequent lung function impairment after inhalation of extremely high concentration of particulate matter are associated with mineral dusts. In some cases hazards involving inhalation of dusts may not be apparent until the effects are observed in exposed individuals. The potentiai health effects may also be difficult to determine since the effects of new or uncommon elements and compounds may not have been evaluated. In particular, toxic elements may not induce any noticeable effects at low doses. As the doses increase, the phenomenon of adaptation may set in whereby a symptom initially associated with a chemical may disappear after some time in spite of continuous exposure. This has led to the promulgation of threshold limit values (TLV) for different chemicals in many Countries (Jackson et al, 1989) as a guide of the permissible exposure to metals and chemical compounds.

Inhalation of mineral dusts may lead to pulmonary diseases. Pneumoconiosis is a special type of lung disease, which is caused by tissue reaction to accumulation of dusts in the lungs. Freshly fractured rocks produce very harmful particles since they tend to be sharp at the edges. Particulate matter from fractured rocks is highly enriched in silica (and other elements) which when deposited at the alveoli of the lungs is phagocytosed by microphages leading to the destruction of the cells. This may lead to production of fibrous material in the lungs as the body attempts to isolate the affected area. Thus, a local area is damaged leading to reduction in efficiency of the lungs. This type of pulmonary disease is called silicosis. It is an irreversible chronic condition with varying degree of severity according to exposure. Silicosis may also predispose patients to pulmonary tuberculosis.

A whole range of metals and chemical compounds found in the environment are known to be harmful. The elements Cu, Zn, Fe, Ca, Sr, Mn, Mo and Cr are essential to biological processes. Their concentrations within the body may vary in normal compared to diseased persons. Ni, Cd, Ba, Al, Pb and Hg are always present in human tissue, but they are generally regarded as non-essential in the biological sense (Butler, 1979). Large concentration of these metals and their chemical compounds in air may result in chronic exposure with symptoms such as nausea, vomiting, irritation of eyes, nose and throat pains and constrictions in the chest with coughing, laboured breathing and severe headaches. Under these circumstances, the incidence of asthma and bronchitis can reach epidemic levels with increasing mortality rate among the older populations.

1.2 Quarry Operations

The quarry operation basically involves the crushing of rocks in order to reduce it to smaller size aggregates. This may proceed through series of steps. Drilling is always the first step. Various shot holes are drilled on a rock deposit using drilling machine. This gives rise to a considerable amount of fine dust particles, which are subsequently dispersed by winds. The various shot holes are subsequently filled with explosives, which are connected together using a string, which also carries explosives. When the explosive is detonated, blasting takes place causing fragmentation of part of the rock deposit and weakening the remaining parts of the deposit.

KASSIM IBRAHIM LIBRARY

In manual quarrying, the weakened rock deposit is beaten continuously with a

large hammer and broken into big rock fragments, which may be further reduced into smaller aggregates. This process generates particulate matter, which are directly inhaled by the worker.

Mechanized quarries on the other hand, employs crushing machine driven by electric motor for the reduction of the big rock fragments into smaller aggregates. The equipment used may consist of one, two or three crushers depending on the sophistication of the industry. A typical quarrying machine assembly is presented in Figure 1.1.

For the purpose of sample collection, mechanized quarries have been classified into MECH1, MECH2 and MECH3, which make use of one crusher, two crushers and three crushers respectively. The most common crushing machine in Zaria is the MECH1 type. It consists of a single crusher with metal screens of varying screen sizes connected underneath it. Crushed rock aggregates of appropriate sizes pass through the sieves before being deposited inside the wheelbarrows placed beneath the screen. The operation of this type of quarry is rather crude and not fully mechanized, as the workers still have to load the big rock fragments into the crusher while the others evacuate the wheelbarrows as they are filled up with smaller rock aggregates. The workers are rather unprotected and are thus directly exposed to immense dust pollution from the crushing activity. This type of machine has a capacity of about 80 tons of rocks per day and operating hours of 6-9hrs.
MECH2 employs primary crusher, and secondary crusher while MECH3 employs primary crushers, secondary crushers and tertiary crushers, each, driven by electric motor. All the crushers and screen units are linked together by conveyor

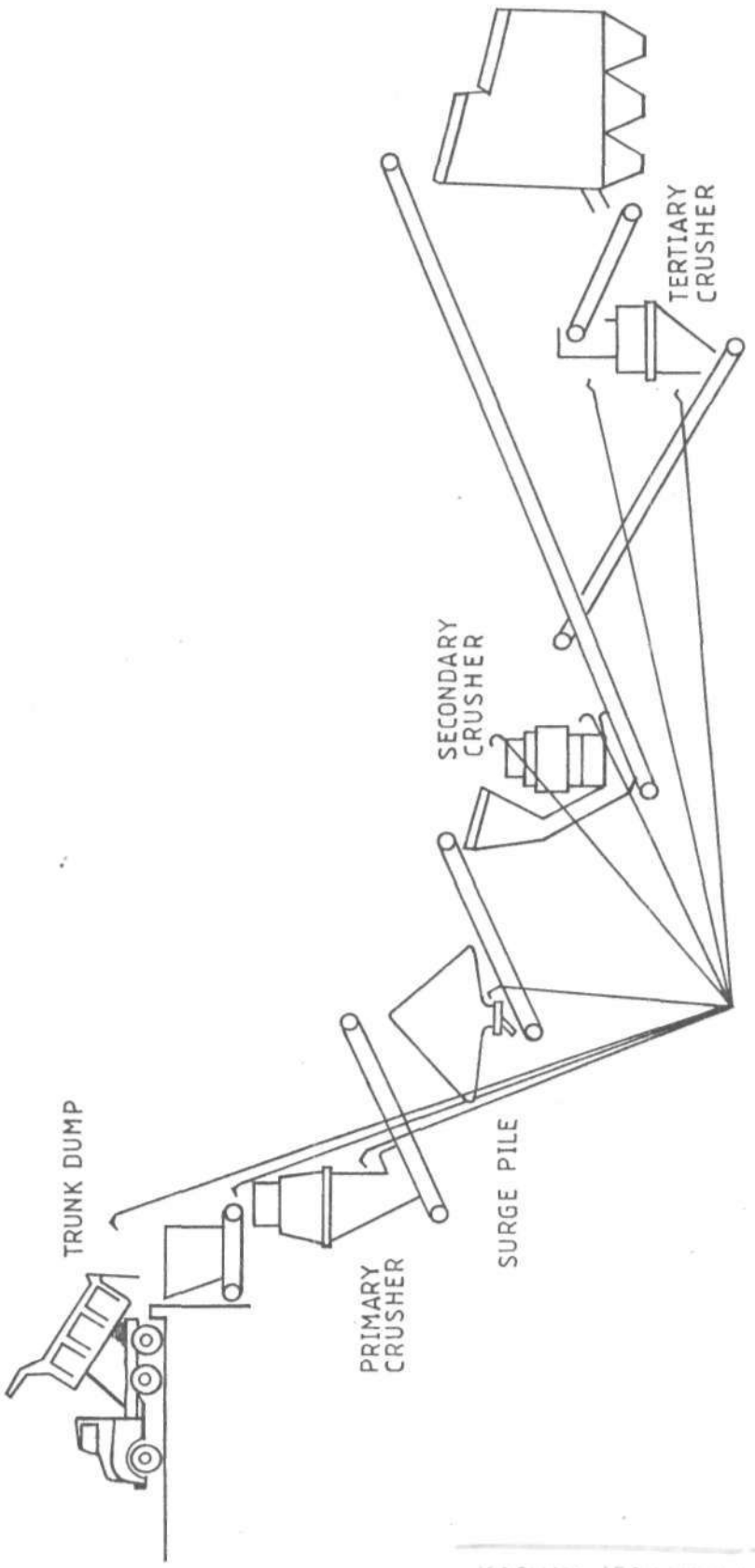


Fig. 1.1: Schematic Representation of a Rock Crushing Plant.

KASHIM IBRAHIM LIBRARY

belts, which are also driven by electric motors. Big rock fragments loaded into the primary crushers by dump trucks are first crushed into smaller sizes and then transferred into the screen unit by conveyor belts before being deposited into the secondary crusher, which also has its own screen unit. The reduced rock aggregates from the secondary crusher are finally transferred into the tertiary crusher for further reduction into smaller aggregates. The crushers and screen units generate dust pollution, making the whole work area dust laden. Apart from the pollutants generated from the above mentioned quarry operations, other sources of pollutants include dust generated from packing and loading and from drilling machine.

1.3 Project Planning

The determining factor in pollution assessment and control is the sampling technique and the strategy adopted since the usefulness of the result of the analytical technique depends on how representative the sample is to the environment under consideration. Before commencing a sampling campaign, a reference technique promulgated by the Federal Regulatory Agency should be considered. The promulgation of such reported method serves to reduce the dispersion in the results reported by the various investigators. However, reported methods may not be representative of all situations encountered and so may not be useful in all circumstances. New methods, which had been subjected to experimental proofs and validations, should serve as a means of updating existing methods.

K BRAHI

The ministry of environment in Nigeria had not promulgated any specific procedure

or technique for collection of inhalable particulate matter (IPM). However, literature search revealed that in Belgium, a filter face velocity of 125cm/s ± 10% is prescribed (Zhang, 1983). The method also allows for free choice of inlet size, but a vertical orientation of the sampling head is specified. The high face velocity is recommended in order to simulate the intake of air by the nose and to ensure high collection efficiency. The requirement of high face velocity can be achieved by either using a high volume sampler or by reducing the inlet size. High volume sampling is not suitable for collection of workplace IPM because its high flow rate has been shown to change the air quality by filtration. Also it does not provide samples with well defined range of particle size and may permit accumulation of windblown dust leading to passive loading on the filter and hence overestimation of its particulate content. A small sample inlet may also cause problems such as small sample size or inhomogeneous distribution of particulate matter over the filter. The latter option was chosen since the project objective is to collect PM10 particulate matter, which are known to have health significance and easily subjected to atmospheric transport to other locations. In addition, the filter used is a "Nuclepore" membrane filter, which has uniform pore size distribution (Spurny et al, 1969) thus leading to uniform deposition of IPM over the filter. Further, the chosen analytical technique can easily handle small sample size as well as compatible with "Nuclepore membrane filter. This led to the modification of the available low volume air sampler by incorporation of PM10 aerosol inlet.

The assessment of pollution at workplace by air monitoring can be carried out using personal aerosol sampler or stationary aerosol sampler. Stationary aerosol sampling does not necessarily provide appropriate data for personal sampling

because of the steep concentration gradient and mobility of the workers. Personal sampling is therefore usually recommended provided personal aerosol samplers can be provided for a large number of workers. In most cases, this is not the case as very few personal monitors are always available. Since the study of effects of pollutants on human health often requires data from a very large population, data provided by a few personal monitors will not allow for proper assessment of exposure and health impact on the population. This is because doses received by a certain population vary largely because of inter-subject variations such as different breathing rate and inhalability characteristics. It therefore follows that any sampling strategy, which will provide data on the average exposure of a certain population, would be appropriate for studies in health impact assessment. The above considerations led to the use of the stacked filter Unit (SFU) aerosol sampler (as stationary aerosol sampler) which has additional advantage of simulating the human respiratory system (Cahill et al, 1977).

With the sampling equipment in place, a reconnaissance visit was paid to the various quarry operations in Zaria and Federal Capital Territory (FCT) with the view to arrive at appropriate sampling strategy for collection of IPM. Thus, the sampling methodology took into consideration the collection of the following types of samples:

(i) Workplace PM10 particulate matter from quarry operations such as manual quarrying, MECH1 type crusher, packing and loading and upwind PM10 particulate matter from MECH3 type crusher assembly.

(ii) Ambient PM10 particulate matter at fixed distances from drilling operation, MECH1, MECH2, and MECH3 type crusher assembly.

473301

(iii) Ambient PM10 particulate matter from MECH2 type crusher assembly during the wet season.

(iii) Ambient background PM10 particulate matter from Zaria and Federal Capital Territory (FCT).

Table 1.1 shows the distribution of various samples collected according to the groupings provided above.

In order to carry out proper assessment of the impact of PM10 particulate matter on the environment and human health, knowledge of its chemical composition is necessary. Owing to the small sample loading due to the inclusion of PM10 aerosol inlet in the sampling line, the method of analysis chosen should be sensitive, specific, accurate and applicable to major, minor and trace constituents. Further, before meaningful inferences can be drawn concerning the impact of pollutant on the environment a large number of data is required. Therefore, speed and ease of analysis is desirable. The multi-element Total Reflection X-ray fluorescence (TXRF) technique, which was employed for analysis of the samples meet all these requirements. It was found to be a powerful tool in the analysis of workplace and ambient PM10 particulate matter from the quarry industry.

Table 1.1: Samples Collected Based on the Various Quarry Operations and Sampling Locations.

SAMPLING DATES	SAMPLE DESCRIPTION	ABBREVIATION	SAMPLE LABEL	SAMPLING LOCATION
6/2/96 to 12/2/96`	Workplace PM10 Source Sample Manual Quarrying	WP-MAN	QC01, QF01,QC02, QF02, QC03, QF03 QC04, QF04 QC05,QF05	Kaduna Road Zaria
27/2/96 to 14/3/96	Workplace PM10 Source Sample MECH1 Crusher	WP-MECH1	QC11, QF11,QC13, QF13, QC15, QF15 QC17, QF17 QC19, QF19	Kaduna Road Zaria.
18/3/96 to 26/3/96	Workplace PM10 Source Sample Packing and Loading	WP-P&L	QC21, QF21, QC22, QF22, QC23, QF23, QC24, QF24	Kaduna Road Zaria.
23/10/96 to 26/10/96	Workplace PM10 Upwind Sample MECH3 Crusher	WP-MECH3	QC35, QF35, QC37, QF37, QC40, QF40, QC42, QF42	Npape Village Abuja.
17/2/96 to 23/2/96	Ambient PM10 at 100m from Drilling Machine	AMB-DRIL	QC07, QF07, QC08, QF08, QC09, QF09	Kaduna Road Zaria.
27/2/96 to 16/3/96	Ambient PM10 At 200m from MECH1 Crusher	AMB-MECH1	QC12, QF12,QC14, QF14, QC16, QF16 QC18, QF18, QC20, QF20	Kaduna Road Zaria.
27/3/96 to 6/4/96	Ambient PM10 at 200m From MECH2 Crusher Dry Season	AMB-MECH2	QC25, QF25, QC26, QF26, QC27, QF27, QC28, QF28, QC29, QF29	Kano Road Zaria.
27/5/96 to 20/6/96	Ambient PM10 At 200m from MECH2 Crusher Wet Season	AMB-MECH2-W	QC31, QF31, QC32, QF32, QC33, QF33, QC34, QF34	Kaduna Road Zaria.
23/10/96 to 26/10/96	Ambient PM10 At 200m from MECH3 Crusher using Wet Rocks	AMB-MECH3	QC36, QF36, QC38, QF38, QC41, QF41, QC43, QF43	Npape Village, Abuja.
14/2/96 to 14/4/96	Ambient PM10 Background Samples From Zaria	AMB-ZBG	QC06, QF06, QC10, QF10, QC30, QF30	Zaria
23/10/96 to 24/10/96	Ambient PM10 Background Samples From FCT	AMB-FCTBG	QC39, QF39	Federal Capital Territory (FCT)

CHAPTER 2

PARTICULATE MATTER CHARACTERISTICS, AERODYNAMIC BEHAVIOUR AND SAMPLING TECHNIQUES

2.1 Introduction

Aerosol is defined as a suspension of a small discrete mass of liquid and/or solid in a gas. In the case of air pollution studies, the gas is the atmosphere. The aerosol may have a complex chemical character as well as diverse physical and aerodynamic characteristics. For example, sizes of aerosols range from about 0.01μm corresponding to molecular size to about 100μm corresponding to the size of a sand particle. It should be noted that the knowledge of the concentration of aerosol is not sufficient. One must also have sufficient information about the size distribution of the toxic components in the aerosol since only limited size range can gain access to the naso-pharyngeal region in the human respiratory tract (Natusch and Wallace, 1974). The present study will give priority to aerodynamic properties of the particles rather than their physical dimensions. The particle is classified as "fine" if its aerodynamic equivalent diameter is less than 2μm and "coarse" if its aerodynamic equivalent diameter is between 2-10μm (Maenhaut et al, 1996).

Atmospheric aerosols have natural and anthropogenic origins with most of it being concentrated within the lower troposphere (about 2km from ground level) where living beings reside. Natural sources of aerosol include mostly volcanic eruptions, soil dust, and burble bursting at the sea surface, all of which are distributed around

the globe. On the other hand, emissions from anthropogenic sources are smaller in magnitude but are highly concentrated in industrialized areas. In such areas, the relative contribution of anthropogenic sources often largely exceeds that of the natural sources and thus may give rise to local air pollution problems.

In order to study the effects of aerosols on the environment, there is need to carry out aerosol sampling. The sampling technique adopted is based on several reasons. Sampling may be to determine the effects of air pollution on public health or to determine compliance with air quality regulations. Alternatively, sampling and analysis may be required for studies such as atmospheric transport of particles, their transformation, deposition and visibility degradation effects. These various reasons lead to different requirements and protocols for air sampling. However, different types of aerosol samplers and filter media are available to meet these requirements. The choice of sampler and the associated filter media will depend ultimately on the purpose for which the data are being sought and the available resources.

This chapter will subsequently consider in detail the physical properties, aerodynamic behavior, sources and sinks of aerosols and sampling techniques for their measurements.

2.2 Physical Properties

2.2.1 Viscosity

Liquids and solids stick to a solid surface so that when they flow their velocity must gradually decrease to zero as they approach the wall of the containing vessel. The

opposition set up by the fluid to shear stress when the fluid flow past a solid surface is called its viscosity. Viscosity may be considered as the internal friction exhibited by all fluids. It arises in liquids as a result of forced movement of a molecule relative to its neighbours as opposed by the intermolecular forces between them.

Unlike liquids, viscosity of a gas increases with temperature. This effect is explained by the kinetic theory of gases according to which gas molecules are separated by distances, which are much larger than the molecular size. The molecules exhibit random motions and collide with each other after traversing a certain distance (called the mean free path) between two successful collisions. In a gas, which is composed of molecular layers moving relative to each other, there is transfer of momentum between the molecules at the upper and the lower layers as a result of acceleration of these layers. This transfer of momentum characterizes the viscosity coefficient η of the gas and it is given by the equation

$$\eta = \frac{\rho_g v_g l_g}{3} \qquad 2.1$$

With:

η = viscosity coefficient

ρ_g = density of the gas

v_g = mean velocity of the gas

l_g = mean free path of the gas

Where:

$$v_g = 1.6\left(\frac{RT}{M}\right)^{\frac{1}{2}} \qquad 2.2$$

With: R = universal gas constant

T = absolute temperature of the gas

M_r = relative molecular mass of the substance.

Equation 2.1 above is analogous to the equation for diffusion coefficient D given by :

$$D = \frac{v_g l_g}{3} \qquad 2.3$$

Since both phenomena involve transport of a certain magnitude (momentum in viscosity and mass in diffusion). In both cases the transport phenomena is irreversible and it continues until the given magnitude is uniformly distributed over the whole gas.

2.2.2 Reynold's number

When the fluid particles passing successively through a given point in a fluid always follow the same path afterwards, the flow is said to be steady and streamlines can be drawn to show the direction of motion of the particles. The Reynold's number denoted by Re is a dimensionless parameter which characterizes fluid flow through a tube or around an obstacle and thus determine the flow regime. It is defined as the ratio of inertial to viscous force. Two types of Reynold's number are in use; the flow Reynold's number and the particle Reynold's number.

The flow Reynold's number denoted by Re_f refers to the critical velocity of a gas in a cylinder and is given by

$$\mathrm{Re}_f = \frac{\rho_g v_g l}{\eta_g} \qquad 2.4$$

Where:

l is the cylinder dimension (cm)

The fluid flow is laminar when $Re_f < 2000$ and turbulent when $Re_f > 4000$.

The particle Reynold's number denoted by Re_p characterizes the resistance of the gaseous medium acting on a moving particle. It is given by

$$\mathrm{Re}_p = \frac{\rho_g (v_p - v_g) d_p}{\eta_g} \qquad 2.5$$

Where:

SULTAN IBRAHIM LIBRARY

v_p = velocity of the particle (cm/s)

d_p = diameter of the particle (cm)

$(v_P - v_g)$ = settling velocity of the particle.

Particle motion is considered laminar when $Re_P < 1$, indicating that the viscous forces are much greater than the inertia forces.

473301

2.2.3 Relaxation time

In many dust control devices, the particles are accelerated to high velocities in order to enhance capture of fine particles. The particle is thus in unsteady motion, and the characteristic time to adjust or relax its velocity starting from its steady state motion is defined as its relaxation time τ. Alternatively, the relaxation time can be defined as the product of mass and mobility *mB*. It can also be expressed in terms of particle diameter as:

$$\tau = mB = \frac{\rho_p d^2 C_c}{18\eta} \qquad 2.6$$

KASTAM IBRAHIM LIBRARY

Where:

ρ_p = particle density

d= particle diameter

C_c = slip correction (to be explained in the following section).

It should be noted that the use of relaxation time as defined in the above equation is limited to particle motion in the Stokes region, *Rep<1*. Relaxation time increases rapidly with particle size since it is proportional to the square of the particle diameter.

2.3 Analysis of Particle Motion in the Gravitational Field

Three types of forces influencing uniform particle motion may be considered. These include external or gravitational force, the resistance force of the medium through which it travels. The third type of force arises from the effects of interaction and only applies to source emission streams and is therefore neglected when considering ambient aerosols.

The resistance force F_R, exerted by a gaseous medium on a spherical particle of unit density is given by Stokes law as:

$$F_R = 3\pi \eta_g v_p d_p \qquad 2.7$$

Where:

η_g = viscosity of the fluid

v_p = particle velocity relative to the fluid

d_p = diameter of a spherical particle.

When the particle reaches its terminal velocity, equilibrium will be established between the resistance force and the gravitational force.

$$F = mg = \frac{\pi d_p^3 g(\rho_p - \rho_m)}{6} \qquad 2.8$$

Thus, equating equations 2.7 and 2.8 gives

$$3\pi\eta_g v_p d_p = \frac{\pi d_p^3 g(\rho_p - \rho_m)}{6} \qquad 2.9$$

from which the particle velocity v_p equal to the terminal velocity v_f can be obtained as:

$$v_p = v_f = \frac{\rho_p d_p^2 g}{18\eta_g} \qquad 2.10$$

where ρ_m, the density of the medium (in this case a gaseous medium) has been neglected.

It should be noted that the application of Stokes law in the present formula is limited to particle size range between 1μm and 100μm, assuming $Re_p < 1$.

The actual settling velocity is greater than that predicted by equation (2.10) with the deviation increasing with decreasing particle diameter. This is because the gas ceases to exist as a continuous medium in the case of sub-micrometer particles since these particles have ability to "slip through" the air molecules and thus experience a reduced resistance force. Cunningham and Millikan extended the application range of Stokes law to particle size range 0.01 - 100μm by the introduction of the Cunningham slip correction factor C in equations (2.7) and (2.10) as follows:

$$F_R = \frac{3\pi\eta_g v_p d_p}{C} \qquad 2.11$$

And

$$v_f = \frac{\rho_p d_p^2 g C}{18\eta_g} \qquad 2.12$$

With:

$$C = 1 + \left(\frac{2\lambda}{d_p}\right)\left(a_1 + a_2 \exp\left(\frac{-a_3 d_p}{\lambda}\right)\right) \qquad 2.13$$

Where:

a_1 = 1.257 (empirical correction factor)

a_2 = 0.400 (empirical correction factor)

a_3 = 0.55 (empirical correction factor)

λ = mean free path for air molecules (6.53 10^{-6}cm)

The slip correction factor ranges from 1.165 for a 1.00μm particle diameter to 22.447 for a 0.01 μm particle diameter.

It should be noted that the above equations assume spherical shape. However in dry conditions spherical shape seldom occurs and therefore a shape factor S must be included in order to correct for the actual resistance force. The dynamic shape factor is defined as the ratio of the actual resistance force of the non-spherical particle to the resistance force of a spherical particle having the same volume and settling velocity. The shape factor has a value of between 1 and 2 for most geometric shapes.

The expression for the terminal velocity in equation (2.9) ignores the acceleration of the particle and considers only equilibrium conditions when the forces acting on the particle are balanced and the velocity is constant. We now consider the acceleration of a particle that is released with a zero initial velocity in still air. Thus equation (2.9) can be re written for this purpose as

$$Mg - 3\pi\eta_g v_p d_p = m\frac{dV(t)}{dt} \qquad 2.14$$

from which we obtain

$$V(t) = V_T\left(1 - \exp\left(\frac{-t}{\tau}\right)\right) \qquad 2.15$$

Equation 2.15 gives the velocity $V(t)$ of a particle released in still air in a gravitational field at time t. If $(V(t)/V_T)$ is plotted against (t/τ), the graph shown in figure 2.1 will be obtained. It is evident from the graph that the particle attains 63% of its terminal velocity after an elapsed time of $t = \tau$ and 95% of its terminal velocity after an elapsed time of $t = 3\tau$.

If on the other hand the particle has an initial velocity of V_0 at time t=0 and V_t is the terminal velocity due to balancing of the forces acting on the particle, then the general equation of motion is

$$V(t) = V_T - (V_T - V_0)\exp\left(\frac{-t}{\tau}\right) \qquad 2.16$$

Equation (2.16) is applicable to the motion of a particle released into a horizontal stream of air moving with velocity U. In this case its initial velocity is zero and its final velocity is U if gravity is neglected. Also in the case of vertical air velocity U including settling, the final velocity is (V_T+U) for positive velocity in the downward direction. In both cases an expression similar to equation (2.15) is obtained.

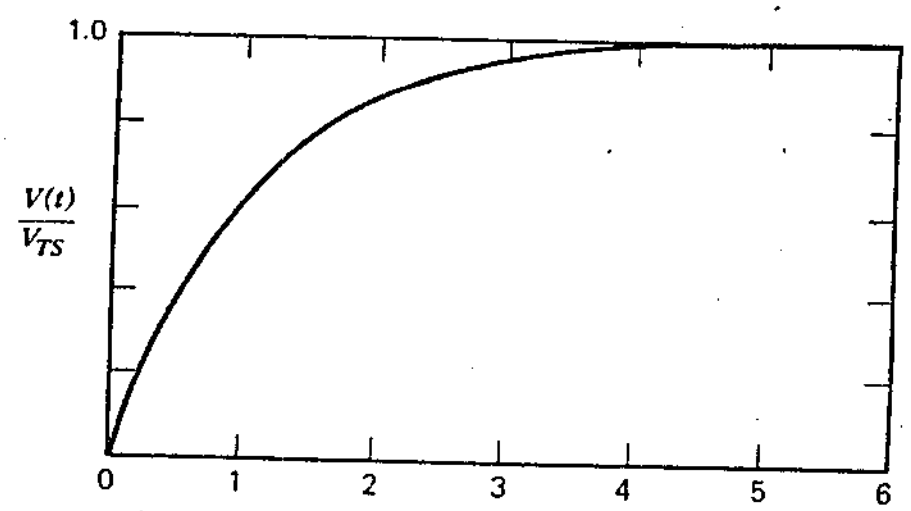


Fig. 2.1: Velocity Versus Time for an Accelerating Particle.

Finally, if the particle motion is affected by a varying external force along an axis, its motion can be readily analyzed if the rate at which the particle adjusts to changes in the force is more rapid than the rate of change of the force. If t_c is the time required for the force to change to *1/e* of its initial value and $t_c >> \tau$ then the particle can be considered to adjust instantly and its velocity at any time is given by

$$V(t) = \tau \frac{F(t)}{m} \qquad 2.17$$

Equation 2.17 is applicable to aerosol flowing in a duct of changing dimension and a particle motion under the influence of centrifugal force.

If *V(t)* in equation (2.16) is replaced by *dx/dt*, the displacement along the x-axis as a function of time denoted by *x(t)* can be obtained as

$$x(t) = V_T t - (V_T - V_0)\,\tau \exp\left(\frac{-t}{\tau}\right) \qquad 2.18$$

In the absence of external forces, $V_T=0$ and $t >> \tau$. In this case the maximum distance *S* covered by a particle with the initial velocity V_0 is given by

$$S = V_0 \tau \qquad 2.19$$

S is called the stopping distance. It can also be defined as the product of the particle mobility and its initial momentum. It represents the ultimate distance covered by a particle in the absence of external force. An important use of the concept of stopping distance is the case of a particle moving in an air stream that is abruptly turned through 90^0. In this case the stopping distance represents the distance the particle continues to travel in its original direction.

The concept of stopping distance can be used to analyze curvilinear particle motion which are important for describing the particle collection mechanisms in a filter, cyclones, lung or cascade impactor where abrupt change in particle motion occurs. Curvilinear motion is characterized by a dimensionless number called Stokes number *Stk* defined as the ratio of the stopping distance of a particle to the characteristic dimension of the obstacle. In the case of a flow perpendicular to a cylinder of diameter *d*, the Stokes number is given by

$$Stk = \frac{2\tau U_0}{d} \qquad 2.20$$

Where U_0 is the undisturbed air velocity farther from the cylinder.

As Stokes number increases from zero, particles, which initially track the gas streamlines perfectly, resist changing their direction with the gas streamlines.

The Stokes number is used to characterize inertia impaction, which is a special case of curvilinear particle motion used in the design of equipment for collection and measurement of aerosol particles.

2.4 Behaviour of Pollutants in the Atmosphere

Pollutants released into the atmosphere are influenced by fundamental physical and chemical processes, which modify the size distribution of these particles. These processes include gas to particle conversion and particle growth by coagulation which are phenomena resulting from interaction and reaction between particles and gaseous molecules to form new particles or modify the existing ones.

2.4.1 Gas to particle conversion

Atmospheric gases and particles can interact and react to form new particles or modify the existing ones. These chemical processes mostly occur in the gas phase. In such cases, gases react to form ultra-fine particles from a gas phase that consists of one or two or more gaseous species. For example, SO_2 reacts in the atmosphere to form H_2SO_4, which are incorporated into the cloud where they can serve as cloud condensation nuclei (Chameides et al, 1982). Thus, the existence of the condensed phase in the atmosphere is an important mechanism in the cycling of sulphur through the atmosphere. Another example is the interaction of nitrogen and sulphur cycles, which occurs when the gaseous species of each cycle react to form an aerosol. For instance, NH_3 and SO_2 tend to ultimately form $(NH_4)HSO_4$ or $(NH_4)_2SO_4$ aerosol which appear to form a major fraction of aerosol particles that are active as cloud condensation nuclei over the ocean (Chameides et al, 1982). Nitrate is another major constituent in atmospheric aerosols. It is an end product of a wide variety of reactions involving primarily NO and $NO_2(NO_x)$. A significant portion of this aerosol is primarily derived from the combustion of fossil fuels and biomass burning.

473301

Another pathway for gas to particle conversion is the growth of pre-existing particle due to deposition of molecules from the gas phase or reaction of gases with particles, which can occur on the surface or the interior of liquid particles.

It should be noted that chemical reactions involving atmospheric trace gases produce reaction products that have a low vapour pressure. This process subsequently leads to super saturation condition of the atmosphere with respect to

the gaseous molecules as more of these secondary volatility products are formed. The degree of super saturation will determine the degree of nucleation (formation of new particles) or condensation (deposition on pre-existing particles).

2.4.2 Particle growth by coagulation.

Particle growth by coagulation proceeds by sequence of events. During each of these events a pair of particle is destroyed and new or larger particles created. Coagulation thus results in continuous reduction in number concentration and an increase in particle size.

Thermal coagulation occurs as a result of Brownian motion of particles, which is responsible for the several collision events. The rate of collision per unit aerosol volume is numerically equal to the rate of change in number concentration *dN/dt*. This can be expressed as

$$\frac{dN}{dt} = -KN^2 \qquad 2.21$$

Where K and N are the coagulation coefficient and number concentration respectively. The coagulation coefficient can be expressed as

$$K = \frac{4KT}{3\eta_g} C \qquad 2.22$$

Where:

k = Boltzman's constant

T = absolute temperature

η_g = viscosity of the gas phase

At standard condition K can be expressed in terms of slip correction factor C as

$$K = 3x10^{-10} C \qquad 2.23$$

Since small particles have significant slip correction, K is therefore significantly altered. For particles larger than 10μm AED, K is independent of the slip correction factor since it is negligible for these particles.

2.4.1 The Multimodal Character of Aerosols

The pollution aerosol distribution in the atmosphere can be classified into three modes. These include the nuclei, fine particle and coarse particle modes. These three modes have different sources, formation processes and atmospheric life times and are removed by different mechanisms.

The nuclei mode can be considered as a transition region in which many chemical and physical processes (nucleation and condensation) occur at high temperatures with fast reaction rates. The high temperature processes, which proceeded in the

The fine particle mode covers particles in the size range 0.1 to 2μm AED, and can be created by coagulation of Aitken nuclei or by condensational growth of Aitken nuclei. This obviously explains the large-scale mass exchange between the nuclei and the fine particle mode. It is remarkable that atmospheric removal of these fine particles is very inefficient. This explains their relatively long resident time of several days in the atmosphere. It also accounts for most of the visibility effects, because maximum light scattering occurs with particles having a size that corresponds to the wavelength of the incident light (0.4 to 0.7μm).

The coarse particle mode is composed of particles ranging from a few micrometers to 100μm AED, and is physically separated from the fine particle mode with a saddle point at about 2μm AED. There is a little mass transfer between both modes; this gives a clue to the origins of the particles. The coarse particle mode is assumed to be generated by mechanical processes, re-suspension of soil and bubble bursting at the sea surface. Their lifetime in the atmosphere can reach several hours before removal by sedimentation, impaction or washout. Figure 2.2 gives the schematic representation of multi-modal character of a typical pollution aerosol and the interactions that modify it.

2.6 Aerosol Removal Mechanisms from the Atmosphere

The atmosphere cleanses itself of large amount of pollutants from natural and anthropogenic sources through deposition phenomenon, which is an efficient process as the concentration of only few gases, mainly CO_2, increases on global scale. Two types of deposition mechanisms can be distinguished: dry deposition and wet deposition. The dry deposition occurs as a result of uptake at the earth's

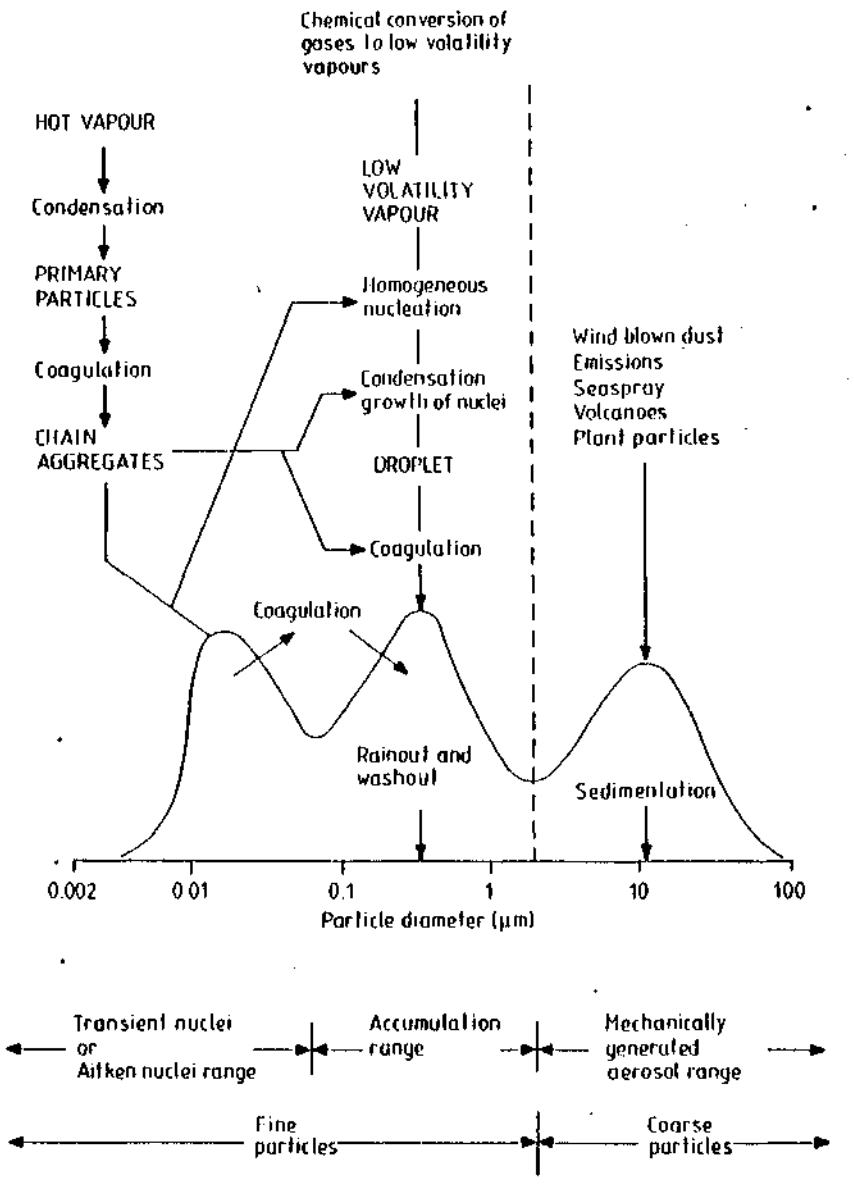


Fig 2.2: Multi-Modal Character of a Typical Pollution Aerosol and the Interactions that Modify it (Whitby, 1977).

surface (soil, water or vegetation) while the wet deposition occurs as a result of absorption of particles into droplets. This may be followed by the droplet's precipitation by rain or impaction at the earth's surface as fog droplets. Wet deposition measurement is generally considered as the most effective method of characterizing removal mechanism than the dry deposition. This is because dry deposition only provides information about pollutants within the atmospheric layer of the sampler location whereas wet deposition mechanism involves several layers from each of which aerosol is collected and hence may reflect more truly atmospheric pollution. Conversely, dry deposition is more useful in assessing health risks and identification of pollution sources than wet deposition since it provides information on shape, size and composition of atmospheric aerosols.

Although the dispersion of pollutants from a source can be calculated to a certain degree on the basis of source characteristics and the meteorological factors, the results obtained still require further correction for the actual removal processes. Recently, deposition processes have received much attention especially in long range transport studies (Pacyna et al, 1984) where the knowledge of these mechanisms is very important in accurate prediction of environmental impacts of pollutants. For this reason, a review of dry and wet deposition processes is provided.

2.6.1 Dry deposition

Dry deposition mechanism is characterized by the dry deposition velocity defined as the ratio of the pollutant deposition flux and the pollutant concentration as

$$V_d = \frac{F}{c} \qquad 2.24$$

Where:

V_d = dry deposition velocity

F = dry deposition flux

c = pollutant concentration

The earth surface is an important sink for removal of particulate matter transported through the viscous boundary layer near its surface. These particles can penetrate through the viscous boundary layer by processes such as sedimentation, impaction and diffusion. Large particles possess deposition velocities dominated by gravitational effects and thus are deposited by sedimentation. Particles in μm size range may be captured by impaction or interception phenomena which are difficult to quantify correctly. Particles in the size range 0.1-1μm have low deposition velocities due to the relative weakness of Brownian motion and gravitational effects. For particles with sizes less than 0.1μm Brownian motion allows rapid movements across the viscous air layer just above the surface. In the case of gases dry deposition is strongly affected by their chemical reaction with the surface. This is verified by the varying deposition velocities of SO_2 for different surfaces (Sehmel, 1980). It should be noted that surface roughness significantly influence the near surface turbulence and hence the rate of pollutant transfer to the surface (Sehmel, 1980)

2.6.2 Wet deposition

Wet deposition occurs when an aerosol is incorporated into water droplets. This is achieved by two complementary processes: washout and rainout.

Rainout occurs when aerosol particles are incorporated into rain droplets owing to the large surface area of cloud droplet and effects of condensation. When formed, such a droplet may then act as sink for smaller Aitken particles, which may attach themselves to an already formed droplet by Brownian diffusion. After leaving the cloud and entering sub-cloud layer, the raindrops may remove aerosol particulates at lower altitudes by essentially inertia impaction mechanism. This second process is called washout.

The efficiency of rain-out has been found to be a function of particle size (Dufour, 1964). Brownian attachment is most efficient for particles less than 0.1μm diameter. Particles in the size range between 10 and 20μm diameter are removed by inertia impaction. The raindrop scavenging efficiency in this case is influenced by the raindrop cross-sectional area and the intensity of the rainfall. From this analysis of precipitation scavenging, it is apparent that there exists a particle size range of 0.1-10μm diameter in which neither Brownian nor aerodynamic impaction can remove aerosol efficiently (Junge, 1970). These particle size range, which include most of the aerosol mass have relatively long atmospheric resident times and thus can be subjected to long range transport.

Assuming that the aerosol concentration is uniform in the troposphere, Junge (1970) showed that where washout is negligible, the amount of aerosols removed from the air after t days can be expressed as

$$\alpha = 1 - \exp\left(-\frac{Eh\rho t}{LH}\right) \qquad 2.25$$

where:

E = rainout efficiency

α = fraction of aerosol removed

L = liquid water content in the cloud

H = depth of the atmosphere to the top of aerosol layer

h = amount of rainfall

ρ = density of water.

The calculation of atmospheric resident time for the removal of a given percentage of atmospheric aerosols shows that as E decreases, atmospheric resident times increases (Larsen, 1969). In particular for E=0.5 for sulfate and lead aerosols, the calculation predicts that about half of the particulate material will remain airborne for at least one week. In time a period as long as this, the aerosol can be subjected to long range transport. The discovery of lead deposits in Greenland and anarctic ice (Murozumi et al, 1969) serves to emphasize this point.

2.7 Sampling Techniques

2.7.1 Principles of air sampling

The objective of any sampling protocol is to obtain representative sample. However, this may not be easy because the very act of sampling itself introduces considerable disturbances within the system that creates differences between the collected sample and the actual sample. This can be minimized by isokinetic sampling in which air is drawn into the sampling unit with the same linear velocity as that of the air flow by the wind at the moment. It has the added advantage of retaining particles larger than 10μm AED. When either calm or turbulent air is being sampled, this is impossible to achieve. The reason is that the passage of the samples into the sampler's chambers can cause aerosol modifications by

precipitation of the larger particles, diffusion of the smaller particles to the tube walls and impaction on the walls.

Since pollutants are reported on concentration basis, an accurate measurement of the volume or weight of the pollutant in a stated volume must be known. For the determination of air volume, two basic types of equipment are in use. These are the flow rate meter (rotameter) and the dry gas meter. A rotameter requires calibration and gives an instantaneous reading of the air flow at the beginning and end of the sampling period. If for any reason sampling is interrupted during this period (e.g. power failure), this will lead to errors. Therefore, dry gas meter is preferred since it provides a more accurate value of the air volume. In either case, the device should be placed behind the pump. It should not be placed between the filter and the pump because of the pressure drop over the filter, which will introduce error owing to the fact that the gas meter is calibrated to work at atmospheric pressure. Also, the gas meter should not be placed before the filter because the gas will interfere with the aerosol sampling on the filter. Another important consideration in aerosol sampling is the leakage of the pump setup. The air leakage from the plastic tubing especially in the connection of the tubing with the filter holder must be avoided to ensure accurate measurement of air volume.

Further, it is essential to employ a reliable pump, which provides a constant flow rate. The exhaust of the pump should however be placed downwind and far away from the sampling location. This is necessary in order to avoid contamination of the filter by exhaust gases which may lead to erroneous measured concentration of elements such as Cu, Fe, Pb etc.

Finally, the collector (e.g. filter) must be efficient. The choice of filter is dictated by the nature of the pollutant and the analytical method to be employed. For particulates, the air is drawn through a filter or series of filters to separate the suspended particulate matter from the air. When this method is used, filter efficiency must considered.

2.7.2 Sampling efficiency

Sampling efficiency is defined as the ratio of the number of particles entering the sampling inlet to the number in the air volume. The capture of particles by filtration is based on five mechanisms: interception, inertia impaction, diffusion, gravitational settling and electrostatic attraction.

Interception occurs when the particle size is larger than the pore size of the filter. This mechanism is independent of the flow rate of the filtration device. The mechanism of impaction relies on the aerodynamic diameter of the particles. They are primarily acting on particles greater than 0.5µm AED and their effect increases with increasing particle size. Diffusion collection is based on Brownian motion of small particles up to 0.5µm, which collide with the gas molecules (Fucks, 1964). It increases with decreasing face velocity. Capture of particles by gravitational settling is not important except when the particle size is large and suction rate is very low. The capture by electrostatic attraction depends on electric charge of the particles and the filter. It is important for porous membrane filters.

In general, the sampling efficiency depends on the wind velocity, filter face velocity and choice of filters.

Influence of the wind velocity

In still air, the ambient air particles can only reach the filter by suction through the sampling inlet. If the particle falling speed exceeds the filter face velocity, the particle will not be sampled. The inertia of suspended particles is affected by high wind speeds. Thus, the stop-distance (and hence the inertia) of the particles increases with increasing wind velocity, which in turn results in increase in Stokes number *Stk*. The increased inertia of the particles implies that a smaller amount of coarse particles will be collected leading to decrease in concentration of the suspended particulate matter. The influence of the wind velocity on sampling efficiency had been demonstrated by field experiments. For example, Barret (1982) observed a decreased sampling efficiency with moderate wind speeds relative to still air using low volume sampler.

It should however be noted that high wind velocity gives rise to considerable accumulation of unwanted particles on the filter leading to passive sampling. This can be avoided by incorporating pre-impaction stage in the sampling line.

Influence of the filter face velocity

The sampling efficiency is also affected by the filter face velocity. It decreases as the face velocity increases. This is due to the loss of sub-micrometer particles through the filter pores at higher face velocity, which results in the re-entrainment of sub-micrometer particles in the air stream. Thus, the sampling efficiency increases as the filter becomes loaded at a low face velocity. However at higher face velocities the efficiency initially increases and then decreases with continued loading of the filter.

Selection of sampling media

A suitable filter should not only be retentive of particles but also permit steady flow of air through it. It should provide sample that can be easily analyzed both by gravimetric and elemental analysis. These simple requirements are however complicated by some other factors that make the choice of filter a difficult task. Often, the choice of filter medium depends primarily on the program objectives, but in most cases, a compromise had to be made in the choice of filter when high sampling efficiency and analytical suitability are considered. For example, fibrous filters have high sample collection efficiency and low pressure drop, but they are rarely used for XRF analysis. This is because of the high blank value of glass filter on one hand and hygroscopic nature, structure and thickness of Whattan 41 on the other hand. Conversely, Membrane filters are favoured for XRF analysis in spite of their lower sample collection efficiency than fibrous filters. This is because they are thin filters and have lower blank value. In addition, they have uniform structure and pore-size distribution that ensures deposition of particles directly on their surfaces so that absorption of the incident and emitted characteristic X-rays is minimized.

2.7.3 Particulate samplers

Introduction

Particulate matter is collected using air samplers. Generally, air samplers consist of aerosol inlet, vacuum pump, air flow regulator, volume meter, filter holder, filters etc. The general concept in air sampling involves drawing a large volume of air through a filter so as to collect the particles present in the air. When the flow rate is appropriately chosen, most of the major elemental constituents of the sampled air

can be observed. In some cases, the sampler is coupled to a device whose function is to modify the sampled air in order to fulfil some predetermined aerodynamic characteristics before it is deposited on the filter. When this is done, only particles meeting these requirements are collected while other components of the aerosol are prevented from reaching the filter. However, in all the cases, the efficiency of the overall sampling setup is determined by the characteristics of the filter upon which the particles are deposited.

Particulate matter may also be collected as deposition samples using dry/wet deposition sampler. The main disadvantage of such samplers is the difficulty in obtaining samples that are representative of the actual dry and wet deposition events.

Various types of aerosol samplers and filters are available. The choice of the sampler and the collection substrate is determined by the project objective and the analytical methodology available for analysis of the sample. For this reason, a review of the commonly used air samplers is presented.

High volume samplers.

High volume samplers which offers high flow rate capability, are widely used for collection of total suspended particulate matter (TSP), most especially to determine compliance with the old U.S. national air quality standard for particulate matter. The size range of particles collected by this type of sampler is not well defined as it is strongly affected by wind speed and direction (Wedding et al, 1977). Another drawback of this type of sampler is that it allows accumulation of

wind blown dust leading to overestimation of the particulate content of the sampled air.

The standard collection substrate is the glass fibre filters. These filters are used because of their high retention capacity for particles greater than 0.3μm. Apart from the fact that this type of filter is unsuitable for ED-XRF and INAA analysis, it has a disadvantage of producing artifact sulphate on the filter (Pierson et al, 1980) and hence causes error in the measurement of TSP. Thus, time consuming sample preparation and analysis procedure is required for analysis.

PM10 samplers

In order to eliminate the drawbacks associated with the high volume sampler and make it suitable for recent air sampling requirements, a PM10 inlet capable of excluding particles greater than 10μm AED is incorporated. The PM10 inlet operates by the principle of impaction on a plate. as explained in section 3.4.2.1 so that only particles above certain effective diameter impact on the plate while smaller particles move with the air stream for subsequent sampling. With this method, it is possible for some of the deposited particles to be re-suspended and move with the air stream. This can be avoided by coating the impaction plate with grease or by the principle of virtual impaction whereby the particles are allowed to impact into a separate volume of air where they are collected by filtration.

Dichotomous sampler

Recent requirements (such as source identification and lung deposition studies) in atmospheric aerosol sampling require collection of aerosol in two separate size

fractions corresponding to bimodal urban aerosols. It has been established that fine particle fraction (<2μm AED) consists of mainly particles from combustion sources while larger particles (2-10μm AED) are generated by mainly natural and mechanical processes. Thus a size cut off of about 2μm to some extent separates the particles according to their origins and chemical properties. The dichotomous sampler is a device used to provide such size separation. It uses the principle of virtual impaction (Dzubay and Stevens, 1975) to separate the aerosol which is initially directed into PM10 inlet (for exclusion of Particle greater than 10μm) into fine and coarse particle fractions. The coarse and the fine particle fractions are sampled at a flow rate of 13.6 litres/min and 0.4 litres/min respectively (Dzubay and Stevens 1975). The collection substrate is a membrane filter such as Teflon, polycarbonate Nuclepore and cellulose acetate filters which provide samples compatible with INAA and ED-XRF. The operating flow rate however depends on the filtration efficiency of the filter and hence must be carefully chosen to avoid clogging of the filters as the particles accumulate.

Stacked filter unit

An alternative and a much less expensive method for collection of bimodal aerosol fractions is the stacked filter unit. It also incorporates a PM10 inlet and uses the different filtration efficiencies of two membrane filters arranged in series to separate the incoming PM10 aerosol into coarse and fine particle size fractions. It has an advantage that pairs of Nuclepore (or Teflon) membrane filters of different pore sizes can be used for size separation. The most commonly used combination of filters are 0.8μm pore size Nuclepore filter for collection of coarse fraction and

0.4µm pore size Nuclepore filter for collection of fine fraction (Cahill et al, 1977; Heidam, 1981).

Cascade impactors

In certain special studies, a detailed size distribution of aerosol may be required This is achieved using cascade impactor. Single or multiple jet cascade impactors are available so that the air is sampled over a wide range of flow rates. In a cascade impactor, the air is drawn through an orifice and particles of appropriate diameter in the resulting jet impact on a plate. Finer particles move with the resulting air stream until they are incident on the next impaction plate with smaller orifice diameter where the jet has a higher speed resulting in deposition on the plate at this stage. The process continues until there is deposition on the plate at the final stage. In this way, an efficient division into various size classes is achieved by arranging several plates in series. For ED-XRF analysis, single jet cascade impactors based on Battelle design (Mitchelle and Pilcher, 1959) are used. Some of the more recent designs have as many as 10 stages made up of 7 regular impaction stage, 2 low pressure stages and a back up filter (Bauman et al, 1981). The particle collection stages should however be thin and flat in order to minimize X-ray absorption effects. A major disadvantage of cascade impactor is particle bounce off which can be minimized by coating the impaction plates with grease.

473301

2.7.4 Filters

There are different types of filters. They can be divided into two categories, i.e. fibrous filters and membrane filters. Fibrous filters are made up of fibres randomly

arranged and bonded together to form a mat so that particles are collected as the air flows around the fibres. fibrous filters include cellulose filters such as whattman 41, glass fibre and quartz fibre filters. Fibrous filters have high sample collection efficiency and low pressure drop. Even though glass filters are very suitable for high volume sampling, they are rarely used because of their high blank value which often invalidates the sample. Whatman 41 also have high collection efficiency and low pressure drop but has to be conditioned to room temp and humidity before usage because of its hygroscopic nature. They are not quite suitable for XRF, as analysis of these types of filters requires absorption correction.

Membrane filters have a much regular structure and smoother surface than fibrous filters. They are made up of thin layer of a polymer, e.g. cellulose ester or Teflon. A particular type of membrane filters, known as Nuclepore filters is composed of thin polycarbonate sheets with fine capillary pores and a uniform structure and pore size distribution (Fleischer et al, 1965; Spurny et al, 1969). One advantage of these types of filters is that they have lower blank values than fibrous filters. In addition, particles are easily collected on the surface thus making them suitable for XRF analysis since X-ray absorption of the incident radiation and the generated characteristic X-rays in the filter material do not need to be considered. They are however more expensive and may be difficult to handle because they become electrostatic. Also, they cannot withstand high flow rate thereby leading to prolonged sampling.

2.7.5 Deposition samplers

Deposition samples are collected on a bulk deposition sampler such as a container placed in open space for extended period of time. In the case of dry deposition samples the container may be dust-fall jars, flat plates or filters while for wet deposition bottles equipped with funnels or rainfall gauge are used. The samples collected are however not representative of the dry and wet deposition phases respectively. The results obtained in such studies are therefore highly suspect.

An improved method for collection of deposition samples is the use of wet/dry deposition collector (Galloway et al, 1982). This device has two collection containers. If the sensing device incorporated into the sampler detects the occurrence of precipitation, the mechanism that exposes the 'wet' collector only is activated and vice versa. In the end wet and dry deposition samples will be collected in separate containers.

Since the wet deposition flux is the ratio of the total concentration of the species in question to the area of the opening of the collector, it is clear that the wet deposition component provides accurate value of wet deposition flux. On the other hand, information obtained from dry collector are not reliable because dry removal processes are extremely size and surface dependent. Reasonable values may be obtained for large-particle size because they are deposited by gravitational settling. On the other hand values for fine particle which are normally removed primarily by diffusion processes are not reliable since the aerosol may be collected by all surfaces of the container. Thus, the collection area is not simply the open area of the collector but rather the entire interior surface.

CHAPTER 3

X-RAY FLUORESCENCE ANALYTICAL TECHNIQUE

3.1 Introduction

X-ray fluorescence (XRF) is a widely used technique for analysis of environmental samples. This is because of its several advantage over the conventional wet chemical methods. These advantages include multi-elemental capability, non-destructive nature, minimum sample preparation, high speed of analysis and good precision, sensitivity and accuracy. Typically, the sample consists of deposits of environmental contaminates collected on a high purity substrate.

Electromagnetic radiation (from X-ray tube or radioisotope excitation sources) or charged particles are used to excite and generate characteristic X-rays from the sample. Traditionally, crystal spectrometers are used to disperse and analyze these X-rays according to their wavelengths by Bragg diffraction from a single crystal. This form of X-rays fluorescence analysis is known as wavelength dispersive X-ray fluorescence (WD-XRF) and was originally and exclusively used for analysis. With the development of high resolution lithium drifted silicon Si(Li) detector and germanium detector capable of separating characteristic X-ray lines according to their energies, another form of X-ray fluorescence technique known as energy dispersive X-ray fluorescence (ED-XRF) came into existence. Both the photon separation techniques have individual advantages and disadvantages so that they have both survived and used in several laboratories worldwide. In spite of the wide spread use of XRF, advances are still being made in order to elliminate

its drawback and limitations. Recent advances are in the development of synchrotron radiation based X-ray excitation source (Gordon, 1982), polarized X-rays and total reflection X-ray fluorescence (TXRF) technique (Prange, 1989) for light matrices and for analysis of minute amounts (of the order of mg) of a sample. TXRF was exclusively applied in this work for analysis of PM10 particulate matter because of the small sample loading on the filters.

The fundamentals, practice and applicability of XRF to analysis of aerosol samples have been described in several books. These include Jenkins et al (1981), Tertian and Classe (1982), Dzubay (1977), and Van Grieken and Markowicz (1993).

3.2 Physics of X-Ray Emission Spectra

X-ray emission spectra may be classified into three groups: continuous spectrum, scattered radiation and characteristic X-ray or line spectrum. Continuous X-rays are produced when electrons or other high-energy charged particles lose energy when passing through the Coulombic field of the nucleus. In this interaction, the energy lost by the electron when they are suddenly brought to rest on striking a target is called Brehmstrahlung. This energy loss (due to high deceleration) can be observed as a pulse of radiation.

The continuous X-ray spectrum generated by electrons in an X-ray tube is characterized by short wavelength limit λ_{min} corresponding to the maximum energy of the exciting electrons and is given by Duane-Hunt law as

$$\lambda = \frac{hc}{} \qquad 3.1$$

where h is the Planck's constant, c is the velocity of light, e is electronic charge and V_o is the potential difference applied to the tube.

Scattered radiation is produced as a result of scattering of X-rays by electrons. Two types of scattered radiation can be distinguished. When the scattered photon has the same energy or wavelength as the incident photon, the scattering is called coherent or Rayleigh scattering. If the energy or wavelength of the scattered photon has been modified, the scattering is called incoherent or Compton scattering (Hubbel et al, 1975). In Compton scattering, the X-radiation scattered by a single electron is changed in wavelength according to the relationship

$$\Delta\lambda = \lambda_{inc} - \lambda_0 = 0.024(1 - \cos\varphi) \qquad 3.2$$

where φ is the angle through which the photon is scattered from its original direction.

As a result of Compton scattering, the total energy of the incident photon is not deposited at the location of the first interaction. For a high-energy photon of the order of MeV, there may be series of Compton scattering events each of which reduces the secondary photon energy, before the sequence ends with photoelectric absorption event. Therefore the energy of the incident photon can be distributed over a significant volume of the material.

Rayleigh scattering is not significant in the energy range considered in X-ray physics. Its effect will tend to cancel in many cases since as many photons may scatter in a particular direction as scatter away from it.

The production of characteristic X-rays involves transitions of the orbital electrons of atoms in the target material. When one or more electrons of an atom is ejected from a K-shell or L-shell of an atom by an electromagnetic radiation, by a charged particle passing through the material or by nuclear processes, the atom becomes ionized and the resulting ion is raised to an excited state. This leaves a vacancy or hole in for example the K-shell. The transition of an electron from any other shell to this hole would reduce the system energy and enhance the return to the ground state configuration. Filling of this vacancy by an electron from the L-shell will be accompanied by emission of an X-ray known as the $K\alpha$ X-ray line which is characteristic of the atom. In principle the excitation of an atom is followed by a sequence of de-excitation transitions each of which may involve emission of an X-ray with an energy that is approximately equal to the difference in energy of the two states.

It should be noted that there are certain transitions that have a very low probability of occurring although they are energetically possible, such as transition from L_1 sub-shell to the K-shell. The restriction on such transitions is explained by quantum mechanical rules involving the angular momentum properties of the atomic states and X-rays (Krause, 1979).

The two additional modes of de-excitation of atomic states are the Auger effect and the Coster-Kronig transitions (McGuire, 1971; Bambynek et al, 1972). For example, if an L-shell electron fills a hole in the K-shell, the most probable result is the emission of $K\alpha$ X-ray. However in a few percent of the cases, the X-ray is not emitted, but rather this energy is transferred to another less tightly bound electron

so that the latter electron is ejected from the atom. This is known as the Auger effect. It has the effect of producing vacancies in the atom. The kinetic energy of the ejected electron is equal to the difference between the expected X-ray energy and the binding energy of the electron before it is ejected.

The combination of X-ray emission process and the Auger process gives rise to radiative Auger process. In this case, a vacancy is filled and an electron and an X-ray are both emitted. In the spectra measured with semiconductor detectors, this results in satellite peaks on the low energy side of the main X-ray peaks (Campbell et al, 1986). These satellite peaks must be taken into account in order to avoid discrepancies between the measured and calculated ratios of intensities of the K_α and k_β X-rays.

The probability that the filling of a hole in the K, L,.... Shell will result in the emission of an X-ray, and not auger electron, is called the K-, L-, ... Fluorescent yield ω_K, ω_L..... respectively (McGuire, 1971).

$$\omega_K = \frac{N(X_K)}{N_0} \qquad 3.3$$

where:

$N(X_K)$ is the number of emitted X_K rays and N_o is the number of K-shell vacancies.

In certain regions of the periodic table of the elements, the energies of the electrons are such that an electron in one sub-shell can move to a lower sub-shell without the emission of an X-ray. These transitions are known as Coster-Kronig transitions. For example L_3 electron might fill a hole in L_2 level. This process is not

of importance here but it makes the definition of the fluorescent yields for the L-sub-shells quite complex. However, since these transitions occur only within a major shell, they do not affect the total fluorescent yield for the whole shell.

3.3 X-Ray Tube Excitation Systems

The electromagnetic radiation needed to excite fluorescence in a sample is generally obtained from the anode of an X-ray tube shown in figure 3.1. This is because of the higher intensity it offers compared to photons from radioisotope sources, thus making it ideally suited for analysis of trace elements in a large number of samples. The X-ray interacts with the sample either by photoelectric effect to produce the required ionization for emission of X-rays or by scattering by electrons to produce background regions in the spectra, which are undesirable.

In order to reduce these background regions in the spectra, monochromatic radiation from the X-ray tube is always preferred. Monochromatic radiation may be obtained by using a thin X-ray filter of typically the same element as the anode material to preferentially transmit the characteristic X-rays generated in the anode. This method has the advantage of providing the most efficient use of the photons generated in the anode. Its disadvantage is the lack of flexibility in the choice of excitation energies. Another method of generating monochromatic X-rays is to operate the tube in a secondary target excitation mode. In this case, the continuum radiation from the X-ray tube is used to excite fluorescence in a secon-

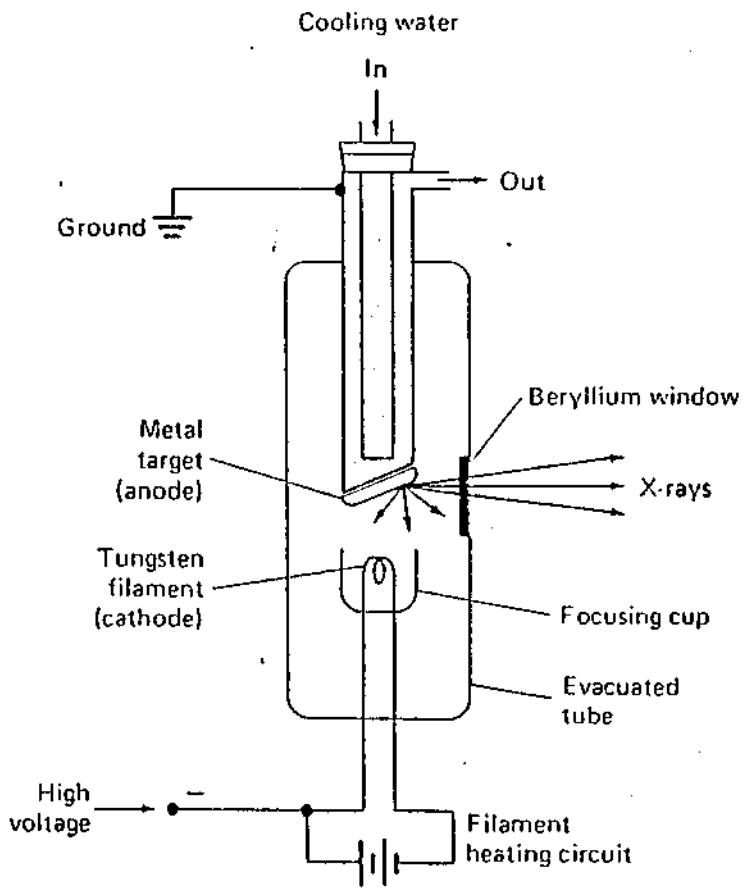


Fig. 3.1: Schematic Diagram of an X-Ray Tube.

-dary target whose characteristic X-rays is then used to excite fluorescence in the sample. This method has the advantage of flexibility in the choice of excitation energies but inefficient in utilizing the output flux.

The monochromatic X-rays generated should be employed with caution. This is because the probability of producing fluorescence in the sample is greatest when the photon energy just exceeds the binding energy of the electrons in the appropriate shells, and this probability decreases as the excitation energy increases. The implication of this is that low-energy characteristic X-rays are not efficiently excited by high-energy monochromatic radiation. The solution to this problem is to select the mono-energetic excitation energy sufficiently far above the absorption edge such that radiation elastically and inelastically scattered from the matrix does not overlap the photo-peaks of the fluorescent X-rays.

The spectral background can also be reduced by reducing the extent of the scattering process and using a highly monochromatic X-ray beam. This can be achieved by using polarized X-ray beam as excitation source or by using the total reflection X-ray fluorescence (Kregsamer, 1991).

It should be noted that the highest possible countrate should be produced from the X-ray tube in order to enhance its sensitivity. One method usually employed is to operate the tube in a pulse mode whereby the X-ray control grid is operated in a feedback loop with the detector output (Jaklevic et al, 1976). When operated this way, the tube will be pulsed off when a signal is being processed and later turned on when a new signal is to be analyzed leading to tremendous increase in the X-

ray flux. A more recent approach used in increasing the flux is the use of synchrotron sources as excitation system (Gordon, 1982, Gilfrich et al, 1983).

3.4 Semiconductor X-Ray Specrometer

A photon spectrum emitted by a source consists of groups of photons, each group being mono-energetic. A detector will convert such a line spectrum into a combination of lines and continuous components. These characteristic lines are used to determine the energies and intensities of the original photons provided they are not lost in the associated continuum. The ability of the detector to produce lines or peaks for mono-energetic photons is characterized by the peak width and the peak efficiency. The peak width is commonly specified by the detector resolution or the full width at half maximum (FWHM). The peak efficiency of the detector is the ratio of the number of counts in the peak corresponding to the absorption of all of the photon energy (full energy peak) to the number of photons of that energy emitted by the source. Both the peak width and the peak efficiency are functions of energy.

X-ray photon detectors follow a series of steps in the detection and measurement process. These include the conversion of photon energy to mainly kinetic energy of electrons by photoelectric absorption and Compton scattering, the production of electron-hole pairs, and the collection and measurement of these charge carriers. The electron-hole pairs produced as a result of ionization are converted into a voltage pulse in a semiconductor spectrometer with the amplitude of this voltage pulse being proportional to the incident energy (Derbertin and Helmer, 1988). In order to maintain the linearity of the voltage signal with respect to the original

charge pulse, specially designed electronics system are used along with the semiconductor spectrometer. A multi-channel analyzer accumulates a histogram of the energy spectrum of the sequential events and stores these data in its memory. The mechanism by which the ionization signal is measured is not limited to a narrow energy region, thus making possible the simultaneous detection of X-rays over a wide range of the emission spectrum. This simultaneous determination of X-rays gives it an advantage of multi-element capability. A typical energy-dispersive X-ray spectrometer is shown in figure 3.2.

3.4.1 Physical processes in semiconductor detectors

Single crystal of semiconductor material such as silicon or germanium consists of sharply defined atomic electron states which are broadened into bands of energy states that are characteristic of the whole crystal. The lowest states called the valence band are separated from the next higher states called the conduction band by the band gap of the order of 1eV. An electron excited from the valence band to the conduction band is free to move under the influence of the external electric field and can be collected at an electrode. The vacancy or hole left in the valence band as a result of electron excitation can also move by the mechanism of electron transfer in a direction opposite to that of the electron. Both the electron and the hole are collected to form a pulse whose shape reflects their differing mobility.

The interaction of a photon with the crystal causes excitation of bound electron from the valence band to the conduction band by the primary electron from the interaction. These secondary electrons if sufficiently energetic can create extra

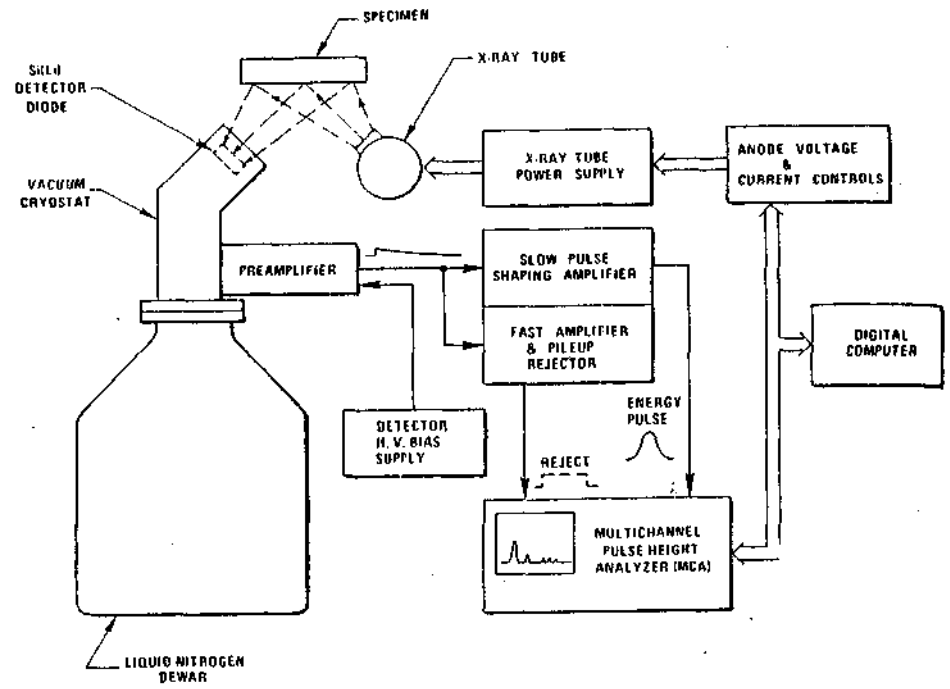


Fig. 3.2: Block Diagram of a Typical Energy Dispersive X-Ray Fluorescence Spectrometer.

secondary electrons, leading to a cascading process. Thus the energy of the primary electron is expended in the production of many electron-hole pairs that are then free to be collected at the electrode of the device. To collect this charge, a bias voltage, which is specific for the particular detector is applied. This voltage is chosen low enough to minimize the probability for a voltage breakdown but high enough to provide good charge collection and hence good peak shapes (Jaklevic and Giauque, 1993).

It should be noted that in the absence of impurities the band gap contains no allowed energy states. However, the presence of impurities in the semiconductor material makes its operation as a photon detector more complex. Impurities with three valence electrons (such as boron or aluminium, gallium or indium) causes introduction of free hole within the crystalline structure and are hence called acceptor impurities. Similarly, impurities with five valence electrons such as (phosphorous, arsenic or antimony) introduce free electrons and are hence called donor impurities. Materials in which the acceptor impurities predominate are called p-type materials while those with primarily donor impurities are called n-type materials.

The motion of these holes or electrons as a result of applied electric field results in an electric current. The statistical variation in this current results in a noise level above, which the pulses for photon interaction must be observed. To reduce this noise level to an acceptable level, it is necessary to create an intrinsic region within the crystal devoid of free charge carriers. This is done by depositing lithium on the upper surface of the p-type crystal and drifting it through the larger part of

its volume (Derbertin and Helmer, 1988). Lithium, an interstitial donor impurity, will compensate the acceptor impurities and thus create an intrinsic region. The germanium detector prepared this way is called lithium drifted germanium, or Ge(Li) detector. In the case of a planar detector, the excess lithium on the upper surface serves as an electrical contact, and a thin uncompensated layer remains on the opposite side. In such a detector, the lithium will continue to drift at room temperature. Therefore, the detector must be kept cold usually at liquid nitrogen temperature at all times.

Another mode of excitation in semiconductor detector is thermal excitation, which has the effect of producing statistical noise background. This noise can be minimized by operating the detector at cryogenic temperature.

3.4.2 Performance characteristics of semiconductor detector

The performance characteristics of semiconductor spectrometer are determined by a number of parameters. These include energy resolution, spectral background, dead time and countrate capability.

Energy resolution

The ability of a semiconductor spectrometer to resolve characteristic X-ray from a multi-element specimen is determined by its resolution. The resolution of the semiconductor detector is equal to the full width at half maximum (FWHM) of the pulse height distribution measured for a mono-energetic X-ray at a particular energy, such as 5.932 keV Mn-kα line. The FWHM for the detector used in this work is 175keV at 5.9 keV. In determining the FWHM, the intrinsic radiation width

may be neglected for low energy X-rays, but for higher energy characteristic X-rays, the intrinsic width must be considered particularly if precision spectral deconvolution is required. If the intrinsic width of X-ray lines are neglected, the resolution of a semiconductor spectrometer is dependent on the properties of the semiconductor (including production of electron-hole pairs and incomplete charge collection) and the associated electronic pulse processing. Thus the FWHM of an X-ray line ΔE_T can be equated to the sum of the contribution due to the detector processes ΔE_D and the contribution associated to the electronic pulse processing ΔE_E (Jaklevic and Giauque, 1993).

i.e.

$$\Delta E_T = \Delta E_D + \Delta E_E \qquad 3.4$$

The detector contribution to the energy resolution is determined by the statistics of the free charge production and the charge collection processes. The statistics of the free charge production process is inherent to each detector material.

The average energy required to produce electron-hole pair in Ge and Si greatly exceeds the band gap energy, with the extra energy being dissipated in the creation of lattice phonons. The division of the photon energy between the different excitation modes causes a statistical distribution in the number of pairs and thus a statistical spread in the amplitude of the pulses produced. The average number of electron hole pairs is equal to the total energy divided by the mean energy required to produce a single electron-hole pair. If the individual electron-hole pairs were independently created, the fluctuation in the average number of pairs created will be governed by Poisson statistics and the variance would be $N^{1/2}$

However, in practice, the creation of electron-hole pairs are not strictly independent and thus there is departure from Poisson behavior. This departure is taken into account by inclusion of the Fano factor in the expression for the detector contribution to FWHM.

i.e.

$$(\Delta E_T)^2 = (2.35)^2 \varepsilon E F \qquad 3.5$$

Where $\in$ is the average energy required to produce electron-hole pair, E is the energy of the photon and F is the Fano factor which can be determined experimentally for the detector. The factor 2.35 converts the root mean square deviation to FWHM.

The next contribution to the resolution is a characteristic of the detector itself and depends primarily on the loss of charge carriers. The most important process responsible for this incomplete charge collection is charge trapping. Trapping occurs when a charge is trapped in one of the states introduced into the energy gap by impurities or crystal imperfections. It has the effect of causing the complete loss of charge or slowing down the rate of charge collection. The loss of charge is observed as a tailing on the peaks in the photon spectrum (Campbell et al, 1986). Further excitation by increase in the bias voltage is required to release the trapped charge and allow it to be collected. The voltage should however be set to a maximum value the detector can take without risk of voltage breaKD own.

The electronics used in the detector introduces a noise level, which must be reduced or eliminated. This contribution is as a result of random fluctuations in the thermally generated leakage current within the detector and the first stage of the

preamplifier. Although these processes are intrinsic to the overall measurement, they can be reduced by cooling the detector and the preamplifier to cryogenic temperatures using the liquid nitrogen reservoir in contact with cold finger on which the detector and the associated components are mounted.

Detector efficiency

The intrinsic efficiency of a semiconductor detector can be calculated using a model which assumes that the X-ray detection probability is equal to the probability of photoelectric absorption within the sensitive volume of the detector. The model is given by

$$\varepsilon(E) = \exp(-\mu t)(1 - \exp(-\sigma d)) \qquad 3.6$$

Where t is the thickness of the absorptive layer between the sample and the detector, $\mu = \mu(E)$ is the mass absorption coefficient of the absorptive layer, d is the detector thickness and $\sigma = \sigma(E)$ is the photoelectric mass absorption coefficient for the detector material.

According to the above model, the Ge(Li) detector should have higher efficiency than the Si(Li) detector because of its higher atomic number and consequently larger photoelectric cross section. It should be noted that at low X-ray energy, the intrinsic efficiency has a low value for both Si(Li) and Ge(Li) detectors. This is due to the combined absorption of the Be cryostat window and the air path between the sample and the detector. However, the intrinsic detection efficiency is near unity over a wide range of useful X-ray energies for both detectors. This is illustrated in figure 3.3.

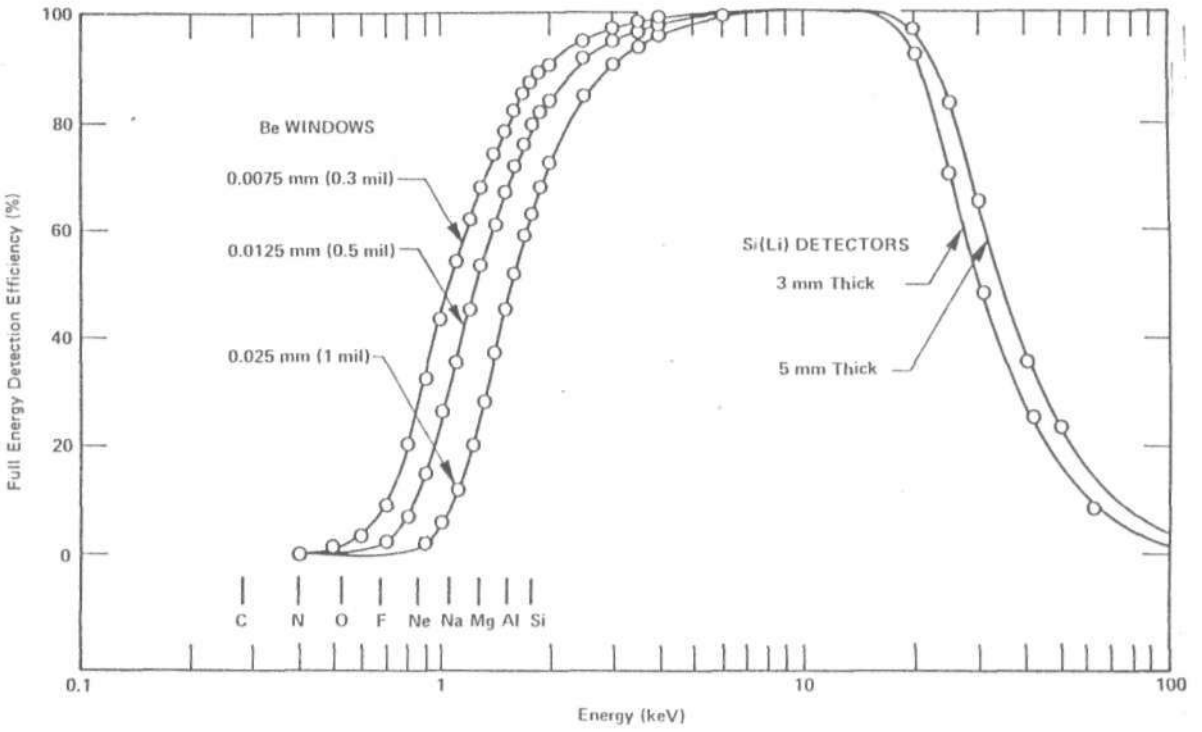


Fig. 3.3: Full Energy Detection Efficiency Versus X-ray Energy for a Si(Li) Detector.

The limitation of the above model is its inability to take into consideration entry window related effects and the presence of absorbing layer on the surfaces of both Si and Ge which reduces the efficiency for low energy photons. Another limitation of the model is the loss of characteristic Ge or Si X-rays from the active volume, which are produced by secondary electrons and the primary photons from the photoelectric absorption events escaping into the active volume of the detector. These escape peaks produce distinct peaks below the full energy peak and has the effect of reducing the amplitude of a given event and thus lower the photopeak efficiency relative to that predicted by the model.

The total detection efficiency E_T can be calculated from the intrinsic efficiency according to the equation:

$$E_T = \frac{\Omega}{4\pi}\varepsilon(E) \qquad 3.7$$

Where Ω is the solid angle of the detector with respect to the sample. It is determined by the area of the detector and the sample-detector distance. Although a higher solid angle may be desired in certain applications, its associated increase in capacitance as a result of increase in detector area results in increase in electronic noise of the system.

It should be noted that for most quantitative applications of EDXRF, it is not necessary to explicitly determine the photoelectric efficiency function since it is included in the overall calibration factor which can be experimentally determined for the particular EDXRF arrangement.

Detector background

The presence of background regions in X-ray spectra have serious consequences on analytical sensitivity and hence represents the limiting factor in establishingstatistical accuracy in trace element analysis. There are two main sources of background in X-ray spectra. The first is the background as a result of deceleration of the electrons when passing through the Coulumbic field of the nucleus. The second type of background is produced when incident photons are scattered from the sample into the detector with very little energy loss. This has the effect of producing composite scatter peaks consisting of both coherent and Compton contributions. The consequence of incomplete charge collection of these events is the presence of continuum background at lower energy in the entire spectra, which will interfere with the lower energy fluorescent X-rays. It has been shown by some authors (Goulding et al, 1972) that scattering background produced as a result of incomplete charge collection from the detector active volume is the dominant contribution to the background in an X-ray spectra. This process is due to non-uniformity in the applied electric field especially at the periphery of the cylindrical detector. The impact of this process on the spectrum can be reduced by preventing the incident radiation from interacting in the periphery of the device. This can be achieved by external or internal collimator arrangement (Jaklevic and Giauque, 1993).

3.4.2 Associated electronics

The associated electronics systems of semiconductor spectrometer is shown in figure 3.2 along with the liquid nitrogen cooled semiconductor detector. The electronic system essentially consists of a detector bias supply, preamplifier,

amplifier, analog to digital converter (ADC), pulse pileup rejector, and a personal computer.

When an X-ray photon interacts with the detector, the electron-hole pairs produced are cleared from the detector diode by the reverse-bias high voltage applied across it. The preamplifier collects these charges on a feedback capacitor to produce an output pulse. The voltage amplitude of this output pulse is proportional to the energy of the original X-ray photon. The initial stage of the preamplifier and feedback elements must be maintained at cryogenic temperature to minimize the electronic noise that was added to the signal during this process.

The weak output signal from the amplifier has a low signal to noise ratio thus requiring the inclusion of the slow pulse shaping amplifier. This amplifier serves the two functions of amplifying the pulse and suppressing extremely low and extremely high frequencies where the signal to noise ratio is poorest in order to obtain improved energy resolution. The consequence of this is that the output pulse from the amplifier is a wide pulse with a slow rise to peak amplitude. Also, this pulse is an analog type but it is proportional to the detected X-ray photon energy.

In order to convert the analog output pulse from the amplifier to digital output pulse, a multi-channel analyzer (MCA) is employed. The MCA performs the analog-to-digital conversion process by measuring the height of each amplifier output pulse and representing this amplitude by an integer. The various pulses arriving at the MCA are processed in this way and a digital histogram of these

events accumulated in the analyzer memory to form the X-ray energy spectrum. Each channel on the MCA represents a particular energy interval. The MCA is normally calibrated in terms of mean energy of each energy interval as x-axis and number of photons counted as y-axis. The MCA is practically installed in form of electronic card in a personal computer where such tasks as specimen presentation, excitation conditions and data accumulation can be controlled. The personal computer is also employed to perform such other functions as spectrum analysis, calibration of the spectrometer, qualitative analysis and quantitative analysis.

In X-ray tube excitation, the available intensity may induce pulse-counting rates that exceed the processing capability of the semiconductor spectrometer. In such situation two events may occur within a time interval less than the shaping time of the amplifier, thereby causing the signals to be indistinguishable and leading to "pileup" of energy pulses. These pileup events can be monitored using fast discriminator. Appropriate logic is then employed to gate the output of the processor to eliminate the resultant ambiguous energy pulses.

In order to correct for pulse pileup rejection, the MCA is equipped with dead time correction circuitry, which uses a live time clock consisting of a gated oscillator and a scaler. The oscillator clock is turned off during pulse processing so that the life time interval is corrected for those periods when the system is incapable of processing a pulse.

3.4.3 X-ray spectrum

The evaluation of X-ray spectrum is complicated by the noise contribution to the spectra. The noise contribution can be classified into amplitude noise and energy noise. The amplitude noise is due to the statistical nature of the counting process in which random events are observed during a finite interval while the energy noise is produced from photon-to-charge conversion and the pulse processing and amplification processes. The effect of these is absence of pure background regions and the broadening of the X-ray peaks. The broadening of X-ray lines places a limit on the energy resolution of the Si(Li) detector spectrometer thus leading to severe overlap of characteristic X-ray lines. Thus, advanced mathematical methods are required for evaluation of the X-ray spectrum. Both linear and non-linear least squares fitting routines have been employed for this purpose. The linear fitting method makes use of library of X-ray spectra for various elements (Arinc et al, 1977) while the non-linear fitting approach involves modeling the X-ray spectra with an analytic function (Nullens et al, 1979).

The latter spectrum evaluation method was used in the development of a software package known as AXIL (Analysis of X-ray Spectra by Iterative Least-squares fitting) that was used for analysis of X-ray spectra from TXRF setup throughout this study.

3.5 Total Reflection X-Ray Fluorescence

3.5.1 Introduction

Total reflection X-ray fluorescence (TXRF) is a variant of energy dispersive XRF which is characterized with a few orders of magnitude better sensitivity than the

conventional XRF. The technique is based on exploitation of two distinct features of total reflection, namely high reflectivity of sample substrate and low penetration depth of primary X-ray beam interacting with the sample at grazing incidence. Thus, in TXRF technique, a highly collimated primary X-ray beam is incident on a smooth plane surface at a glancing angle (of a few mrad) less than or approximately equal to the critical angle at which total reflection of X-rays occurs. The plane smooth surface is either a sample support upon which a few µl volume of sample solution had been deposited (thin film analysis) or is itself the object to be examined for impurities either on the surface or within a small depth of about 100nm in the sample (surface analysis).

The main reasons for the very high sensitivity in thin film analysis is because the intensity of an X-ray beam grazing an interface at a sub-critical angle is drastically reduced inside the reflecting material and thus scattered and fluorescent radiation contributed by the sample carrier is very much reduced. In addition, the excitation of the sample is increased because of the small incident angle and because of the elongated path of the beam through the sample due to reflection. These features of TXRF results in very low background levels in the fluorescence spectra thus making possible determination of picogram amount in samples of favourable matrices. In the case of surface analysis, the total reflection arrangement allows high selectivity with respect to the atoms in the near surface layers, thus resulting in low penetration of primary X-ray beam.

3.5.2 Physics of TXRF

At the interface between two different media, reflection and refraction of X-rays occur. The refractive index for X-rays is a complex quantity in which the real part describes the dispersion of X-rays while the imaginary component represents the absorption within the material of the reflector. The refractive index n is given by

$$n = 1 - \delta - i\beta \qquad 3.8$$

Where:

$$\delta = \frac{n_e e^2 \lambda^2}{2\pi mc^2} \qquad 3.9$$

$$\beta = \frac{\mu^* \lambda}{4\pi} \qquad 3.10$$

$$n_e = \frac{\rho N_A Z}{A} \qquad 3.11$$

μ^*= linear absorption coefficient

λ = wavelength of the radiation.

n_e = electron density

e = electronic charge

c = velocity of light

N_A = Avogadro's number

Z = atomic number

A = atomic weight

The total reflection of X-rays is based on the fact that the real part of the refractive index n is less than unity, with $\delta \approx 10^{-5} - 10^{-6}$ in the X-ray energy range. The requirement for total reflection to take place is that the incident angle of X-rays must be smaller than the critical angle for the total reflection φ_C, which is defined

from Snell's law as

$$\cos\Phi_c = 1-\delta \qquad 3.12$$

Where φ_C is the angle of incidence for which the angle inside the reflector is approximately equal to zero. Expansion of cosine in equation yields

$$\Phi_c = (2\delta)^{\frac{1}{2}} = \frac{99.1}{E\left(\frac{Z\rho}{A}\right)^{\frac{1}{2}}} \text{ min } utes\ of\ arc \qquad 3.13$$

in terms of experimental viewpoint φ_C gives an estimate of the range of angles for which total reflection can be observed. For example φ_C for quartz reflector and for the X-rays of energy 17.4 keV is approximately 1.8 mrad.

3.5.3 Basic experimental arrangement

In order to obtain optimum detection limit, the design consideration of TXRF setup should take into account both the minimization of background levels via total reflection and the maximization of analyte signal intensity. This can be achieved by ensuring that solid angle losses are minimized by ensuring close distances between the anode of the X-ray tube and the sample position and by ensuring proper focussing of X-ray beam.

In general, the basic experimental arrangement for TXRF analysis of deposit of materials removed from filter on quartz sample carrier is shown in figure 3.4. It consists especially of the following components;

(i) X-ray tube with Mo-anode and fine focus;

(ii) A collimator for narrowing the X-ray so that a fine beam is obtained;

(iii) A goniometer for adjustment of the incident angle of X-rays

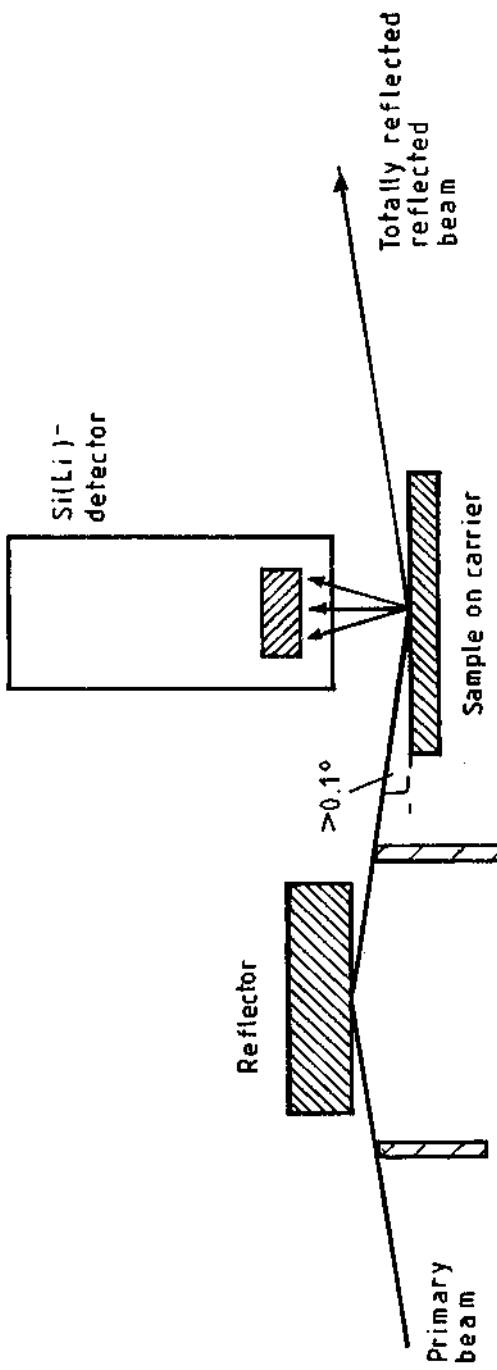


Fig. 3.4: Basic Instrumental Arrangement for TXRF Set Up.

(iv) A Si (Li) detector based spectrometer as explained in section 3.4

(v) A cut-off reflector or multi-layer monochromator;

The slits of the collimator is about 10cm away from the anode focus and about 0.05mm wide in order to collimate the beam with a divergence less than 0.5mrad. A narrow primary beam emerging from a narrow aperture is reflected at a mirror or Bragg reflector and is consequently either filtered or monochromatized. The beam of X-rays finally hits the Quartz sample carrier under grazing incidence and consequently undergo total reflection. The sample placed on the carrier is passed through and is excited to fluorescence. The function of the cut-off reflector (made from Duran glass) is to suppress the high energy part of the beam which when scattered by the sample and detected by the Si(Li) detector will produce low energy background due to Compton scattering in the Si crystal. The cut-off reflector is mounted on a goniometer, which makes possible the adjustment of proper incident angle for total reflection of the beam.

A highly polished quartz disc 30mm diameter and 3mm thickness was used as substrates. The sample itself consists of tiny drop of PM10 particulate matter dried under infra-redlamp. The source – sample distance was limited to 0.5cm in order to allow for effective excitation of the sample.

A Canberra Si(Li) detector based X-ray spectrometer was used for spectral data acqusition and storage. It was arranged parallel to the sample plane at a distance of 0.5cm in air. The radiation is indicated as MCA based Si(Li) detector Energy dispersive spectrum. Spectral data reduction was accomplished by means of the AXIL software package already described.

CHAPTER 4

METHODOLOGY OF PM10 SAMPLING AND LABORATORY ANALYSIS

This chapter deals with the methodological aspects of sampling and elemental analysis of inhalable particulate matter from the Quarry Industry. The sampling procedure adopted limits the sample collection to PM10 particulate matter because of their lung deposition characteristics and long-range transport to other locations far from the source.

However, the sampling procedure provides small sample loading on the filter and hence analysis of such samples require a sensitive analytical technique capable of analyzing major, minor and trace constituents of the PM10 particulate matter. Total reflection X-ray fluorescence analysis was exclusively used for analysis of all the samples collected after developing appropriate analytical procedures for analysis of the samples as explained in detail in the later part of this chapter.

4.1 Methodology of PM10 Sampling

Sampling of particulate matter is a very important and initial step in air pollution assessment. The sampling process is performed by pumping a representative volume of air through a filter in order to collect the particles present. An inlet is an important part of the sampling equipment, which allows all particles of interest to arrive at the collection zone while excluding unwanted particles. It is essential that the theory and limitations of various combinations of sampling devices and analytical procedures be properly understood in order to obtain meaningful results.

Adequate considerations must be given to the various aspects such as leakage of the pump, inlet size, flow rate etc. These are necessary because the final results and its interpretation depend on the accuracy of the sampling procedure.

Sampling conditions (such as sampling time, sampler location etc) depends on the method used in crushing of rock deposits to reduce them into smaller size aggregates. Since the operation of the Quarry Industry ranges from the simple manual quarrying using big hammer for crushing of the rocks to more complex fully mechanized quarrying with multiple crushers each driven by electric motor, the amount of dust generated by the various quarry operations will exhibit large variation. Thus for the purpose of sample collection for pollutant transport studies and assessment of occupational exposure, the quarry operation was classified into manual quarrying and mechanized quarrying. Mechanized quarries are further grouped into Drilling Machine, MECH1, MECH2 and MECH3 involving the use of single crusher, double crusher and multiple crushers respectively. For each of these quarry operations, appropriate sampling time was chosen in such a way that there is no filter overloading which may lead to clogging of filters.

It is worth mentioning that this investigation does not include dust from "Blasting" using explosives. The reason is that this aspect of quarrying is mostly carried out at night and also there is restriction of movements around the location where blasting is to take place in order to avoid accidents. Furthermore, dust emission from blasting is somewhat instantaneous, thus rendering the interpretation of sampling data almost impossible.

Various aspects of aerosol sampling will be discussed in the following subsections. These include sampling equipment, sampling criteria, and sampling programme. These will be followed by discussion of the results obtained.

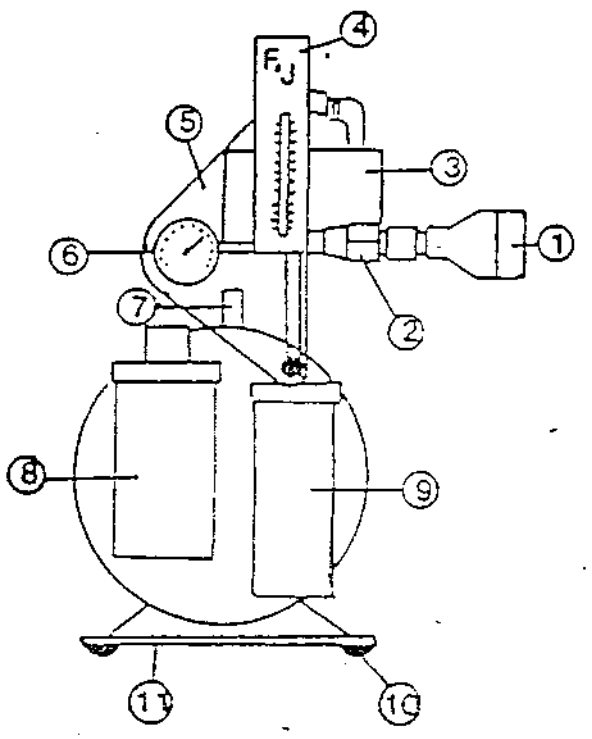
4.1.1 Sampling equipment

The available sampling equipment is a low volume air sampler (FJ specialty products Inc., Florida, U.S.A.). This type of sampler has a disadvantage that its open-faced combination filter holder collects the various particle size groups of the particulate matter without size discrimination. Thus there is possibility that unwanted particles such as wind blown dusts, re-suspended dusts etc which usually consists of very large particles may be collected, thus invalidating the sampling data. Thus important modifications to the original sampling equipment were found necessary for particulate sampling in order to realize the project objectives. A brief description of the sampling equipment and the applied modifications will be presented in the following section.

General description of low volume air sampler

The low volume aerosol sampler is schematically presented in figure 4.1. Its major components include an oil-less vacuum pump, plastic combination filter holder, air flow regulator and flowmeter (or rotameter). The carbon vane vacuum pump consists of permanently lubricated ball bearings and thus the internal workings require minimal maintenance.

The plastic combination filter holder accommodates 47mm diameter particulate filter paper for sample collection. The dual O-rings on the filter holder ensures that



1. Combination Filter Holder
2. 3/8" Quick Disconnect Fitting
3. Constant Air Flow Regulator
4. Flowmeter
5. Face Plate
6. Vacuum Gauge
7. Handle
8. Muffler Jar
9. Intake Filter Assembly Jar
10. Non-Skid Rubber Feet
11. Base Plate

Fig. 4.1: Schematic Diagram of a Low Volume Air Sampler.

the airflow path is through the filter and not around it. The filter holder is also provided with quick disconnect coupling which enables its easy connection and disengagement from the pump chassis.

The constant air flow regulator is used to regulate air flow during long periods of operation. This is achieved by holding a constant pressure drop across an on-line orifice by varying a bye-pass valve into the pump. The orifice itself is adjustable so that flow-rate values up to 100litres/min can be obtained. The flow-rate can thus be increased by rotating a knob at the bottom of the regulator in anti-clockwise direction or reduced by rotating the knob in clockwise direction.

The total volume of air to be sampled is obtained with the aid of rotameter consisting of a tube with a float in it. When the pump is in operation the air flow traverses the tube from the bottom to the top. Therefore, the balance of the drag force of the air flow at a given pressure drop against the force of gravity gives a measure of the flow rate (Urone and Ross, 1979). The rotameter is always positioned vertically. It is calibrated based on the pressure drop and the flow characteristics. The result of such calibration exercise using NBS dry gas meter is presented in Table 4.1.

Modification of low volume air sampler to stacked filter unit aerosol sampler

In order to use the low volume air sampler to collect fractionated PM10 particulate matter, two major modifications were applied. The first is the incorporation of PM10 aerosol inlet, which restricts the size of particles entering the sampler to diameters of less than or equal to 10μm AED. The other modification is the

Table 4.1: Calibration of Low Volume Aerosol Sampler

Rotameter Flow rate (L/min)	Atmos. Pressure (mmHg)	Inlet Temp (^{0}F)	Correction for Temp and Pressure	Calculated flow rate (litres/min)	Corrected NBS Flow rate (litres/min)	Deviation
100.86	30.01	70	0.98	98.86	102.86	4.9%
80.86	30.01	70	0.98	79.14	81.43	2.8%
60.57	30.01	70	0.99	60.00	60.00	0.0%
40.29	30.01	70	0.99	40.29	41.43	4.5%

replacement of the combination filter holder with stacked filter cassette holder. These modifications are discussed in detail in the following section.

(a) PM10 Aerosol Inlet

(i) Impactor Theory

The PM10 aerosol inlet is a device used to exclude particles with diameter greater than 10μm AED. It operates by the principle of impaction on a plate. The air to be sampled is directed through a narrow opening onto a plate causing the streamlines to deflect abruptly through 90^0 as shown in figure 4.2. The particles in air are under the influence of the viscous force, which is proportional to the particle diameter. They are also affected by the inertia, which is proportional to the particle volume. Therefore, by appropriately adjusting the flow-rate, the inlet size and the distance between the impaction plate and the lower end of the inlet, particles above certain effective diameter will be deposited on the plate by impaction. The smaller particles however continue their motion along with the air stream. In this way, unwanted particles are excluded.

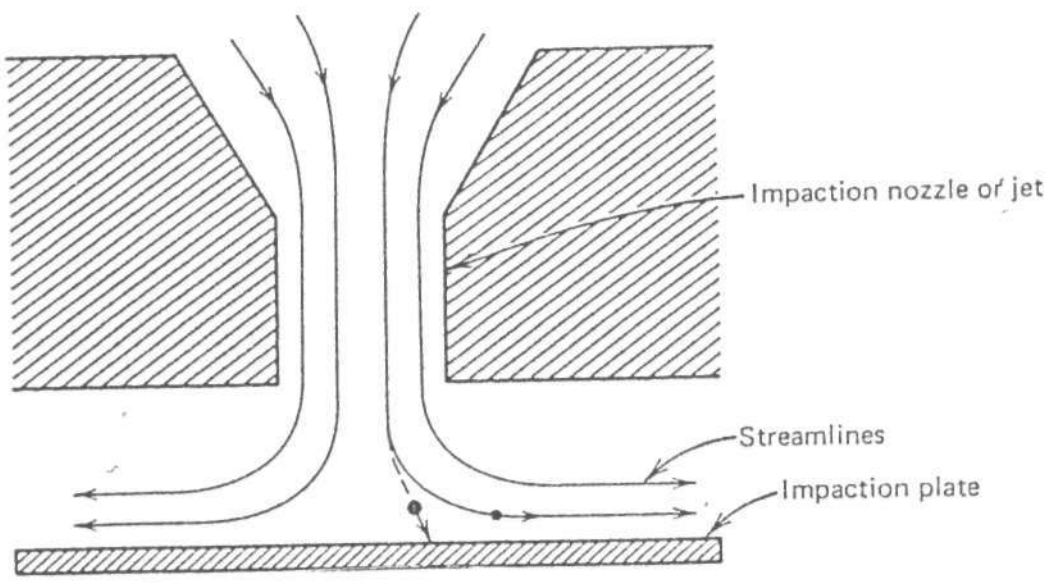


Fig. 4.2: Schematic Representation of Impaction Phenomenon.

The PM10 impactor is characterized by the collection efficiency versus particle size curve shown in Figure 4.3 (Hinds, 1982). The parameter that governs the collection efficiency is the Stokes Number or impaction parameter defined as the ratio of the particle stopping distance at the average jet exit velocity U to the jet radius $D_j / 2$.

Since

$$\tau = mB = \frac{\rho_p d_p^2 C_c}{18\eta} \qquad 4.13$$

$$Stk = \frac{2\tau U}{D_j} = \frac{\rho_p d_p^2 U C_c}{9\eta D_j} \qquad 4.14$$

Where m = particle mass, B = Particle mobility, ρ_p = particle density, η = viscosity, d_p = particle size and C_c = slip correction.

In general, the collection efficiency curve for an impactor is plotted as efficiency versus the square root of Stokes number $\sqrt{Stk}$, which is directly proportional to the particle size. The theoretical determination of the characteristic efficiency curve for an impactor is rather complex and thus requires the use of a computer model. The above equation (called Navier-stokes equation) is first solved for the particular impactor geometry and particle trajectories is then determined for each entering streamline for a given particle size. The fraction of particle trajectories that intercept the impaction plate is equivalent to the efficiency (Hinds, 1982). The process is repeated for many particle sizes to obtain the characteristic efficiency curve in figure 4.3. A single number Stk_{50}, the Stokes number that gives 50% collection efficiency, characterizes ideal impactors (i.e. impactors with sharp cut-off). The mass of particles larger than the cut-off size that pass through such

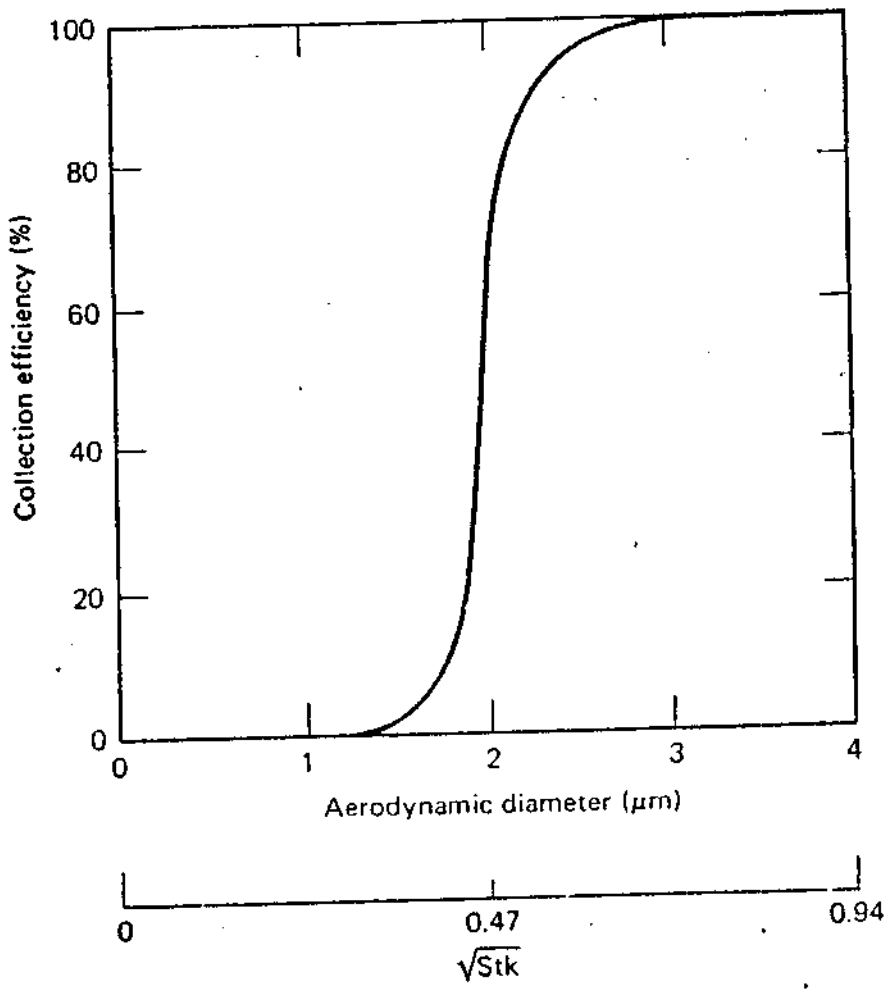


Fig. 4.3: Typical Impactor Efficiency Curve.

impactor can be assumed to be equal to the mass of particles below the cut-off size that are collected on the plate.

Equation 4.1 can be rearranged to give the particle diameter having 50% collection efficiency, d_{50} in terms of Stk_{50};

$$d_{50}\sqrt{C_c} = \left[\frac{9\eta D_j \, Stk_{50}}{\rho_p U}\right]^{\frac{1}{2}} \qquad 4.15$$

This equation is easily solved if slip correction is neglected. The equation shows that a sub-micrometer cut-off diameter requires a small diameter nozzle operating at high velocity.

(ii) Impactor Design Parameters

Based on the above theoretical considerations, the impaction parameters were determined for PM10 pre-impaction stage (Maenhaut et al, 1995). These parameters are presented in Table 4.2 and were used in construction of PM10 aerosol inlet. Figure 4.4 shows the schematic diagram of the PM10 aerosol inlet, which was constructed locally.

Table 4.2: Impactor Design Parameters

Jet Inlet Diameter	30mm
Jet Exit Diameter	10mm
Dist. Bet. Exit diameter and Plate	10mm
Diameter of Impaction plate	10mm
Air Flow rate	15litre/min
Face velocity	35.41cm/s

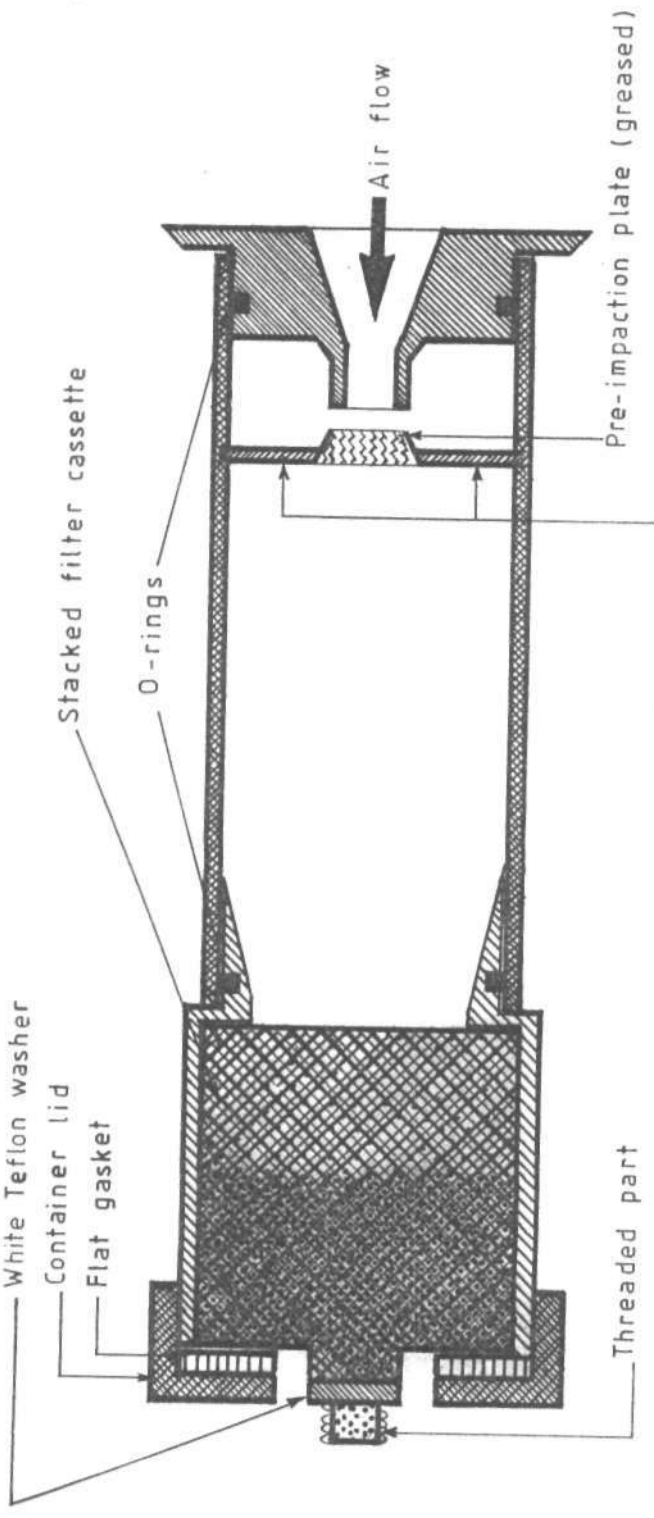


Fig. 4.4: PM10 Aerosol Inlet Consisting of Polyethylene Container and the Stacked Filter Cassette.

When air is drawn into the inlet at a flow rate of 15litres/min, it provides a cutoff for particles greater than 10µm. Thus only particles less than or equal to 10µm AED follow the air stream and are subsequently sampled. To prevent errors due to particle "bounce off ", the impaction plate is regularly coated with grease.

(b) Stacked Filter Cassette

The second modification to the low volume air sampler is the substitution of the combination filter holder with stacked filter cassette. The stacked filter cassette consists of two filter holders arranged in series. Each of the filter holders has a dual O-rings which ensures that the air pass directly through the filter and not around it. The first filter holder accommodates 8µm pore-size "Nuclepore" membrane filter while the second filter holder accommodates 0.4µm pore size "Nuclepore" membrane filter. At a flow-rate of 15 litres/min, the 8µm pore-size (coarse) filter provides cut–off point of 2µm for PM10 particulate matter. Thus, only PM10 particles with aerodynamic equivalent diameter of 2-10µm are collected on the surface of this filter while the second (fine) filter collects particles less than or equal to 2µm AED directly on its surface. The "Nuclepore" membrane filters are preferred because of their uniform pore-size distribution, surface deposition properties, low blank weight, and low hygroscopicity (Spurny et al, 1969). These characteristics make them suitable for both gravimetric analysis and elemental analysis by X-ray fluorescence.

4.1.2 Evaluation of stacked filter unit aerosol sampler

PM10 aerosol inlets utilizing the above design parameters and the complete Stacked Filter Unit sampling system have been subjected to series of evaluation

studies (Maenhaut et al, 1995). One of such studies was performed by P. K. Hopke at the Clarkson university in postdam, New York State. The impaction plate of the PM10 inlet was covered with a 0.4μm pore size Nuclepore filter and also greased piece of the same filter was placed at the coarse position in the SFU cassette. A number of ambient aerosols were collected at the Clarkson University in postdam, New York State. The particles on the greased Nuclepore filter (Impaction Plate) and on fine filter were examined with an optical microscope. Aerodynamic equivalent diameter was calculated for each individual particle, and the number of particles per μm EAD size interval on both the greased and the fine Nuclepore filter was counted. On the basis of these data and after correcting for wall loses, a 50% cut point of 10.5 to 11μm EAD was derived.

The stacked filter unit has also been evaluated both through studies of the collection efficiency of each filter using monodisperse aerosols and through field studies using ambient and quasi-ambient aerosols (Cahill et al, 1977). Figure 4.5 illustrates both the particulate capture efficiency of the upper respiratory tract versus particle diameter (ICRP, 1966) and that of 8μm and 0.4μm nuclepore membrane filters (Cahill et al, 1977). The closed symbols are derived from data on particulate capture using monodisperse aerosols directly as in the case of 0.4μm filter. In the case of 8μm filter, the data were obtained by extrapolation to lower flow rates. The SFU thus provides a simple way to approximate lung behaviour.

4.1.3 Criteria for accurate sampling

Sampling errors arise because some particles fail to enter the inlet with the air. The ratio of the number of particles entering the inlet to the number in the original

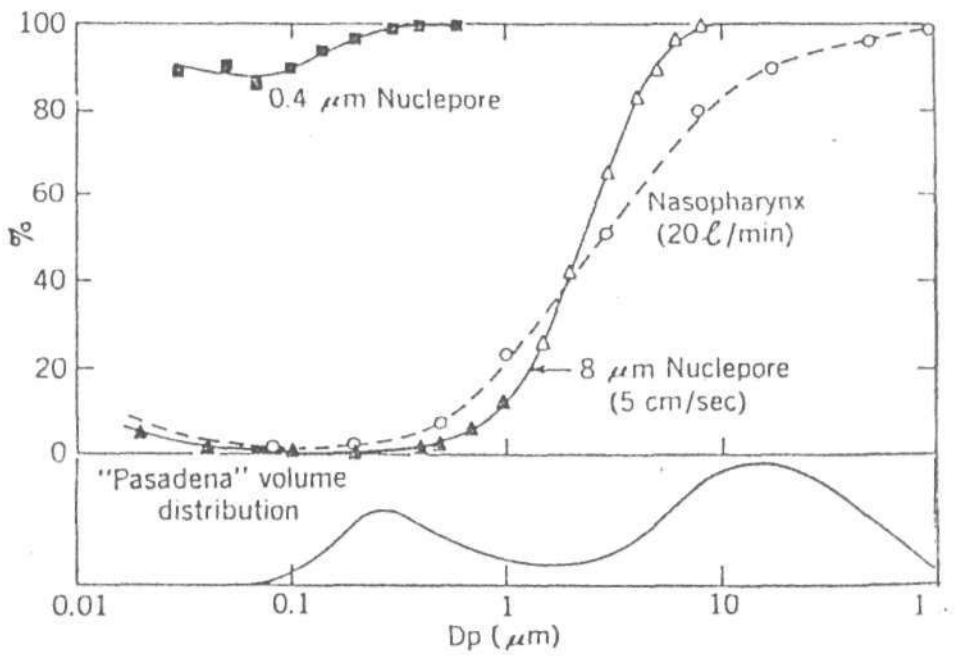


Fig. 4.5: Aerosol Collection Efficiency Curves for the Naso-Pharynx and Nuclepore Filters Of 8 and 0.4μm Pore-Size Arranged in Series (Cahill, 1977).

air volume, defined as the intake sampling efficiency, is thus affected. The sampling of particles in still air is susceptible to two sources of error. These include the inertia of the particles, which prevent them from following the motion of the air in which they are suspended and also the additional downward pull due to gravity. As a result, it is most important to test whether the sampling equipment conforms to established criteria for accurate sampling.

Theoretical basis of criteria for accurate sampling

Davies (1968) established the criteria necessary to ensure negligible sampling errors from the two sources of errors mentioned above. These criteria are based on the ratio of the stop-distance to the inlet diameter. Davies pointed out that when the filter face velocity U is much greater than the terminal settling velocity V_T:

$$\frac{V_T}{U} << 1 \qquad 4.1$$

provided the inertia of the particles and orientation of the sampling head are neglected. He specifically suggested a value of 0.04 for this ratio to ensure a ±4% error due to the settling motion of the particles in the worst cases. This criterion can be expressed in terms of the sampling flow rate Q, inlet diameter D_I and relaxation time τ .

Since

$$Q = \frac{U \times \pi D_I^2}{4} \qquad 4.2$$

473301

And

$$V_T = \tau g \qquad 4.3$$

According to Davies Criteria for which relative settling speed is less than 0.04

$$D_I = \frac{2}{5}\left[\frac{Q}{\pi \tau g}\right]^{\frac{1}{2}} \qquad 4.4$$

As mentioned above, the inertia of the particles can also introduce error during sampling. A particle velocity increases as it approaches the inlet along a curved streamline. If the particle has enough inertia, its stop-distance will become relatively large compared to the size of the inlet and thus may be thrown away from the inlet and not collected. This is more significant for larger particles and higher face velocity of the inlet.

Davies criterion for this bias is given by

$$D_I >> \left[\frac{Q\tau}{4\pi}\right]^{\frac{1}{3}} \qquad 4.5$$

He also suggested a factor of 10 for sampling losses to be less than 1.6%

$$D_I >> 10\left[\frac{Q\tau}{4\pi}\right]^{\frac{1}{3}} \qquad 4.6$$

Recall that the Stoke's number S_{tk} is given by

$$Stk = \frac{2\tau U}{D_I} \qquad 4.7$$

And from Equation (4.2)

$$Q = \frac{U \times \pi D_I^2}{4} \qquad 4.8$$

Thus, S_{tk} becomes

$$Stk = \frac{8\tau Q}{\pi D_I^{\,3}} \qquad 4.9$$

Combining this with the inertia criterion given above (equation 4.6), Davies inertia criterion can be written as

$$Stk \leq 0.32 \qquad 4.10$$

Davies criteria defines a sampling condition that ensures unbiased sampling, but they are somewhat over restrictive as they require high flow rates and large inlets which are unsuitable for sampling in still air and at workplace.

Agarwal and Liu (1980) however presented a relatively simple criterion, which is independent of the inlet velocity and flow rates and furthermore remove practical restrictions on still air sampling of PM10 particulate matter. They used a mathematical simulation of the flow field around a sampling inlet to calculate the particle trajectories. The intake efficiency of the inlet is then determined from the calculated particle trajectories. This criterion, which is supported by experimental verification with American sampler types leads to the following conclusion:

(i) The intake velocity is generally affected by Stokes number *Stk* and the ratio V_T/U.

(ii) Accurate sampling, defined as an entry efficiency greater than 90% in calm air is obtained when the product of the Stokes number and the relative settling velocity of the particle is smaller than 0.1.

$$Stk\left(\frac{V_T}{U}\right) \leq 0.1 \qquad 4.11$$

Combining with equations (4.3) and (4.7), Agarwal and Liu Criterion can be expressed in terms of inlet diameter and particle relaxation time as:

$$D_i \geq 20\tau^2 g \qquad 4.12$$

This criterion thus shows greater flexibility in the choice of aerosol inlet and applies to efficient entry of particles into the sampling inlet. It should however be noted that filtration property of the filter medium plays the most important role in obtaining high sampling efficiency.

Application of sampling criteria to SFU

The above criteria of Davies on one hand and that of Agarwal and Liu on the other hand, were applied to the presently used stacked filter unit aerosol sampler. Table 4.3 and 4.4 summarize the most relevant parameters used in calculating the sampling efficiency in both cases. Figure 4.6 shows the criteria for accurate sampling according to Davies criteria and that of Agarwal and Liu. The region below 90% efficiency line represents all possible conditions that will result in accurate sampling according to the criteria of Agarwal and Liu. It is readily observed that in calm air condition, the SFU will attain accurate sampling of particles even up to 100μm AED. The SFU also meets the Davies criteria as the criteria are satisfied for particles up to approximately 20μm AED.

Table 4.3: Characteristics of Stacked Filter Unit Aerosol Sampler

Average flow rate	15 litres/min (0.9 m^3/hr)
Filter medium	membrane filter (0.4 & 8μm pore size)
Inlet diameter	4.0cm
Filter diameter	4.7cm
Exposed filter diameter	4.05cm
Effective inlet area	7.07cm^2
Face velocity	35.41cm/s

4.1.4 Sampling programme

Installation of SFU sampling line

The Stacked filter unit aerosol sampling line consists of the following components:

(i) A cylindrical shaped polyethylene housing for PM10 pre-impaction stage and stacked filter cassette which accommodates 8μm pore-size and 0.4μm pore-size "Nuclepore" Membrane filters respectively;

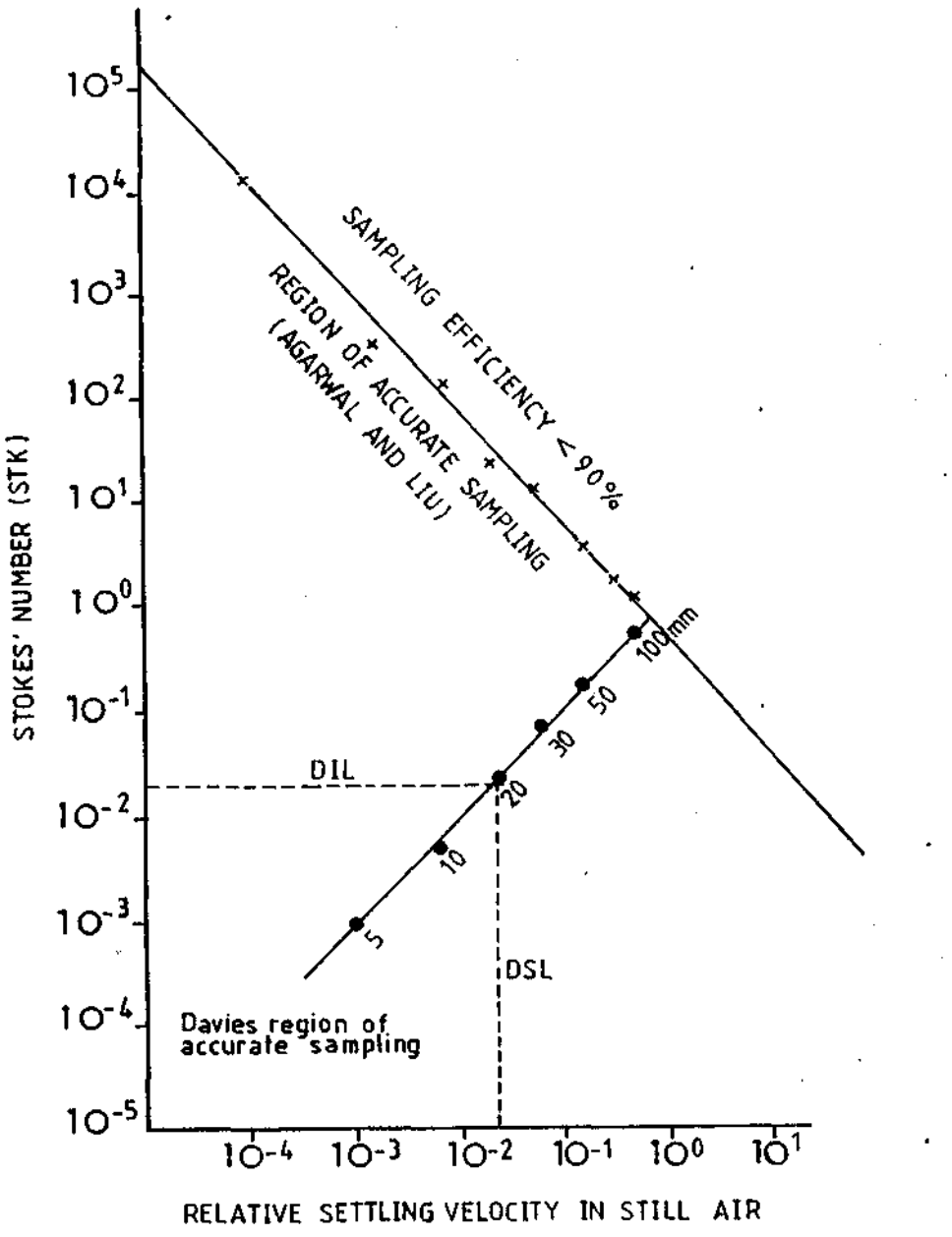


Fig. 4.6: Criteria for Accurate Sampling in Calm Air as Applied to SFU.

Table 4.4: Aerodynamic Characteristics of Aerosol Particles

Aerodynamic diameter (μm)	Relaxation Time (τ) (s)	Settling velocity(V_T) Cm/s	Relative settling velocity (V_T')	Stoke's Number (S_{tk})	$S_{tk} \times V_T'$
1	4.57×10^{-6}	4.50×10^{-3}	9.88×10^{-5}	8.43×10^{-5}	8.33×10^{-9}
5	7.91×10^{-5}	7.76×10^{-2}	2.19×10^{-3}	1.86×10^{-3}	4.07×10^{-6}
10	4.11×10^{-4}	4.05×10^{-1}	8.61×10^{-3}	7.34×10^{-3}	6.32×10^{-5}
20	1.23×10^{-3}	12.1×10^{-1}	4.42×10^{-2}	2.90×10^{-2}	9.92×10^{-4}
30	2.77×10^{-3}	27.2×10^{-1}	7.68×10^{-2}	6.54×10^{-2}	5.02×10^{-3}
50	7.68×10^{-3}	75.3×10^{-1}	2.1×10^{-1}	1.81×10^{-1}	1.88×10^{-2}
80	1.96×10^{-2}	171×10^{-1}	4.8×10^{-1}	4.63×10^{-1}	6.7×10^{-1}
100	4.06×10^{-2}	248×10^{-1}	7.0×10^{-1}	7.22×10^{-1}	15.2×10^{-1}

(ii) A short transparent tubing with SWAGELOCK nylon Connector at one end and another SWAGELOCK connection at the other end for connecting the stacked filter cassette to the POLY-FLO tubing;

(iii) A POLY-FLO tubing (1/4" inner diameter) with SWAGELOCK brass connector mounted at each end for connecting the pump set-up to the transparent tubing;

(iv) Constant air flow regulator;

(v) vacuum gauge;

(vi) low volume vacuum pump

(vii) flow-meter (rotameter);

(viii) A programmable timer (and stop watch);

(ix) A wooden pole for mounting the polyethylene cylinder.

It should be noted that the constant air flow regulator, the vacuum gauge, the vacuum pump, the timer and the flow-meter are assembled in the pump set-up. In

addition, the polyethylene cylinder containing the PM10 pre-impaction stage and the stacked filter cassette form a complete Stacked Filter Unit. The schematic representation of the stacked filter unit sampling line (Maenhaut et al, 1995) is shown in figure 4.7.

The SFU sampling line should normally be installed on an open area far away from structures such as buildings, walls, large vegetation etc. This sampling campaign particularly took cognizance of this as it has an added advantage in the application of Gaussian model (for dispersion studies) that was used in studying transport of pollutants into the environment. The SFU sampling line was assembled as shown in Figure 4.7. The SFU was mounted on a wooden pole with the polyethylene container placed vertically downwards at a distance of 1.6m above the ground level. It should be noted that if the SFU is positioned upwards there is possibility of deposition of rain or dust fall directly on the filter. In addition, horizontal positioning of the inlet may cause variation in the collection of particles due to variable wind speed and direction. To prevent contamination from the pump, which may lead to erroneous measured concentration of elements, the exhaust of the pump was positioned far away from the sampling site and downwind from it using long POLY FLO tubing.

Furthermore, Initial inspection of the SFU was carried out to ensure that all connections are leak free before sample collection. This was done by checking properly whether the SFU sampling line including the short transparent tubing gives appropriate flow-rate when the air flow regulator is turned completely counterclockwise without the SFU. It was also checked whether it remains airtight

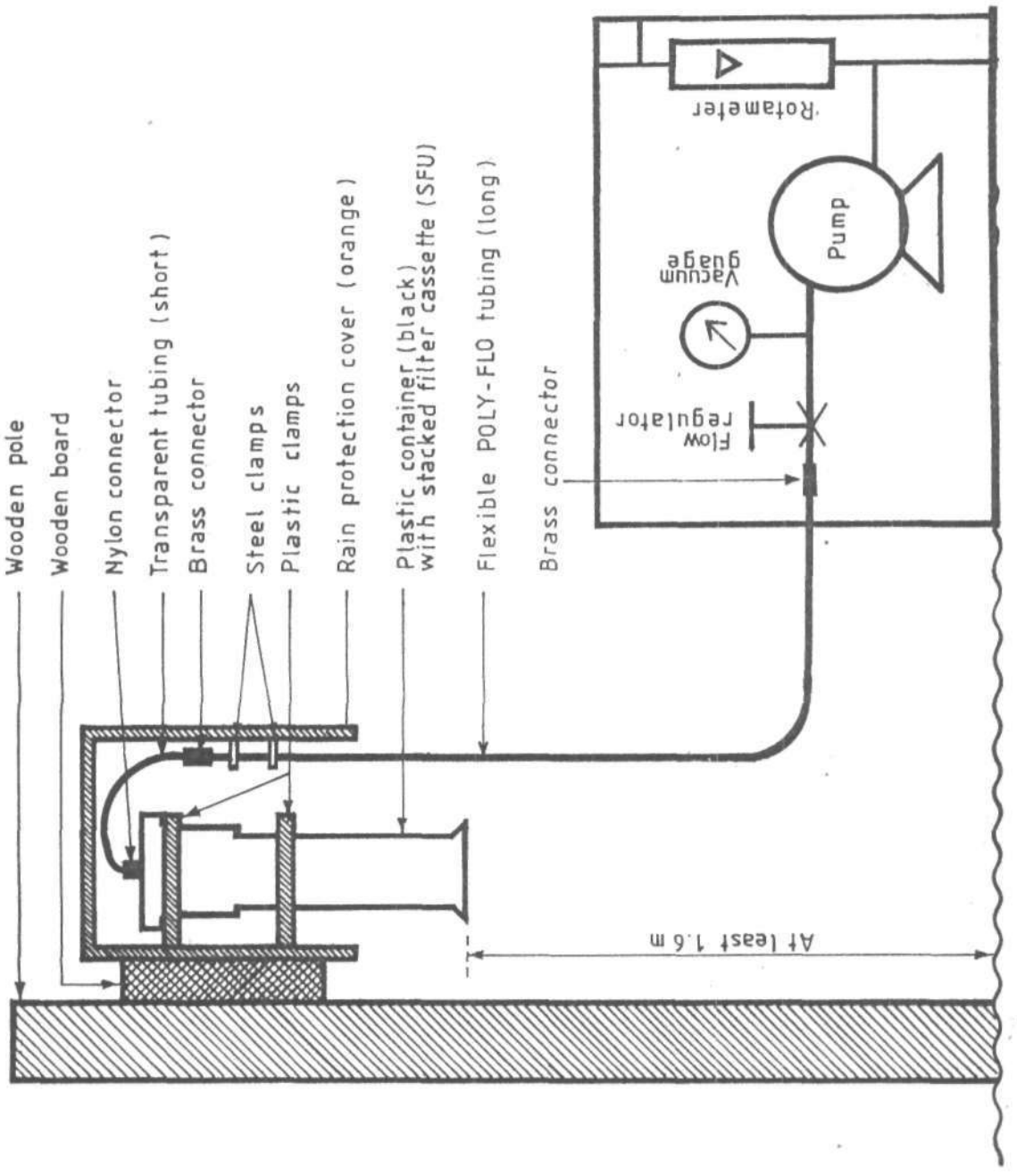


Fig 4.7: Schematic Representation of SFU Sampling Line.

when the transparent tubing is completely closed, i.e. the rotameter should be zero.

The loading of the stacked filter cassette was separately carried out in the laboratory ensuring that the shining side of the filter faces the air intake. After sample collection, the filter is placed in a specially designed polyethylene container (petri dish) to avoid contamination during transportation to the laboratory. Prior to loading of the stacked filter cassette, both the coarse and fine filters were weighed in the laboratory using sensitive balance. To avoid contamination from direct contact with the filter, handling of the filters was performed with stainless steel tweezers.

Additional precaution taken to monitor filter contamination during transportation from the field was collection of blank samples in which a blank filter was placed inside the sampling device without sucking air through it.

Throughout the sampling campaign, the rotameter was set at a flow-rate of 15litres/min. With the timer switch appropriately set, (and the stopwatch started), the sampling of particulate matter was conducted for specific time period depending on the dust loading. It should be noted that the rotameter was continually checked and the air flow regulator appropriately adjusted to ensure that the flow-rate remains constant throughout the sampling period. All observations for each sample were properly recorded in a logbook. The information recorded include

(i) Sample label;

(ii) Sampling date;

(iii) Time at the beginning of sampling and at the end of sampling;

(iv) Rotameter flow-rate at the beginning and end of sampling;

(v) Distance between the pollution source and the sampler

(vi) Unusual events such as plant breaKD own, power cut etc.

It is worth mentioning that this sampling programme did not make use of isokinetic sampling which is rather difficult to realize. This is because this method of sampling is only significant for large particles and atmospheric deposition studies. It is not very relevant for collection of PM10 particulate matter.

Sampling locations and sampling strategy

Table 4.5 and 4.6 show the various sampling dates, sampling locations and sampling conditions for the period 6th Feb, 1996 to 26th Oct, 1996. It should be noted the Quarries investigated in Zaria are located along a major road while those monitored at the Federal Capital Territory are located within a village.

Two major types of sample were collected. These include workplace PM10 particulate matter and ambient PM10 particulate matter. It should be noted that workers involved in operation of MECH1 quarry are directly exposed to immense dust pollution. This is because these workers are involved in loading of the crusher and evacuation of the crushed rocks deposited inside the wheelbarrows placed beneath the crushers. Workers involved in operation of the more mechanized Quarries such as MECH2 and MECH3 are exposed to less dust pollution as they are not directly involved in loading of the crushers and evacuation of the crushed rocks. In addition, these workers are always located at positions upwind from the

source. Similarly, emission from the drilling operation is always in opposite direction to the location of the drilling machine and its operator and so the operator is exposed to minimal dust pollution. On the other hand, Workers involved in manual Quarrying and in packing and loading of the crushed rocks, are directly exposed to dust pollution. Thus, there is need to carry out occupational exposure assessment using personal respirable sampler. However, previous studies in an iron foundry (Zhang, 1983) had shown that there is good agreement between personal air sampler and stationary air sampler for measurement of PM10 particulate matter. Further, the collection efficiency curve for SFU is similar to that of human upper respiratory tract as explained in section 4.1.2.2 and thus the SFU is suitable for occupational exposure studies.

The collection of ambient PM10 particulate matter was limited to drilling, MECH1, MECH2, and MECH3 Quarry operations. In each case, the sampler was placed at a fixed distance from the source depending the dust loading in the environment.

Results and discussion

The measurement of inhalable particulate matter in the present study was performed with the Stacked Filter Unit (SFU) aerosol sampler. The dust laden air at the various Quarry industries was sucked through a PM10 pre-impaction stage which provide a cut-off point of 10μm AED for the air-stream incident on the SFU. With the flow-rate set at 15litres/min, the stacked filter assembly further fractionates the particulate matter into coarse and fine components. The exposed filter area for the coarse and fine filter is 14.88cm^2. Sampling time varies depending on the dust loading at the various Quarry operations in order to avoid

Table 4.5: Sampling Data for PM10 Particulate Matter (Coarse Fraction)

SAMPLE LABEL	SAMPLING LOCATION	SAMPLING DATE	SAMPLING TIME Mins	AIR VOL. m^3	NET PM10 MASS µg	PM10 CONC $\mu g/m^3$
QC01	KD Rd Zaria	6/2/96	540	8.1	1900	234.57
QC02	KD Rd Zaria	7/2/96	360	5.4	1300	240.74
QC03	KD Rd Zaria	8/2/96	540	8.1	1900	234.57
QC04	KD Rd Zaria	10/2/96	540	8.1	1800	222.22
QC05	KD Rd Zaria	12/2/96	360	5.4	1400	259.26
QC06	Zaria BG Site	14/2/96-16/2/96	1440	21.6	1100	50.93
QC07	KD Rd Zaria	17/2/96&19/2/96	1200	18.0	1000	55.56
QC08	KD Rd Zaria	20/2/96-21/2/96	1200	18.0	1200	66.67
QC09	KD Rd Zaria	22/2/96-23/2/96	1200	18.0	1100	61.11
QC10	Zaria BG Site	24/2/96-26/2/96	1440	21.6	1000	46.30
QC11	KD Rd Zaria	27/2/1996	60	0.9	2600	2888.89
QC12	KD Rd Zaria	27/2/96-29/2/96	1440	21.6	2200	101.85
QC13	KD Rd Zaria	4/3/96	60	0.9	2500	2777.78
QC14	KD Rd Zaria	4/3/96-6/3/96	1440	21.6	2100	97.22
QC15	KD Rd Zaria	7/3/96	60	0.9	2600	2888.89
QC16	KD Rd Zaria	7/3/96-9/3/96	1440	21.6	2000	92.59
QC17	KD Rd Zaria	11/3/96	60	0.9	2700	3000.00
QC18	KD Rd Zaria	11/3/96-13/3/96	1440	21.6	2000	92.59
QC19	KD Rd Zaria	14/3/96	60	0.9	2600	2888.89
QC20	KD Rd Zaria	14/3/96-16/3/96	1440	21.6	2200	101.85
QC21	KD Rd Zaria	18/3/96	60	0.9	1600	1777.78
QC22	KD Rd Zaria	19/3/96	60	0.9	1500	1666.67
QC23	KD Rd Zaria	25/3/96	60	0.9	1700	1888.89
QC24	KD Rd Zaria	26/3/96	60	0.9	1600	1777.78
QC25	KN Rd Zaria	27/3/96	720	10.8	1600	148.15
QC26	KN Rd Zaria	28/3/96	720	10.8	1500	138.89
QC27	KN Rd Zaria	2/4/96	720	10.8	1700	157.41
QC28	KN Rd Zaria	4/4/96	720	10.8	1900	175.93
QC29	KN Rd Zaria	6/4/96	720	10.8	1800	166.67
QC30	Zaria BG Site	12/4/96-14/4/96	1440	21.6	800	37.04
QC31	KD Rd Zaria	27/5/96-29/5/96	1440	21.6	400	18.52
QC32	KD Rd Zaria	4/6/96-6/6/96	1500	22.5	500	22.22
QC33	KD Rd Zaria	10/6/96-12/6/96	1440	21.6	400	18.52
QC34	KD Rd Zaria	18/6/96-20/6/96	1380	20.7	400	19.32
QC35	FCT	23/10/96	180	2.7	700	259.26
QC36	FCT	23/10/96	540	8.1	1600	197.53
QC37	FCT	24/10/96	180	2.7	800	296.30
QC38	FCT	24/10/96	540	8.1	1700	209.88
QC39	FCT BG Site	23/10/96-24/10/96	720	10.8	500	46.30
QC40	FCT	25/10/96	180	2.7	700	259.26
QC41	FCT	25/10/96	540	8.1	2000	246.91
QC42	FCT	26/10/96	150	2.3	600	266.67
QC43	FCT	26/10/96	480	7.2	1500	208.33

Table 4.6: Sampling Data for PM10 Particulate Matter (Fine Fraction)

SAMPLE LABEL	SAMPLING LOCATION	SAMPLING DATE	SAMPLING TIME Mins	AIR VOL. m^3	NET PM10 MASS µg	PM10 CONC $\mu g/m^3$
QF01	KD RD Zaria	6/2/96	540	540	600	74.07
QF02	KD RD Zaria	7/2/96	360	360	500	92.59
QF03	KD RD Zaria	8/2/96	540	540	600	74.07
QF04	KD RD Zaria	10/2/96	540	540	600	74.07
QF05	KD RD Zaria	12/2/96	360	360	500	92.59
QF06	Zaria BG Site	14/2/96-16/2/96	1440	1440	600	27.78
QF07	KD RD Zaria	17/2/96&19/2/96	1200	1200	600	33.33
QF08	KD RD Zaria	20/2/96-21/2/96	1200	1200	700	38.89
QF09	KD RD Zaria	22/2/96-23/2/96	1200	1200	600	33.33
QF10	Zaria BG Site	24/2/96-26/2/96	1440	1440	600	27.78
QF11	KD RD Zaria	27/2/1996	60	60	500	555.56
QF12	KD RD Zaria	27/2/96-29/2/96	1440	1440	900	41.67
QF13	KD RD Zaria	4/3/96	60	60	500	555.56
QF14	KD RD Zaria	4/3/96-6/3/96	1440	1440	900	41.67
QF15	KD RD Zaria	7/3/96	60	60	500	555.56
QF16	KD RD Zaria	7/3/96-9/3/96	1440	1440	900	41.67
QF17	KD RD Zaria	11/3/96	60	60	500	555.56
QF18	KD RD Zaria	11/3/96-13/3/96	1440	1440	900	41.67
QF19	KD RD Zaria	14/3/96	60	60	500	555.56
QF20	KD RD Zaria	14/3/96-16/3/96	1440	1440	900	41.67
QF21	KD RD Zaria	18/3/96	60	60	300	33.33
QF22	KD RD Zaria	19/3/96	60	60	400	44.44
QF23	KD RD Zaria	25/3/96	60	60	400	44.44
QF24	KD RD Zaria	26/3/96	60	60	400	44.44
QF25	KN RD Zaria	27/3/96	720	720	700	64.82
QF26	KN RD Zaria	28/3/96	720	720	700	64.82
QF27	KN RD Zaria	2/4/96	720	720	700	64.82
QF28	KN RD Zaria	4/4/96	720	720	700	64.82
QF29	KN RD Zaria	6/4/96	720	720	700	64.82
QF30	Zaria BG Site	12/4/96-14/4/96	1440	1440	600	27.78
QF31	KD RD Zaria	27/5/96-29/5/96	1440	1440	400	18.52
QF32	KD RD Zaria	4/6/96-6/6/96	1500	1500	400	17.78
QF33	KD RD Zaria	10/6/96-12/6/96	1440	1440	400	18.52
QF34	KD RD Zaria	18/6/96-20/6/96	1380	1380	400	19.32
QF35	FCT	23/10/96	180	180	300	111.11
QF36	FCT	23/10/96	540	540	600	74.07
QF37	FCT	24/10/96	180	180	300	111.11
QF38	FCT	24/10/96	540	540	600	74.07
QF39	FCT BG Site	23/10/96-24/10/96	720	720	400	37.04
QF40	FCT	25/10/96	180	180	300	111.11
QF41	FCT	25/10/96	540	540	600	74.07
QF42	FCT	26/10/96	150	150	300	133.33
QF43	FCT	26/10/96	480	480	600	83.33

clogging of the filters.

Prior to sampling, gravimetric measurements were performed on each filter using sensitive digital balance, ensuring that stainless steel tweezers were used for filter handling throughout.

Table 4.7 provides the summary of the emission data for Workplace PM10 particulate matter and ambient PM10 particulate matter for the various Quarry operations. It is readily observed that the highest concentration of workplace PM10 is from MECH1 Quarry operation. This is as a result of the fact that the sampler was located very close to the source in order to reflect the exposure conditions of

Table 4.7: Summary of the Emission Data for Workplace and Ambient PM10 Particulate Matter for Various Quarry Operations

SAMPLING LOCATION	SAMPLE DESCRIPTION	MEAN CONC. FINE ($\mu g/m^3$)	MEAN CONC. COARSE ($\mu g/m^3$)	MEAN CONC. PM10 ($\mu g/m^3$)	COARSE-FINE RATIO	REMARKS
KD RD Zaria	WP-MAN	81.48	238.27	319.75	2.92	Workplace PM10 Particulate Matter
KD RD Zaria	WP-MECH1	555.56	2888.89	3444.45	5.20	
KD RD Zaria	WP-P&L	416.67	1777.78	2194.45	4.27	
FCT	WP-MECH3	116.67	270.37	387.04	2.32	
KD RD Zaria	AMB-DRILL	34.95	61.73	95.68	1.82	Ambient PM10 Particulate Matter
KD RD Zaria	AMB-MECH1	41.67	97.22	138.89	2.33	
KN RD Zaria	AMB-MECH2	64.81	157.41	222.22	2.43	
KD RD Zaria	AMB-MECH2-W	18.53	19.65	38.18	1.06	
FCT	AMB-MECH3	76.39	215.66	292.05	1.85	
Zaria	AMB-BGZ	27.78	44.75	72.53	1.61	Background PM10 Samples
FCT	AMB-BGFCT	37.04	46.30	84.34	1.25	

the workers. These workers are directly exposed to the emitted dust because of their direct involvement in manual loading of the crusher and the evacuation of the crushed rock aggregates. A similar situation exists in packing and loading of the crushed rocks into tippers for commercial purposes, hence the high value of mean PM10 concentration. It should however be pointed out that this operation is Performed within a relatively short time and not even on daily basis. PM10 output for manual quarrying has the lowest value. This is evident from the fact that the dust emission is a relatively slow process. However, the workers suffer from longer time of exposure compared to other Quarry workers. The table also shows that occupational exposure to PM10 for MECH3 crusher with a capacity of 800 tons per day is lower than that of MECH1 with a capacity of about 80 tons per day. This is because the rocks and the surroundings are wet with water before the crushing operation. In addition, the quarry operation is fully mechanized starting from loading of the crusher and collection of the crushed rock aggregates. This necessitated the location of the workers at the upwind positions from the source, and hence the positioning of the sampler at upwind position.

473301

On the other hand, Comparison of the ambient PM10 for the various mechanized quarry operations shows that MECH3 crusher has the highest concentration in spite of the fact that adequate measures were taken to suppress the dust output. This is because the capacity of MECH3 crusher greatly exceeds that of MECH2 and MECH1 (which do not employ any dust suppression mechanism) by a factor of 4 and 10 respectively. Further, the table shows that the PM10 concentration of samples collected during the dry seasons greatly exceeds those collected during wet season as indicated in the results for MECH2 crusher assembly. This shows

that application of wetting agents e.g. water greatly reduces particulate matter pollution.

In general, there is large variation in the mean gravimetric concentration of PM10 particulate matter for the various Quarry operations. This is because the PM10 concentration varies according to the capacity of the crushing equipment, scope of operation, and the distance between the source and the sampler. The table also shows that the concentrations of the fine fractions are lower than those of coarse fractions as indicated by the coarse/fine ratio, which is greater than 2 for the various quarry operations. It can thus be inferred that the emitted PM10 particulate matter is highly enriched in coarse fraction compared to the fine fraction just like any other particulate matter generated by mechanical action.

4.2 Analytical Procedures

The stacked filter unit aerosol sampler is generally characterized with low sample loading thus requiring sensitive analytical technique for analysis. As a result of its high sensitivity and small sample requirement, TXRF technique was exclusively applied for analysis of major, minor and trace elements in the samples collected from various quarry activities. In the following section, the principal components of TXRF will be described. This will be followed by the description of adjustments that must be effected before total reflection X-rays can be observed. Furthermore, the calibration protocol and quantitative analysis method used will be provided. Finally, the results of the analysis will be extensively discussed.

4.2.1 Description of the principal components of TXRF

Figure 4.8 shows the technical drawing of the TXRF components. A Base Plate is fixed (with 4 M4 screws) to the X-ray tube housing with height adjustable L-support mounted on it. The Al-base plate of the TXRF unit is then mounted on this L-support. Also, the Brass Collimator is mounted on the Al Base Plate and adjusted to the exit window of the X-ray tube. The TXRF unit consists of three main parts; the collimator unit, the cut-off reflector unit and the sample holder unit. The collimator Unit consists of two narrow slits S1 and S2 which can be adjusted vertically and even rotated using the screws on the L- support. The cut-off reflector unit consists of a flat brass piece with the reflector made of Duran glass at its center and a beam stopper. This brass piece is pressed with three steel springs against the screw heads. Clockwise rotation of the screws moves the reflector downward while counterclockwise rotation moves it upwards. The sample reflector holder unit consists of an Al base plate with 3 micrometer screws and a spring load fixing mechanism of the reflector. The glide and rotation pieces are used for adjusting vertical and rotation movements.

4.2.2 Practical adjustment procedures for the TXRF set-up

Proper adjustments of the various components of the TXRF setup has to be carried out before total reflection of X-rays can be observed. These adjustments include, coarse adjustment involving the slits through which the primary X-ray beam passes, adjustment of cut-off angle, filtering of the high energy part of the primary beam, adjustment of the sample reflector and adjustment of the Si(Li)

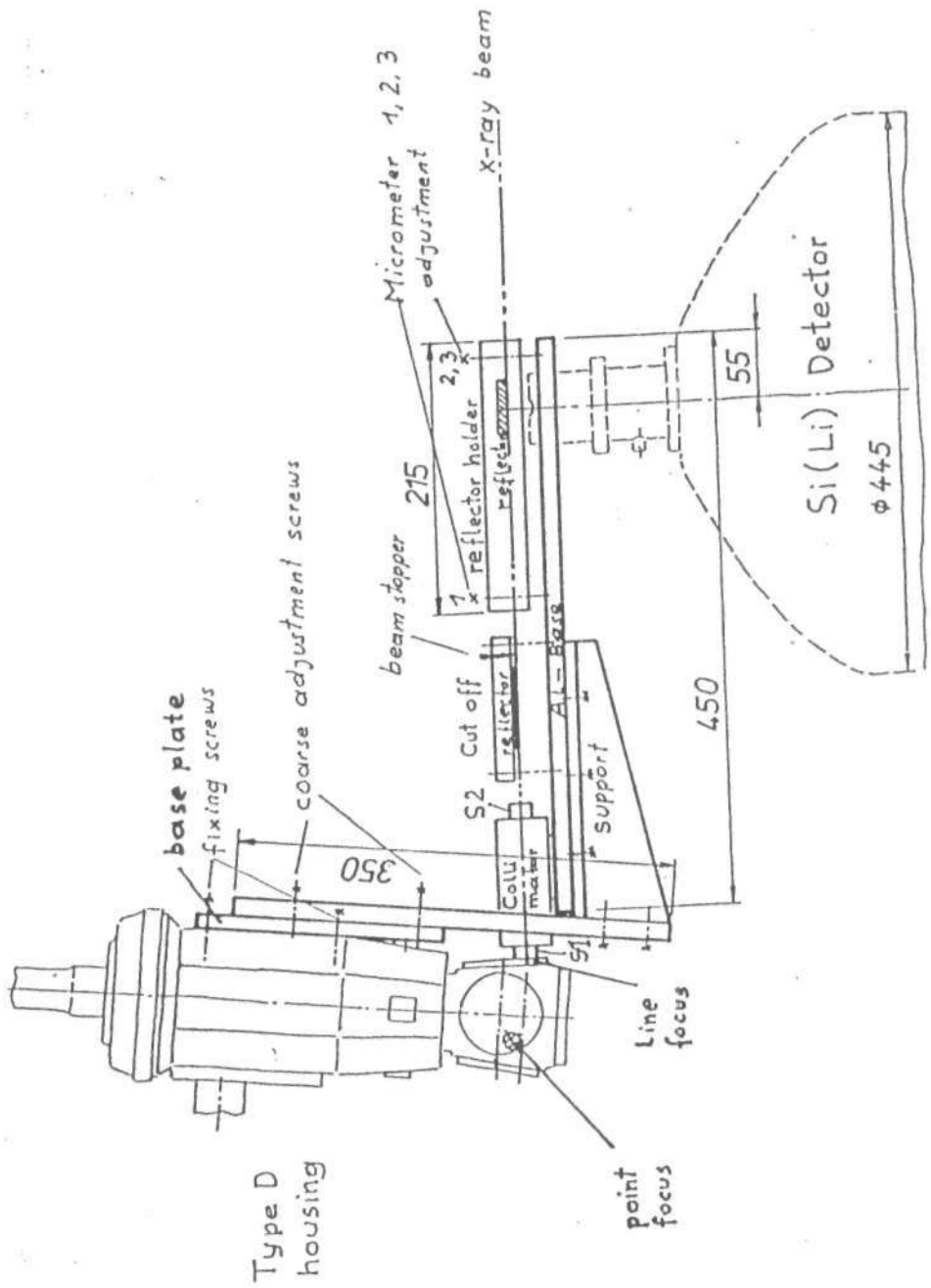


Fig 4.8: Technical Drawing of TXRF Components.

detector with respect to the specimen in order to obtain of maximum fluorescent intensity. Each of these adjustment procedures are briefly explained further.

Coarse adjustment

Slit 2 is first removed from the Collimator Unit and height and rotation adjustment of slit 1 (using screws) performed in order to adjust the slit parallel to the emittingbeam. This adjustment is continued until an intense sharp beam is observed on ZnS screen optically. Slit 2 is then replaced and adjusted by rotation and vertical motion parallel to slit 1 so that the image on the ZnS screen is a sharp rectangle.

Adjustment of cut-off angle

The beam stopper is first removed from the cut-off. With the beam stopper at 0.5m, the reflector is adjusted parallel to the beam at first and then lowered down gradually as long as its shadow appears on the screen. Then it is rotated gradually by turning a screw to obtain a certain angle at which reflection occurs. At this position the passing and reflected beam will be visible on the ZnS screen.

Filtering

Having obtained the correct cut-off angle, the passing beam must be absorbed (filtered) using the beam stopper so that the upper beam is completely absorbed and only the reflected beam is observed on the screen. The spectral distribution can be observed by inserting any low Z scatterer in the beam path.

Adjustment of sample reflector

The sample reflector is inserted and fixed with the spring load mechanism. It is then moved down by turning the micros counterclockwise. The reflector is firstmoved parallel to the beam and then moved further down and rotated until two separate beams of almost equal intensity are visible on the ZnS screen.

Maximum fluorescent intensity

The Si(Li) detector is moved very close (about 0.5cm) to the sample reflector which is spiked with the sample material. The position of the maximum intensity is observed on the MCA by rotating micro. screw 3 to move the reflector up and down. In each position, the peak intensity is observed on the MCA. At the position where the beam optimally interacts with the sample good peak to background ratio was observed.

4.2.3 Elemental analysis procedures

The concentration of 12 elements and 9 elements in the coarse and fine fractions respectively were determined by the chemical analysis of the PM10 particulate matter retained on the coarse and fine membrane filters. The applied analytical techniques were gravimetry and Total Reflection X-ray Fluorescence (TXRF). Isotopic source based XRF could not be applied because the intensities of the 5mCi ^{109}Cd and ^{55}Fe sources are too low to cause excitation of X-rays because of the relatively small sample loading of the filters. Similarly, secondary target tube XRF could not be used because of the diminishing intensity of the X-ray tube and problems associated with the design of the collimator, which could not provide appropriate source-sample-detector positions for efficient excitation of X-rays. On

the other hand, TXRF provides favourable experimental conditions for excitation of X-rays in the sample. This is because, the sample substrate used is effectively thin so that the X-rays penetrates only a few nm into the depth of the sample reflector at small incident angles, thereby reducing scattering background to the barest minimum. Also, excitation of the sample is increased by a few order of magnitude because of the small incident angle and increased path of the beam through the sample due to reflection.

Sample preparation

The fine and coarse membrane filters (47mm diameter) were cut into two. One portion was used for TXRF analysis, while the second portion was kept for subsequent analysis. It was ensured that all the filters were weighed on a clean bench and handled with stainless steel tweezers.

The sampled material was removed from the filter using 65% ultra-pure nitric acid (Merck, D-6100, Darmstadt) diluted to twice its volume (i.e. 32.5% nitric acid) and further diluted by addition of Ga solution which was used as internal standard (Klockenkamper and von Bohlen, 1996). It should be noted that the extraction of the sampled material is greatly aided by the surface deposition property of the Nuclepore membrane filter. To avoid contamination of the filter by the container, contact between the filter and the container wall was avoided as much as possible. About 5µl of dissolved material and particulate matter was then deposited on the quartz sample carrier and dried under infrared light. For the analysis of Si, plexi glass was used as sample carrier instead of quartz. This is because of the high silica content of quartz.

Calibration of the TXRF set-up.

(a) Energy Calibration

The spectrum analysis is preceded by energy calibration protocol, which is re-checked daily or anytime there is alteration in the setting of the shaping time, amplification time etc. Typical equipment settings throughout this work were characterized with the energy calibration gradient of about 25eV/channel, resolution (noise) of about 230eV, and Fano factor of about 0.137.

(b) Sensitivity Calibration

Single element AAS standard solutions were used for the calibration of the TXRF. Different concentrations, (i.e. 5,10,15 and 20 ppm) of the different elements K, Fe, Cu, Zn, Co, Sr, Ba and Pb were prepared from the mixtures of aliquots taken from the initial solution and made up to 100mls. Great care was taken to ensure that the choice of elements for the mixtures does not give rise to overlap of X-ray lines. Each of the mixtures, (i.e. 5,10, 15,and 20 ppm of elements K, Fe, Cu, Zn, Co, Sr, Ba and Pb) was spiked with 10ppm of Ga solution which was used as internal standard.

Aliquot of about 5µl of each of the mixtures was deposited in separate quartz sample carrier and dried under infrared lamp. The prepared specimens were measured for 1000s at a voltage of 40KV and current of 30mA. The calibration curves for the different elements used, as standards are straight lines independent of matrix effects usually observed in conventional XRF. These are presented in Figure 4.9 to 4.16. Thus the slopes of the straight line graph for each element is equal to the sensitivity S for that element.

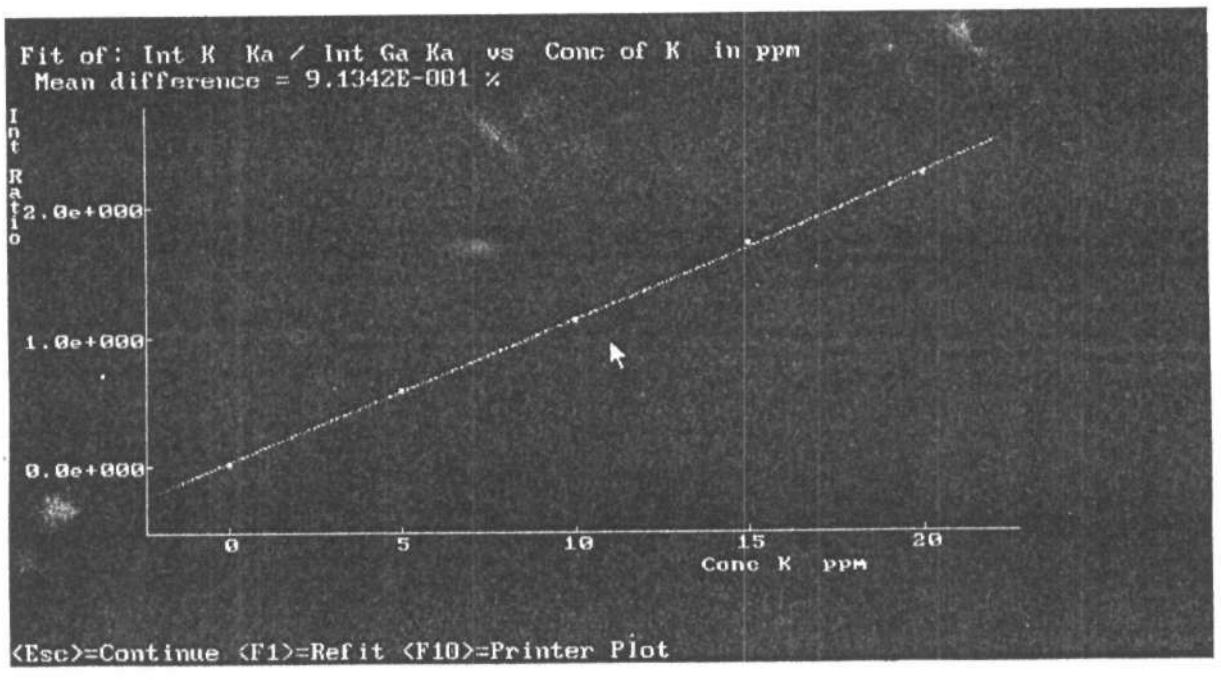


Fig. 4.9: TXRF Calibration Line for K

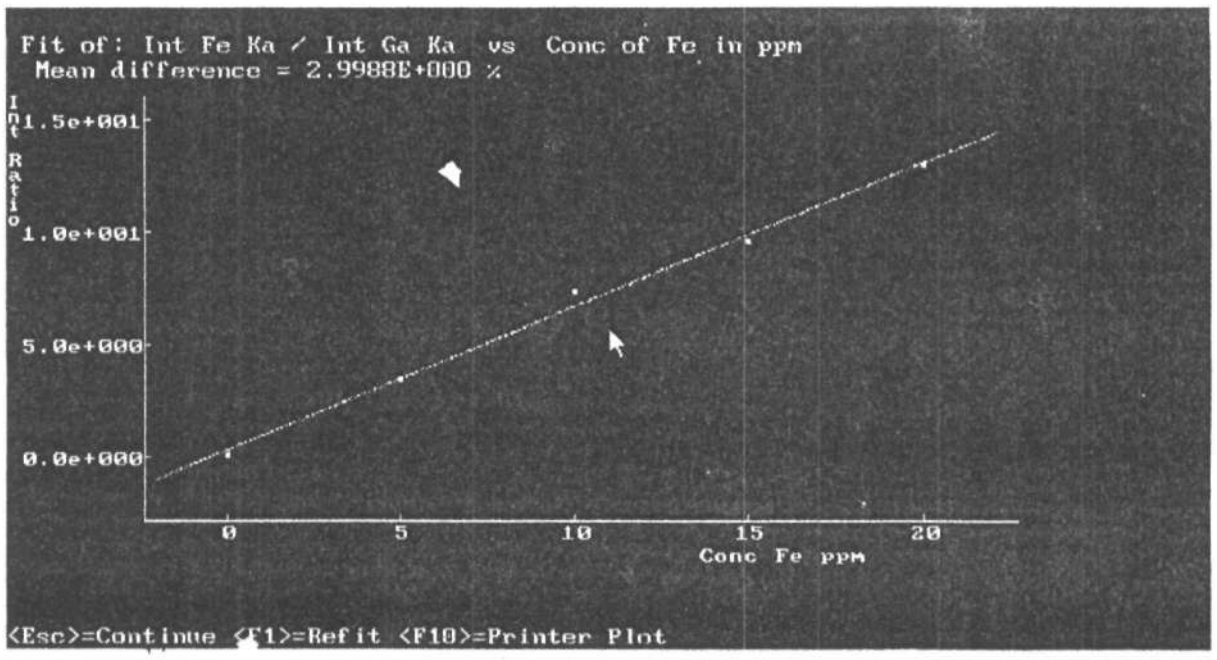


Fig.4.10: TXRF Calibration Line for Fe

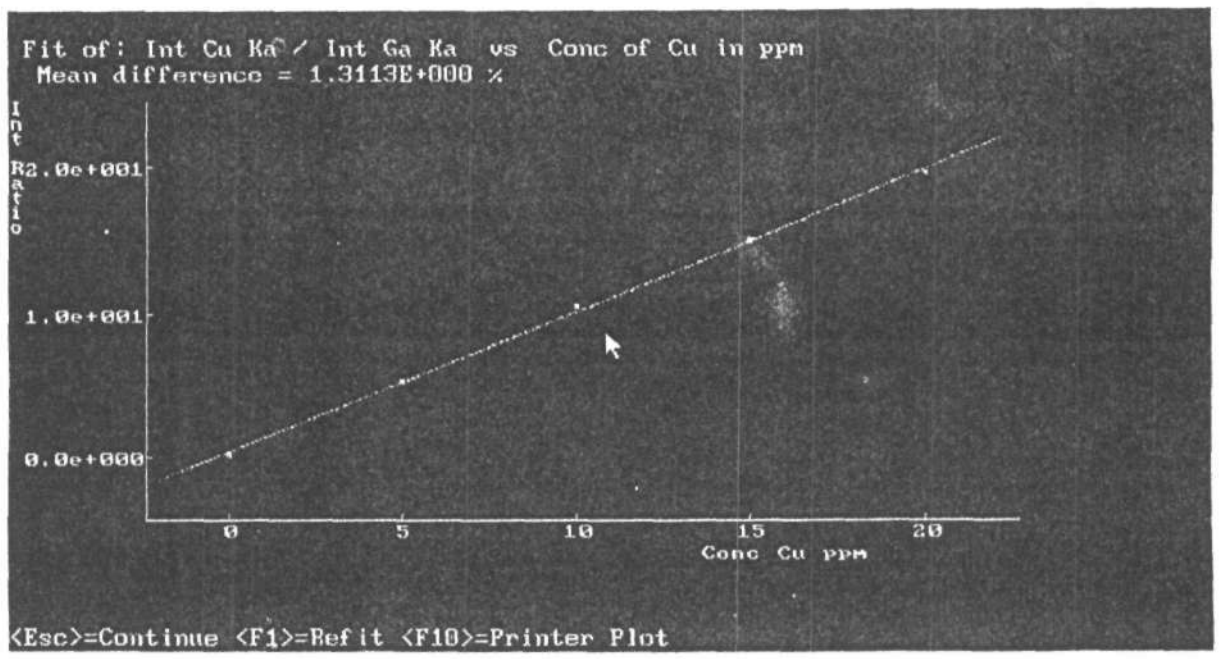


Fig.4.11:TXRF Calibration Line for Cu

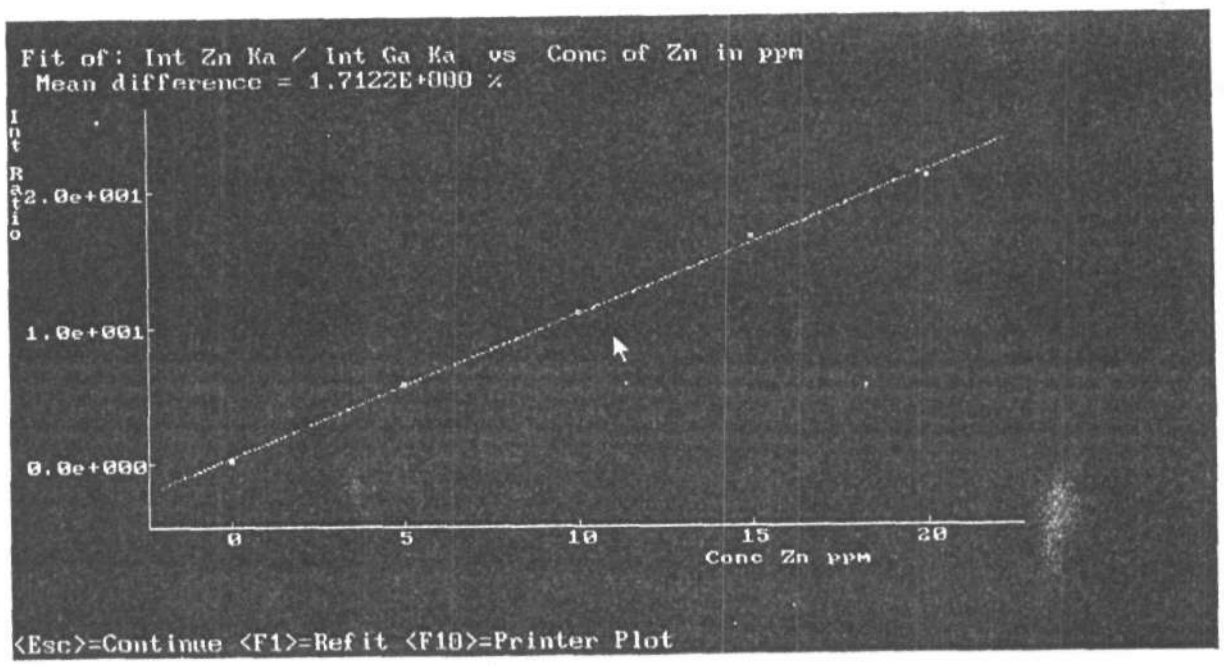


Fig.4.12:TXRF Calibration Line for Zn

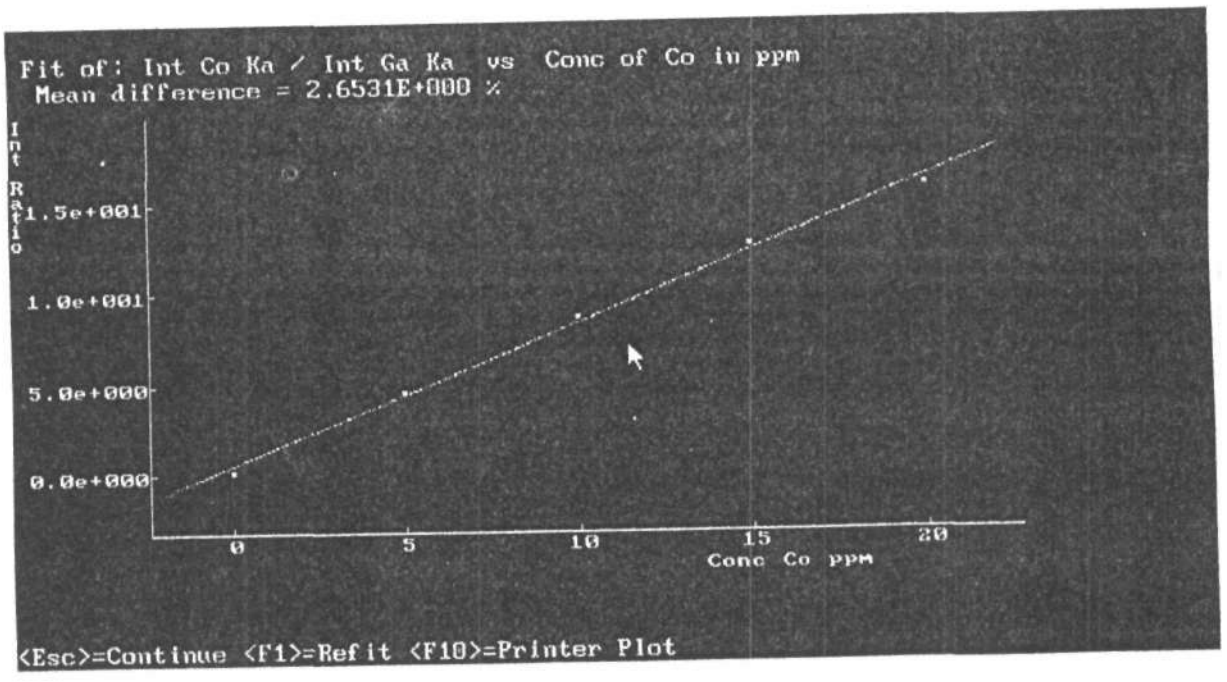


Fig. 4.13: TXRF Calibration Line for Co

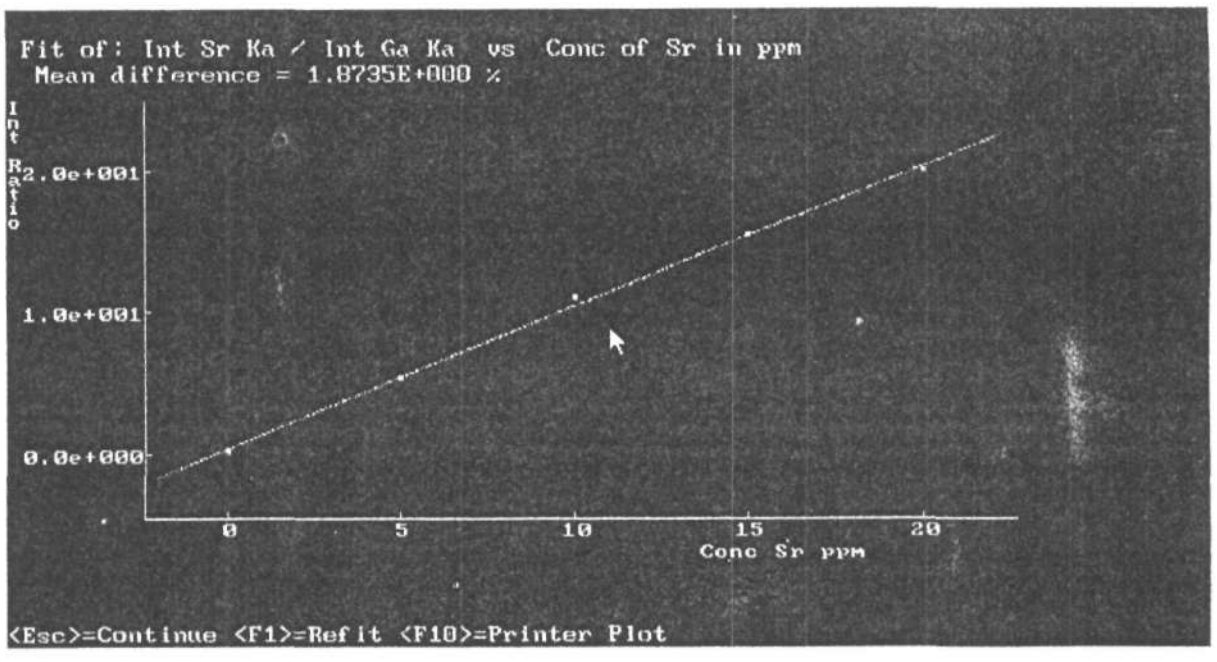


Fig. 4.14: TXRF Calibration Line for Sr

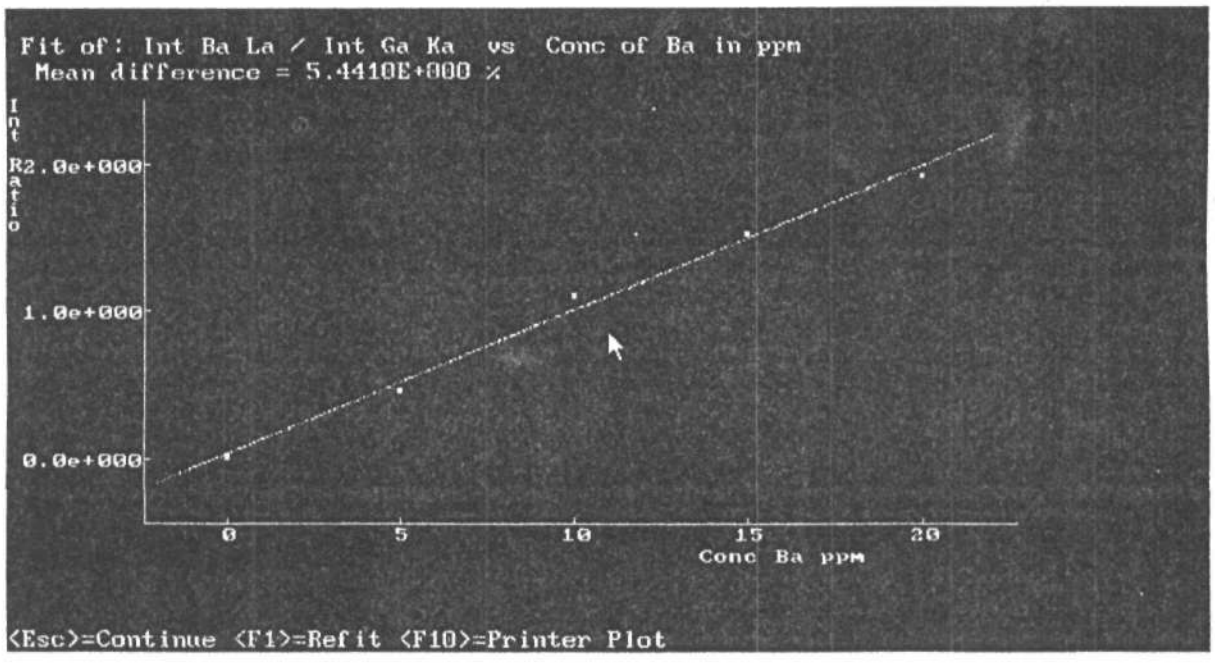


Fig. 4.15: TXRF Calibration Line for Ba

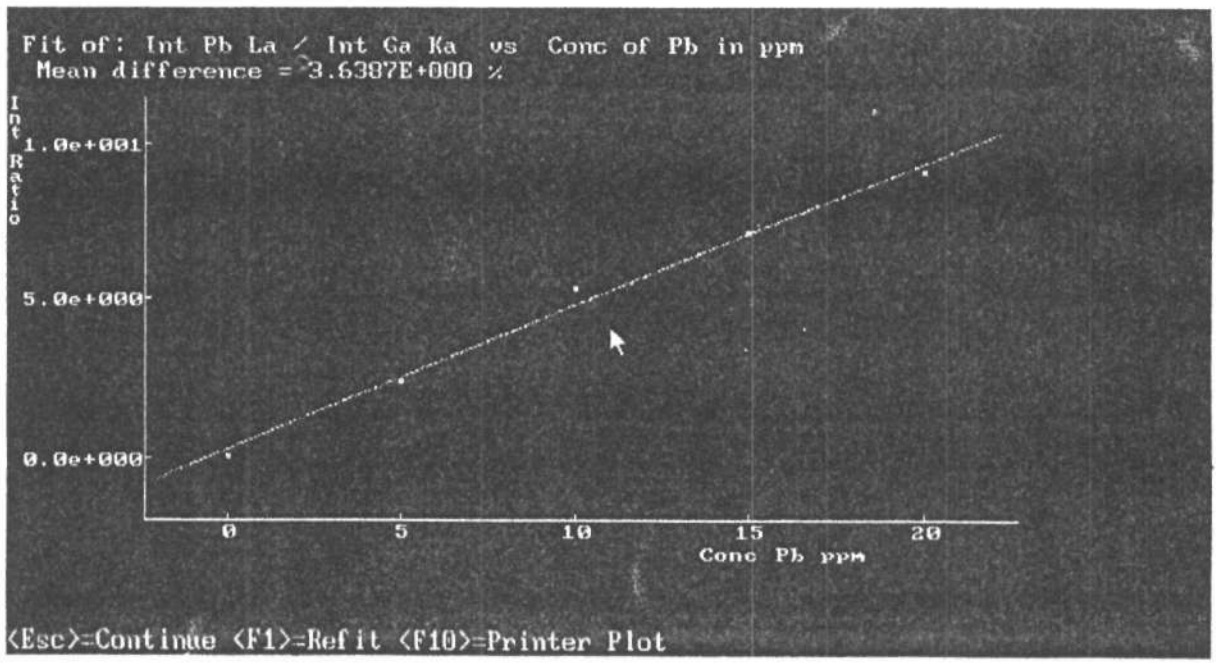


Fig. 4.16: TXRF Calibration Line for Pb

Spectrum analysis

interest in the spectrum using AXIL was preceded by such initial tasks as: The TXRF spectrum for a coarse and fine filter samples are presented in figures 4.17 and 4.18 respectively. The fitting of X-ray spectrum within a chosen region of

(i) Creation of parameter or model file which can be amended and used repeatedly as appropriate;

(ii) Energy and resolution calibration;

(iii) Identification and selection of characteristic X-ray line groups with flexibility for inclusion of escape peaks and peak shape correction; and

(iv) Selection of suitable background fitting model of appropriate order among the various options such as linear, exponential, Bremstrahlung, filter and orthogonal background models.

The least-squares fitting was based on minimization of Chi-square as defined in the theory of non-linear function fitting (Nullens et al, 1979). The optimization was done by means of Marquardt algorithm (IAEA, 1995). This method changes the model parameters in an iterative manner and stops the iterations if certain set conditions are fulfilled. These include preset Chi-square value, percentage difference between two consecutive Chi-square values compared to a preset value, or preset maximum number of iterations. The actual Chi-square value is an indicator of the level of agreement between the fitted model and the measured spectrum. Furthermore, evaluation of the spectrum was performed by inspecting the residual plot of the spectrum.

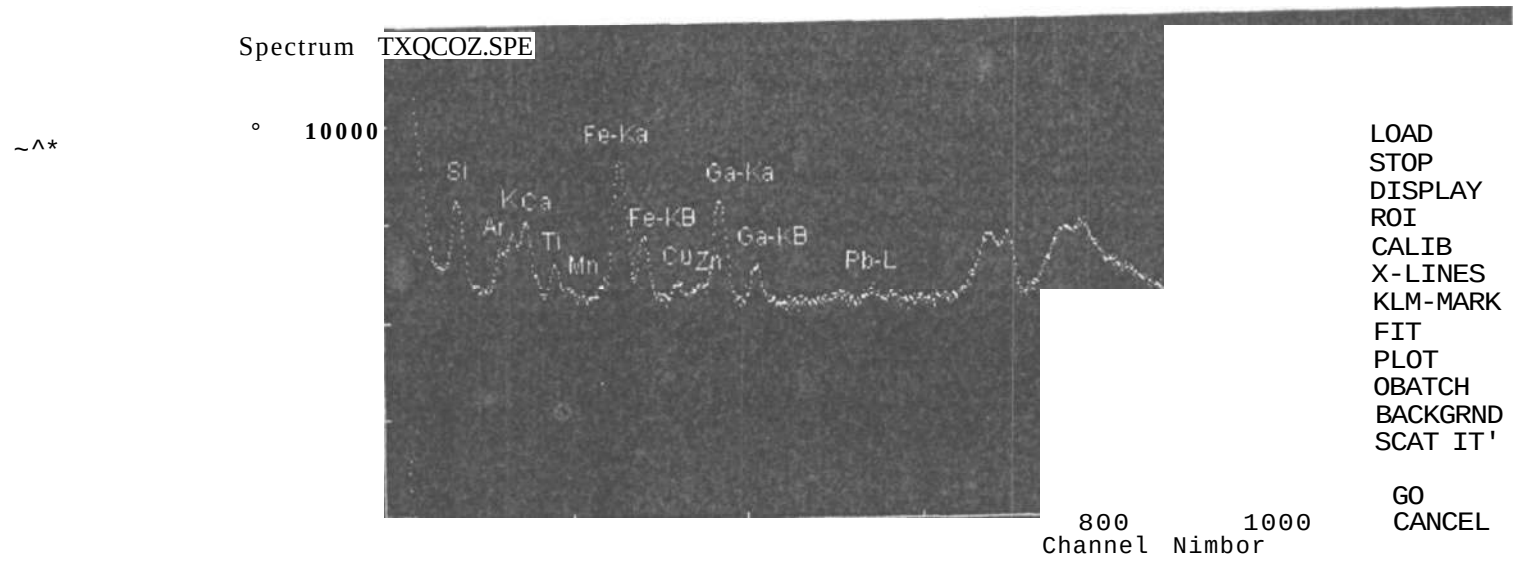


Fig. 4.17: Typical TXRF Spectrum for Coarse PM10 Sample.

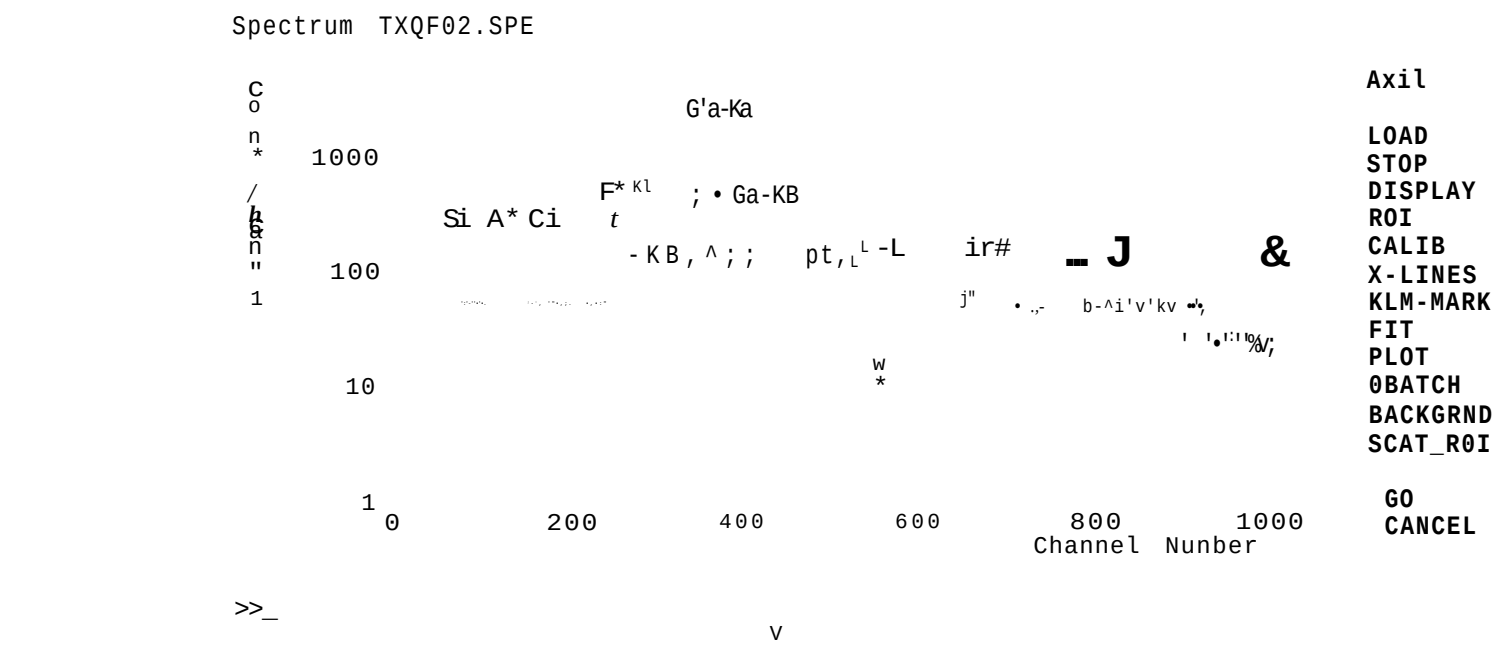


Fig. 4.18: Typical TXRF Spectrum for Fine PM10 Sample

The program automatically prepares an analysis report at the end of the fitting process. The report allows one to retain or reject any of the X-ray lines included in the fit based on the corresponding net peak area and its uncertainty, which are calculated during the spectrum fitting. The criterion used was to remove a line from the model if its peak area is smaller than three times its standard deviation.

Quantification in TXRF

Since a small amount of the sampled material is deposited as a thin layer on the quartz sample carrier, the matrix effect of the conventional XRF is negligible as evident in the calibration lines for the various elements used as standards. On the basis of the sensitivity values determined for each element used in the calibration, quantification was carried out by addition of single element internal standard at a known concentration. The unknown concentration C_x of any other element is determined using the following equation;

$$C_x = C_i \frac{I_x / S_x}{I_i / S_i} = \frac{C_i I_x S_i}{I_i S_x} \qquad 4.14$$

Where:

C_i = Concentration of element used as internal standard (i.e. Ga)

I_x = intensity of element to be measured

I_i = Intensity of element used as internal standard

S_i = Relative sensitivity of internal standard

S_x = Relative sensitivity of measured element

In this way, the concentration of the various elements in the PM10 particulate matter dissolved in acid-Ga solvent was determined. The summary of the applied

procedures for elemental analysis of coarse and fine filters for the various samples using TXRF is provided in appendix 1and 2.

Accuracy

The validity of analytical measurements is determined by accuracy. Accuracy is influenced by faulty standards or calibrations, use of erroneous physical constants, matrix effects, calculation of errors and unknown sources of error. Thus it is necessary to establish the accuracy of experimental results prior to the analysis of the samples. This is normally carried out using certified reference materials (CRM) or standard reference materials (SRM) which must be analyzed under similar conditions as routine analysis. However, it has been established that analysis involving use of carefully prepared calibration standards or commercial standards introduces negligible error provided the standards are subjected to similar experimental conditions as the samples. Since the analytical work in TXRF involves use of calibration standards and further additions of internal standard during sample analysis, the accuracy is greatly enhanced. This is because of elimination of matrix effects as a result of presentation of the sample as a thin film and addition of internal standard to control the errors that may be introduced by the residual matrix. The measured intensity depends only on the fluorescent yield, geometric parameters of the instrument, and detector efficiency of the elements of interest, all of which remain stable over long periods. Also, the slope of the calibration curve does not depend on the properties of the sample. Thus quantification of all the detected elements in any sample is facilitated provided internal standardization of the sample by an element not present in the sample is done. For example, the accuracy of TXRF has been established using this

technique (i.e. calibration standards and internal standardization of the samples) in analysis of reference samples and in inter-comparison tests of river water of estuarine origin (Klockenkamper and Bohlen, 1996). In all these cases, TXRF shows high performance that is comparable with established techniques such as instrumental neutron activation analysis (INAA), atomic absorption spectrometry (ET-AAS) and inductively coupled mass spectrometry (ICP-MS).

In this work, accuracy of the technique could not be assessed using certified reference materials since such reference materials are not readily available for aerosol filters. However, the accuracy was tested using a mixture of single elemental standards prepared from a stock solution different from the one used for sensitivity calibrations. Table 4.1 shows the results of such exercise. It is readily observed from the table that TXRF shows good performance for the elements measured.

Table 4.8: Comparison of Measured Concentration of a Multi-element Standard Using TXRF with Actual Values.

ELEMENT	INDICATIVE VALUE (ppm)	MEASURED CONC. (ppm)
Cr	8.0000	7.978±0.202
Mn	0.2125	<0.256
Co	4.000	4.296±0.065
Cu	10.000	10.913±0.086
Se	2.500	2.514±0.029
Ba	20.000	24.400±1.349

Detection limit

The detection limits are determined by the sensitivity and by the background counting rates in the X-ray spectrum. It is assumed that the background fluctuations are determined solely by random Poisson statistics. As this background is ultimately controlled by extent of scatter from the aerosol substrate, thin films are desirable.

The minimum detection limit Mdl is given by

$$M_{dl} = \frac{3.29\sqrt{\frac{RB}{t}}}{S} \qquad 4.15$$

Where R_B is the background counting rate in Counts/sec under the X-ray peak, t is the time interval of the measurement and S is the sensitivity of the instrument for a specific element.

Equation 4.15 can also be written in terms of the known concentration of element in the standard C_s and net intensity under the X-ray peak I_{NET} as

$$M_{dl} = \frac{3.29C_s\sqrt{\frac{RB}{t}}}{I_{NET}} \qquad 4.16$$

Table 4.10 shows the minimum detection limit for various elements using TXRF technique.

It should be noted that the single element detection limit quoted above merely represents optimistic predictions regarding the statistical accuracy of any such measurement. Possible systematic errors or erroneous background

determinations could increase the detectable limit. Analysis of realistic samples can further complicate matters because of X-ray absorption and enhancement effects, inter element interference and possible changes in the background characteristics.

Table 4.9: Analytical Detection Limits of TXRF Spectrometer

ELEMENT	DETECTION LIMIT (ppb)
K	10.45
Fe	1.80
Co	1.40
Cu	1.52
Zn	1.32
Ga	1.38
Sr	1.05
Ba	15.30
Pb	3.33

4.2.4 Results and discussion

The concentration of the various elements calculated using equation 4.4 is actually the volumetric concentration of the various elements with respect to the acid-Ga solvent that was used for removal of particles from the filter and internal standardization. This concentration in itself is not useful unless it is related to the air volume. Thus, the conversion factors in Appendix 1 and 2 were used to normalize the volumetric concentration in solvent (μg/ml of solvent) to concentration in air (μg/m^3 of air). The concentrations of elements Al, Si, K, Ca, Ti, V, Mn, Fe, Cu, Zn, Sr, and Pb in a total of 86 samples collected between 6th Feb. and 26th Oct 1996 are summarized in Tables 4.10, 4.11, 4.12 and 4.14 by their

arithmetic means and their combined uncertainties. It should be noted that background values of the measured elements are also very important as they must be considered in the final computation of the elemental concentrations of PM10 from the various Quarry operations. The time average concentrations of the various elements and their uncertainties in the background samples collected at Zaria and FCT are presented in Table 4.10.

Workplace PM10 concentrations for various quarry operations.

The variability of the PM10 concentration for selected elements in identical samples collected from various quarry operations is very minimal as demonstrated in figure 4.19. Thus the average concentration values of the various elements in identical samples will be close to their representative values. Table 4.11 and 4.12 shows the time average elemental concentration for coarse and fine fractions of the samples collected for the purpose of monitoring occupational exposure from the various Quarry operations relative to the background values. The concentration of all the elements monitored shows high variation for the various quarry operations, which is as a result of the high variations of PM10 concentrations. It is readily observed that all the elements have peak concentration values for WP-MECH1. This is as a result of the large amount of PM10 particulate matter produced relative to the location of the sampler. In spite of the fact that MECH3 crusher has a capacity of 800tons per day, which is an order of magnitude greater than that of manual quarrying, their workplace concentration values are comparable and also the lowest. This is as a result of the fact that extra precaution, involving wetting of the rocks and the whole work area undertaken by the operators of this quarry. It should be recalled that in this case the siting of the

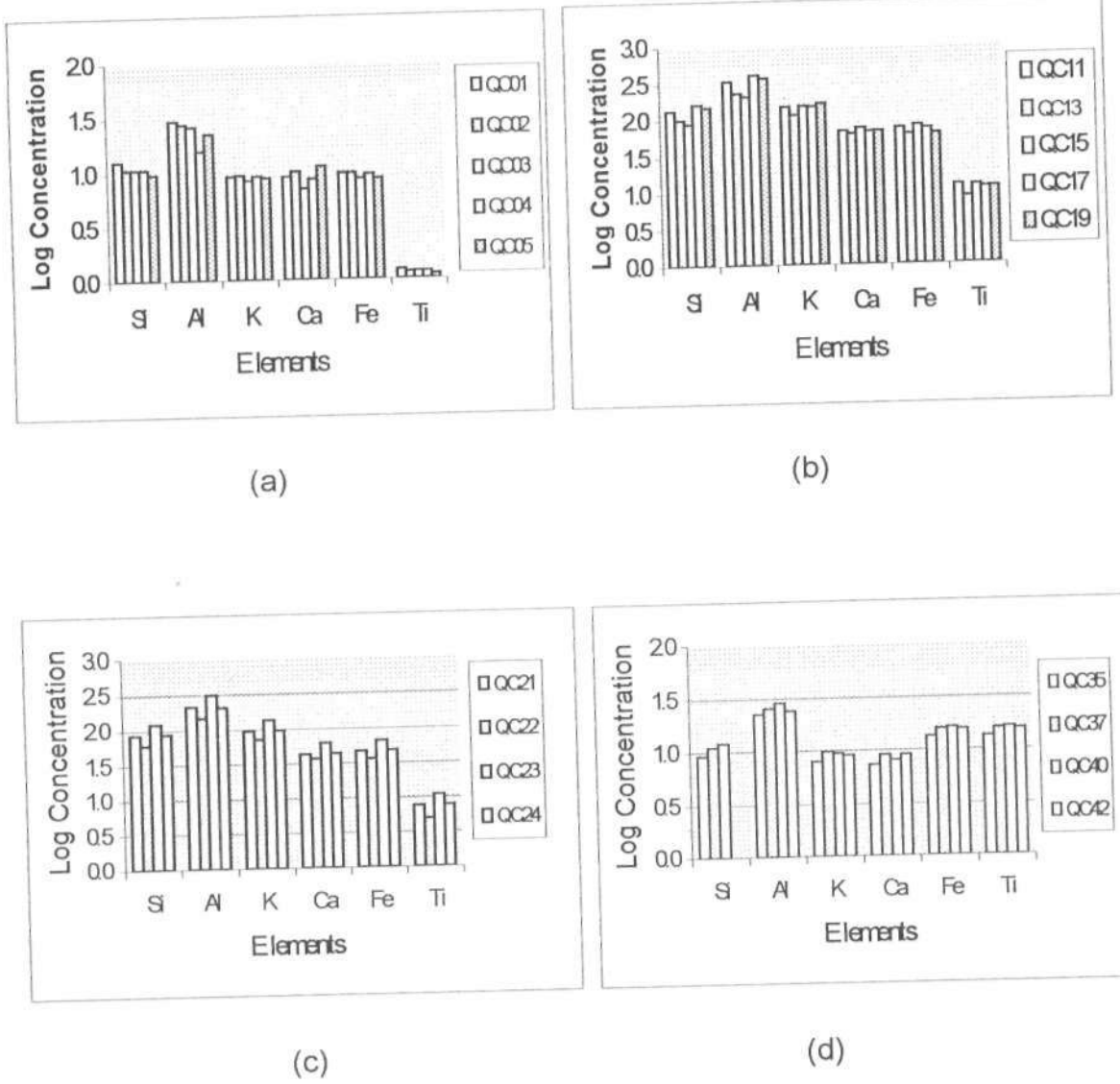


Figure 4.19: Variability of Selected Elements in Workplace PM10 Samples from (a) Manual Quarrying (WP-MAN) (b) Semi-Mechanized Quarry (MECH1) (c) Packing and Loading (WP-P&L) and (d) Fully Mechanized Quarry (WP-MECH3).

Table 4.10: Mean Elemental Concentration of Background PM10 particulate matter for Zaria and FCT.

ELEMENT	ZARIA BACKGROUND CONCENTRATION (μg/m^3)		FCT BACKGROUND CONCENTRATIONS (μg/m^3)	
	COARSE	FINE	COARSE	FINE
Al	-	-	-	-
Si	-	-	-	-
K	1.288±0.057	0.507±0.030	1.146±0.088	1.349±0.078
Ca	1.309±0.040	0.400±0.018	1.316±0.052	1.086±0.052
Ti	0.289±0.017	0.037±0.007	0.195±0.017	0.135±0.018
V	-	-	-	-
Mn	0.049±0.007	-	0.051±0.011	-
Fe	2.431±0.016	0.294±0.006	1.947±0.023	1.222±0.018
Cu	0.127±0.009	0.118±0.006	0.139±0.013	0.255±0.044
Zn	0.126±0.008	0.087±0.007	0.117±0.018	0.266±0.032
Sr	-	-	-	-
Pb	0.141±0.023	0.116±0.015	0.149±0.035	-

sampler was at the upwind position because the whole operation is fully mechanized and the workers are always located at the upwind position.

Table 4.12 shows the recommended threshold limit values (TLV)(ACGII, 1971) and the concentration of some of the elements measured from workplace PM10 aerosols. In spite of the various health effects associated with these elements, it is readily observed that the exposure level of workers at the various quarry operations does not exceed the recommended TLV's even for workers at MECH1 quarry. This does not necessarily imply that the workers are not in any danger since long time exposure may still be accompanied by the various health effects listed. In addition, the promulgated TLV's are based on total suspended particulate

Table 4.11: Mean Elemental Concentration Of Workplace PM10 particulate Matter (Coarse Fraction) for Various Quarry Operations

ELEMENT	WORKPLACE ELEMENTAL CONC.(µg/m³) FOR VARIOUS QUARRY OPERATIONS (COARSE FRACTION)			
	WP-MAN	WP-MECH1	WP-P&L	WP-MECH3
Al	10.757±0.621	127.176±4.783	87.666±3.466	10.803±0.675
Si	26.172±1.410	311.218±3.711	215.729±3.203	25.256±0.347
K	7.632±0.044	144.141±0.358	95.298±0.261	8.017±0.065
Ca	7.172±0.037	66.419±0.255	44.432±0.184	7.101±0.047
Ti	0.865±0.015	10.774±0.089	7.510±0.071	1.534±0.017
V	0.097±0.007	0.910±0.056	0.491±0.035	-
Mn	0.176±0.007	1.763±0.045	1.234±0.038	0.406±0.010
Fe	6.652±0.017	66.827±0.125	45.800±0.101	13.455±0.038
Cu	0.330±0.009	3.635±0.066	2.327±0.046	0.083±0.011
Zn	0.310±0.010	4.874±0.047	3.190±0.037	0.123±0.011
Sr	0.321±0.020	3.201±0.235	2.068±0.129	0.230±0.009
Pb	0.382±0.026	3.351±0.178	2.549±0.110	0.132±0.023

matter without any size consideration. Previous studies (Natusch and Wallace, 1974) had shown that particles larger than 10µm have negligible probability of penetrating the respiratory tract and are also characterized with short life time so that they cannot be subjected to long range transport. Furthermore, PM10 particulate matter fraction in the TSP for mechanical action based pollution source is very low but yet had been known to be associated with health effects. It can thus be concluded that the promulgated TLV's cannot be used to assess the health impact of PM10 particulate matter pollution.

Table 4.12: Mean Elemental Concentration Of Workplace PM10 Particulate Matter (Fine Fraction) for Various Quarry Operations

ELEMENT	WORKPLACE ELEMENTAL CONC. (μg/m^3) FOR VARIOUS QUARRY OPERATIONS (FINE FRACTION)			
	WP-MAN	WP-MECH1	WP-P&L	WP-MECH3
Al	-	-	-	-
Si	-	-	-	-
K	1.349±0.040	31.815±0.588	22.307±0.562	2.209±0.078
Ca	1.620±0.022	13.619±0.362	12.147±0.421	1.424±0.048
Ti	0.011±0.006	-	-	0.153±0.019
V	-	-	-	-
Mn	-	-	-	-
Fe	0.714±0.007	8.784±0.092	6.740±0.085	1.786±0.018
Cu	0.373±0.012	7.307±0.164	4.722±0.119	0.328±0.041
Zn	0.363±0.013	5.661±0.234	3.600±0.166	0.338±0.027
Sr	-	-	-	-
Pb	0.453±0.030	7.363±0.291	4.674±0.241	-

The effect of high concentration of Si in the respiratory system has been stressed (Jackson et al, 1989). Si is solely responsible for a dangerous respiratory disease known as silicosis. Once Si particles reach the alveoli of the lungs, they are phagocytosed by macrophages and in the process the toxic Si destroys the cell thereby causing permanent damage to that cell. Although Al becomes toxic only at high concentration, long time exposure may lead to pulmonary fibrosis, as it is not easily expelled from the lungs after deposition. Lead is regarded as highly toxic cumulative element in man. Long- term exposure has been recognized as causing anemia and affecting the nervous system.

Table 4.13: Comparison of Measured workplace PM10 Concentration with Threshold Limit Values for some Elements

ELEMENT	TLV ($\mu g/m^3$)	CONC. RANGE IN QUARRY DUST ($\mu g/m^3$)	EFFECTS ON LUNGS
Al	-	10.8-127.2	Pulmonary fibrosis (95000$\mu g/m^3$ respirable dust)
Fe	1000	7.4-75.6	Siderosis, increased risk of lung cancer.
Cu	100	0.4-10.9	Acute irritation in the upper respiratory tract.
Mn	5000	0.2-1.8	Pneumonia, bronchitis
V	500	0.1-0.9	Irritation of the upper respiratory tract
Zn	5000	0.5-10.5	Pneumonitis, pulmonary edema

Ambient PM10 concentrations for various quarry operations.

The composition of ambient PM10 concentration for coarse and fine samples relative to the background values is summarized in Tables 4.14 and 4.15 by their arithmetic means and combined uncertainties. The arithmetic means are also adopted in this case because of the slight variability of the elements measured in identical ambient samples. It should be noted that, for this purpose, the sampler was stationed at about 200m from the quarry. At this distance, the sampler is free from topographic obstructions such as trees, tall buildings etc which would have introduced error in the application of Gaussian plume dispersion model that will be used to calculate the source strengths for the various quarry operations.

It is readily observed that there is again a large variation in the concentration values of the various elements measured. This occurs as a result of the varying

capacity of the equipment used for the various quarry operations and variability of wind speed and direction. For example, MECH3 crusher has a capacity of 800 tonnes per day as compared to MECH2 and MECH1 crushers of about 150 tonnes per day and 80 tonnes per day respectively.

Using the individual fine and coarse ambient concentration data, fine/coarse ratios were calculated for each of the elements K, Ca, Ti, Fe, Cu, Zn, Pb in every ambient PM10 sample and these ratios were subsequently averaged over all the samples. The mean fine/coarse ratios are shown in figure 4.18. For the elements K, Ca, Fe, Ti which are typically predominantly from crustal origin, the mean fine/coarse fraction in both fractions are of the order of 0.2 to 0.4. The typical anthropogenic elements Cu, Zn, Pb have fine/coarse ratios above 2. These values are in agreement with the values obtained for ambient air in GENT using stacked filter unit aerosol sampler (Maenhaut et al, 1995). In addition, it is clearly observed from Table 4.14 that ambient PM10 is generally dominated by coarse fractions for the major elements Si and Al for all the quarry operations. These elements are not even measurable in the fine fractions. The same behaviour is exhibited by the other major elements K, Ca and Fe except for the drilling operation. It can thus be concluded that the PM10 particulate matter from the various types of crusher are dominated assembly are dominated by coarse fractions for all the major elements measured. On the other hand, the fine fractions are highly enriched in trace elements Cu, Zn and Pb compared to the coarse fractions for the various quarry operations.

Table 4.14: Mean Elemental Concentration of Ambient PM10 particulate Matter (Coarse Fraction) for Various Quarry Operations

ELEMENT	AMBIENT ELEMENTAL CONC. (µg/m^3) FOR VARIOUS QUARRY OPERATIONS (COARSE FRACTION)				
	AMB-DRIL	AMB-MECH1	AMB-MECH2	AMB-MECH2-W	AMB-MECH3
Al	2.820±0.212	5.209±0.202	8.411±0.500	-	8.098±0.504
Si	5.458±0.161	14.372±0.151	24.480±0.294	-	22.188±0.307
K	0.387±0.031	4.749±0.032	7.946±0.043	0.920±0.011	5.786±0.056
Ca	0.419±0.022	1.526±0.023	1.608±0.027	0.314±0.006	5.052±0.040
Ti	-	0.174±0.009	0.167±0.011	0.026±0.002	1.112±0.014
V	0.007±0.001	0.044±0.004	-	-	-
Mn	-	0.027±0.004	0.031±0.005	0.010±0.001	0.295±0.009
Fe	-	0.473±0.010	0.627±0.012	0.260±0.002	9.717±0.029
Cu	0.032±0.005	0.031±0.005	0.102±0.007	0.054±0.003	0.029±0.009
Zn	0.024±0.005	0.085±0.055	0.085±0.008	0.048±0.003	0.064±0.010
Sr	0.144±0.011	0.134±0.010	-	-	0.174±0.007
Pb	0.041±0.018	0.034±0.015	0.134±0.029	0.061±0.013	0.063±0.021

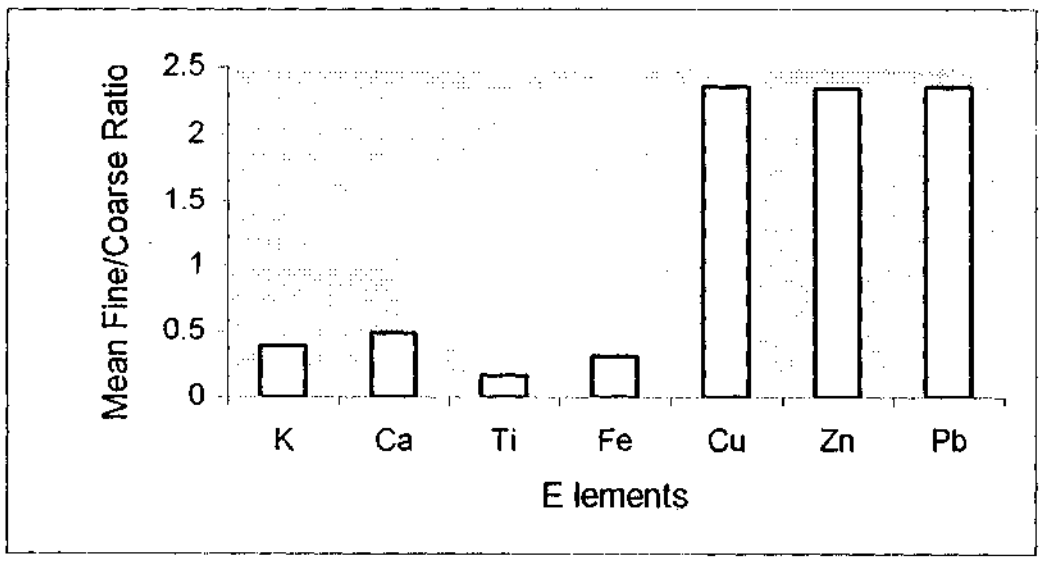


Figure 4.20: Mean Fine/Coarse Concentration Ratios for Selected Elements in PM10 Samples Collected near Mechanized Quarries.

Table 4.15: Elemental Concentration of Ambient PM10 particulate Matter (Fine Fraction) for Various Quarry Operations

ELEMENT	AMBIENT ELEMENTAL CONC. (μg/m^3) FOR VARIOUS QUARRY OPERATIONS (FINE FRACTION)				
	AMB-DRIL	AMB-MECH1	AMB-MECH2	AMB-MECH2-W	AMB-MECH3
Al	-	-	-	-	-
Si	-	-	-	-	-
K	0.610±0.036	0.891±0.031	1.277±0.026	0.603±0.023	1.247±0.063
Ca	0.480±0.021	0.210±0.019	0.561±0.016	0.293±0.012	0.754±0.040
Ti	0.017±0.006	-	-	-	-
V	-	-	-	-	-
Mn	-	-	-	-	0.073±0.015
Fe	0.354±0.007	0.103±0.005	0.306±0.005	0.151±0.004	0.972±0.014
Cu	0.142±0.007	0.198±0.008	0.220±0.007	0.169±0.007	0.165±0.033
Zn	0.104±0.009	0.157±0.011	0.244±0.007	0.159±0.007	0.170±0.023
Sr	-	-	-	-	-
Pb	0.139±0.018	0.203±0.015	0.260±0.019	0.186±0.031	-

Table 4.14 also shows that the concentration of the major elements Al, Si and K is greater for MECH2 crusher with a crushing capacity of 150 tonnes of rock per day than for MECH3 crusher with a capacity of 800 tonnes per day. This is due to the application of wetting agents to the rocks and at each crusher /screen units which reduces the dust output. It should be noted that, even though, the concentration of major element Ca is higher for MECH3 crusher compared to MECH2 crusher, the difference is not commensurate with the difference in their respective capacities, thus showing the effect of wetting agent on the amount of Ca in the PM10 output. Fe appears uninfluenced by the application of wetting agents, this may not be necessarily true since the PM10 output from MECH3 crusher is highly enriched in Fe as confirmed by its high concentration in Workplace PM10. The effect of

wetting agents is also evident in the composition of ambient PM10 from MECH2 crusher during the dry and wet season. Comparison of their elemental composition for coarse fraction, shows that the concentration of major elements K, Ca, Ti, and Fe are reduced by 88, 80, 84 and 58% respectively while the concentrations of trace elements Cu, Zn and Pb are reduced by 47, 44 and 54% respectively. For fine fraction, the concentrations of major elements K, Ca, and Fe are reduced by 53, 48 and 51% respectively while the concentration of trace elements Cu, Zn and Pb are reduced by 23, 35 and 38% respectively. It should be noted that Al and Si are not even detected in PM10 samples collected during the wet season. This clearly shows that application of water alone completely removes Al and Si particles from quarry dust but it is not very efficient in removing the other elements especially when they are in the size range less than 2μm.

CHAPTER 5

HEALTH IMPACT OF PM10 AEROSOLS FROM THE QUARRY INDUSTRY

5.1 Introduction

The harmful effects of particulate matter pollution are only established after the onset of disease or on death of an individual. Detrimental effects of pollutants on humans are either observed or predicted. Many effects are not immediately obvious because of the efficiency of the body's response to stimuli as it attempts to retain internal stability. However social stresses such as marital, occupational and psychological problems and state of health of individual may compound the effect of the pollutant. The response of a population to a pollutant has a wide spread making determination of the actual impact of the pollutant difficult. For this reason, researchers resort to the use of inference or extrapolation techniques in implicating the suspected pollutant.

Humans can respond to pollutants based on its visible, olfactory, or pathogenic effects. Pathogenic effects may arise from the immediate toxicity of the pollutant or its long-term effects. The problem pollutant may not be easily identified because the most obvious pollutant may not actually be the most harmful (e.g. an odorous chemical). It is however clear that certain diseases such as respiratory diseases are linked to the levels of pollutants in the atmosphere. Thus, our health impact assessment of particulate matter pollution will be discussed both in terms of its deposition and clearance mechanisms in the human respiratory tract.

In the following subsection, the structure of human respiratory system and deposition mechanisms of dust pollutants in the system will be discussed in detail. This will be followed by actual computation of the amount of heavy metals deposited in the various compartments of the respiratory tract of workers at the quarry industry and urban population in Zaria and FCT exposed to PM10 particulate matter from the quarry industry. This was done using the multi-elemental PM10 data for the various quarry operations and EPA model. Further, a brief discussion on the clearance mechanisms will be presented.

5.2 The Human Respiratory System

The respiratory system comprises of both the lungs and the airways. Everyday, about 10 to 15m^3 of air is breathed into the lungs by the action of the respiratory muscles. The lungs are very elastic and their volumes vary with inspiration and expiration. The airways on the other hand are built in such a way that they are always open and in free connection with the outside world.

For the purpose of studying deposition of particles, the human respiratory tract shown in figure 5.1 can be divided into three anatomical compartments which have important functional distinctions and radiobiological implications: (ICRP, 1966) as follows:

(1) The nasopharyngeal region (N-P), which begins with the nose, mouth and extends downwards to the level of larynx;

(2) The tracheobronchial (T-B) region, which includes the airways from the larynx to the terminal bronchioles;

(3) The pulmonary region (P), which consists of several structures, respiratory

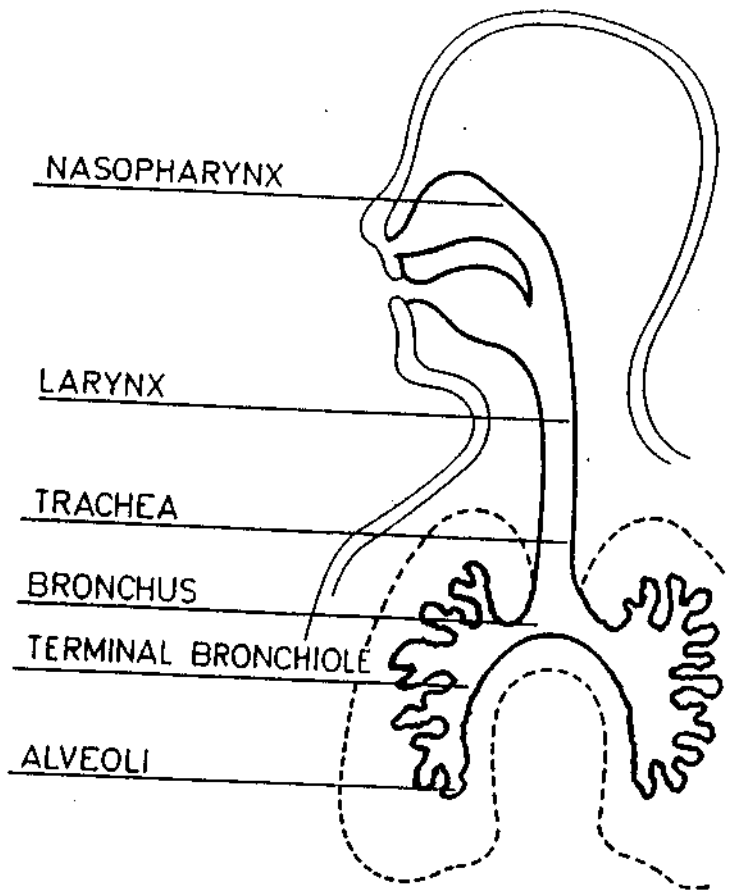


Fig. 5.1: The Human Respiratory System.

bronchioles, alveolar ducts, atria, alveoli and alveolar sacs.

Air is inhaled through the nose, which presents the first line of defense against airborne particulates. The nasal hairs filter out dusts greater than 10μm AED, depending on the dust loading in the environment. The trachea and all other parts of the bronchial tract (except the alveoli) are lined up with slowly oscillating hairs called the cilia. Particles impacting on the sides of the wall are thus trapped both by the cilia and mucous secretions and slowly advected to the top of the oesophagus, where they are then swallowed and eventually excreted. The trachea divides at the top of the chest into two bronchi which themselves subdivide several times into bronchioles of decreasing size until reaching the air sacs or alveoli. There are about 3×10^8 alveoli each about 0.2mm in diameter. The consequent surface area, across which oxygen diffuses into the blood and carbon dioxide out of it is about $50m^2$. Further, the inner side of the respiratory system is covered with a mucous blanket, which is moved to the pharynx by the aid of cilia.

5.3 Theory of Particle Deposition in Human Respiratory Tract.

Deposition is the process determining what fraction of the inhaled particulate matter will be caught in the respiratory tract. Inhaled particles deposit in the various regions of the respiratory system by five mechanisms namely, impaction, sedimentation, diffusion, interception, and electrostatic deposition (Vanoeteren et al, 1986). Inertia impaction causes the major portion of aerosol deposition on mass basis, with the maximum deposition occurring near the carina, the first airway bifurcation. The impaction probability depends on the ratio of the particle stopping distance to the airway dimensions. Sedimentation is most important in the smaller

airways and the alveolar region, and is maximal in those airways that are oriented horizontally. Deposition caused by Brownian motion of sub-micrometer particles is most likely to occur in the smaller airways where resident times are comparatively long. It is the predominant mechanism for particles smaller than 0.5μm in diameter. Interception and electrostatic deposition are less important mechanisms in the human respiratory tract and thus will not be emphasized here. It should be noted that the deposition efficiency depends on the aerodynamic properties of the particles, the anatomy of the airways, the geometric pattern of the air stream, and breathing pattern.

In determining dust deposition in the respiratory system, one of the requirements is the compartmentalization of the respiratory system into three anatomical compartments and the development of a method by which dust deposition can be quantitatively estimated for each of the compartments (ICRP, 1966). The procedure adopted in determining these deposition estimates must take into consideration the aerodynamic characteristics of the air-borne dust particles because of their role in deposition processes. Also, the respiratory system must be considered as a dynamic system, responsive to the activity states of the individuals. The activity condition of man affects deposition primarily as a result of its action on ventilation (ICRP, 1966). The usual psychological response to the demands of increased minute ventilation is to increase the tidal volume more than the respiratory frequency. It should be noted that the greatest change in deposition throughout the respiratory tract is easily accomplished by an increase in tidal volume at a constant respiratory frequency. Studies on relatively sustained work states show changes in minute volumes of the order of 2 or 3 (ICRP, 1966). For

this reason, application of more than one ventilatory states at a respiratory frequency of 15cycles per min should be considered in the determination of deposition.

5.4 Quantitative Determination of Deposition in Human Respiratory Tract.

The mass deposition fraction f_i for the various compartments of the human respiratory tract is determined using standard deposition curves, which relate deposition in the respiratory tract to some parameter of aerosol distribution such as aerodynamic equivalent diameter. In practice, calculations cannot be carried out for all possible breathing patterns or for all possible aerosols. Therefore, the fit to the curve constructed by the EPA (USEPA, 1982) based on the works of various authors for different breathing patterns, variety of size distributions and for N-P and T-P respiratory compartments were used. For the pulmonary region, high and low estimates were determined (because of wide variations of data) using two curves that envelope the data (Milford and Davidson, 1985). The deposition curves for f_i constructed by the US Environmental Protection agency are presented in Figures 5.2, 5.3 and 5.4 for N-P, T-B and P compartments respectively. All of the data are deduced from mouth breathing with respiration rates of 7.5-30 litres per minute and tidal volume of between 1.0 and 1.5 litres.

5.4.1 Determination of fractional deposition estimates

Ideally, the mass median diameter for each size interval should be used to determine the f_i values especially when multistage cascade impactor is used for sample collection. This is not possible with the stacked filter unit (SFU) aerosol

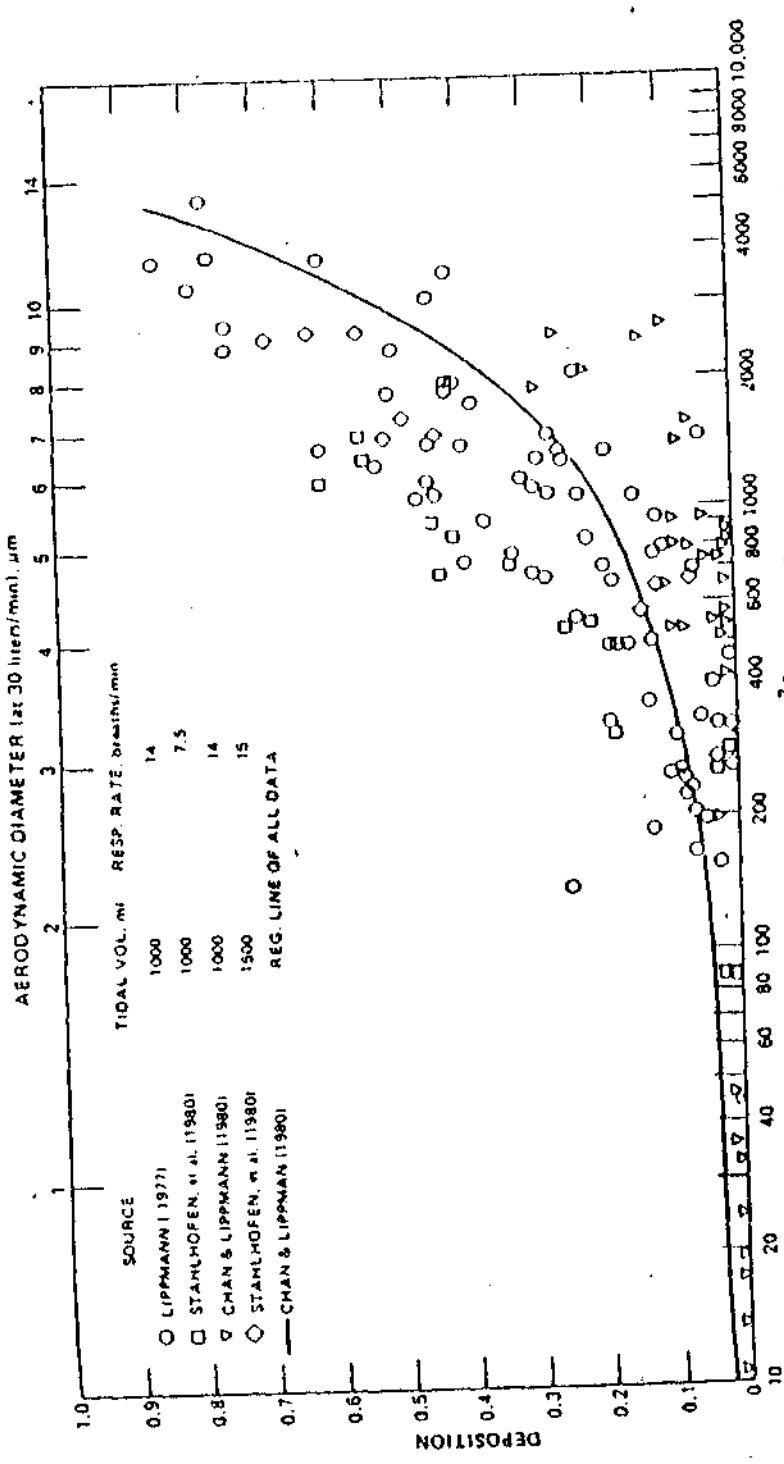


Fig. 5.2: Deposition Curves for the Naso-Pharyngeal (N-P) Region.

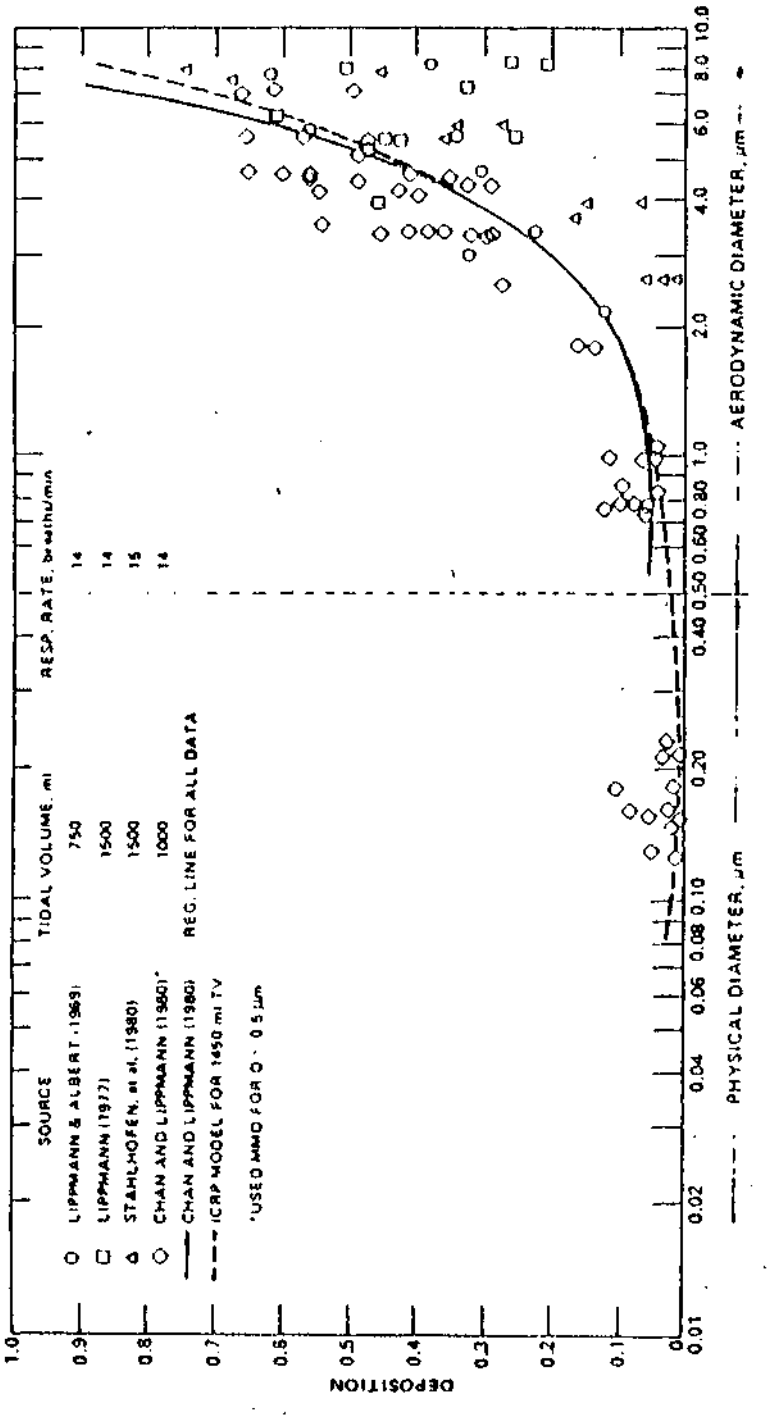


Fig. 5.3: Deposition Curves for tracheo-Bronchial (T-P) Region

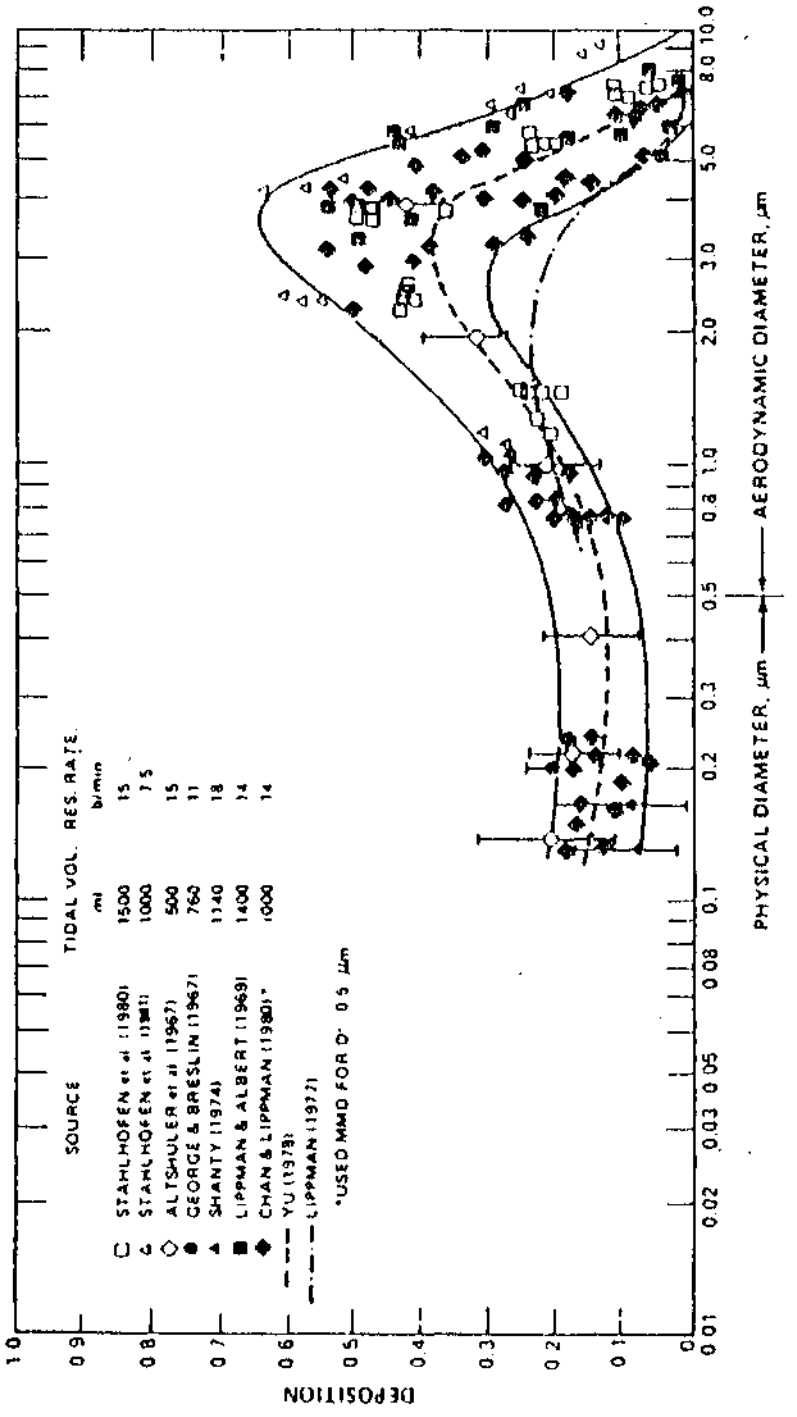


Fig. 5.4: Deposition Curves for the Pulmonary (P) Region.

sampler used for sample collection, because of its bimodal size distribution. However, consideration of uniform deposition of mass on the Nuclepore membrane collection media because of its regular structures and uniform pore size distribution led to the adoption of average f_i values of particle in the size ranges encountered in the SFU. For example for the coarse fraction (2-10μm AED), the average value of respective deposition fraction for 2, 3, 4, 5, 6, 7, 8, 9 and 10μm for the various compartment of human respiratory tract obtained from the EPA curves was adopted. Similar procedure was used in determining the mass deposition fraction for fine filters. The fractional deposition estimates (f_i values) for fine fraction (>2μm AED) and coarse fraction (2-10μm AED) of PM10 particulate matter for the quarry industry are presented in Table 5.1.

Table 5.1: Fractional Deposition Estimates for Fine and Coarse Fraction of PM10 Particulate Matter from the Quarry Industry

RESPIRATORY COMPARTMENT	MASS DEPOSITION FRACTION	
	>2μm	2-10μm
Naso-Pharyngeal region (N-P)	0.033	0.227
Tracheo-Bronchial region (T-B)	0.071	0.268
Pulmonary region (P)	0.146, 0.311 (low and high estimates respectively)	0.196, 0.398 (low and high estimates respectively)

5.4.2 Determination of regional deposition

Principles

the overall deposition fraction F for any of the above anatomical compartments of human respiratory tract is given by

$$F = \frac{\sum f_i \Delta C_i}{\sum C_i} \qquad 5.1$$

Where

f_i is the mass deposition fraction in a compartment of the lung corresponding to size range i,

ΔC_i is the airborne elemental concentration in that size range.

Values of the overall deposition fraction F thus calculated represents the total mass of an element deposited in a specific compartment of the respiratory system divided by the total mass of metal inhaled.

Results and discussion

Calculated values of the total regional deposition fraction F for N-P, T-B and P compartments for elements Al, Si, K, Ca, Fe, Cu, Zn and Pb based on workplace and ambient air concentration data for the various quarry operations using Equation 5.1 and Table 5.1 are presented in Table 5.2. The results obtained suggest deposition fraction ranging from 0.37 to 0.68 for elements Pb, Zn, Cu, Fe, Ca, K, Si, and Al.

The result obtained for total deposition is comparable to that obtained from previous estimates of lung deposition by Milford and Davidson (1985). These investigators also used the US EPA model in obtaining their estimates. For example the total deposition (low) obtained for elements Al, Fe, Zn and Pb are 0.63, 0.61, 0.39 and 0.29 respectively as compared to the values of 0.68, 0.61, 0.34 and 0.34 respectively for the same elements. However, there is considerable

Table 5.2: Regional Deposition Fraction for N-P, T-B and P Compartments of the Human Respiratory System for Various Elements

Element	Extra-Thoracic	Tracheo-Bronchial	Pulmonary (Low)	Pulmonary (High)	Total Deposition (Low)	Total Deposition (High)
Al	0.227±0.019	0.258±0.021	0.196±0.016	0.398±0.033	0.681±0.033	0.852±0.042
Si	0.227±0.011	0.259±0.013	0.196±0.010	0.398±0.020	0.682±0.020	0.853±0.026
K	0.183±0.006	0.216±0.007	0.181±0.007	0.378±0.014	0.580±0.012	0.775±0.017
Ca	0.184±0.007	0.217±0.008	0.182±0.007	0.379±0.015	0.583±0.013	0.778±0.018
Fe	0.198±0.006	0.228±0.007	0.186±0.006	0.385±0.012	0.612±0.011	0.799±0.015
Cu	0.084±0.007	0.123±0.010	0.147±0.013	0.334±0.028	0.354±0.018	0.604±0.032
Zn	0.099±0.010	0.136±0.010	0.153±0.022	0.341±0.047	0.388±0.026	0.630±0.053
Pb	0.092±0.020	0.129±0.015	0.145±0.030	0.338±0.064	0.366±0.039	0.612±0.072

difference in regional estimates obtained for some of the elements. For example, the fraction for Pb in ET, TB and P compartments were estimated as 0.11, 0.07 and 0.11 respectively, and for Fe as 0.34, 0.15 and 0.12 respectively; whereas the fractions obtained in the present study for Pb in ET, TB and P compartments are 0.10, 0.13 and 0.14 respectively and for Fe are 0.20, 0.23 and 0.19. The wide variation in concentration data of workplace and ambient PM10 particulate matter is probably responsible for the slight difference.

5.5 Clearnce of Particles from the Respiratory System

Even though the lung is continuously exposed to particulate matter, the surfaces of the respiratory tract are relatively free of foreign matter. It has been observed that even the diseased and the blackened lungs of miners contain less than 10% of the dust originally deposited there (Vanoeteran et al, 1986). This is because the

respiratory system has a complex defense mechanism, which prevents particle entry as well as remove particles that have been deposited. The efficiency of the clearance decreases with increasing lung burden, decreasing particle size and with fibrous nature of the inhaled dust.

Highly soluble particles and gases dissolve rapidly and are directly absorbed into the blood while less soluble particles deposit on the mucous blanket covering the pulmonary airways and are transported towards the pharynx by the cilia. Similarly, particles deposited on the ciliated mucous membranes of the nose are propelled towards the pharynx where mucous cells and debris mix with salivary secretions and are swallowed. These particles are removed with half- lives of minutes to hours but the particles deposited in the non-ciliated compartments have much longer resident times.

The alveolar surfaces are kept clean and sterile by the alveolar microphages. The lytic enzymes kill and digest bacteria. This digestive capacity may eventually damage pulmonary tissues, e.g. during the development of emphysema. Increased deposition of inert and infectious particles act to recruit additional macrophages and thus the effect may be reinforced. Phagocytosis also plays an important role in the preventing entry of particles into the fixed tissues of the lungs. Once particles leave the alveolar surface and penetrate into the fixed tissues subjacent to the air-liquid interface their removal is slowed down. Particles remaining on the surface are cleared with biological half times estimated to be 24hrs in humans, while particles that have penetrated into fixed tissues are cleared with half times ranging from few days to several years. Most particles

deposited in the alveoli are ingested by alveolar microphages and some of these find their way to the bronchioles and are then carried to the pharynx by ciliary action. The extent by which each pathway is used depends on the sizes, solubility and chemical properties of the deposited particles, on time elapsed after the exposure and individual factors.

CHAPTER 6

IMPACT ASSESSMENT OF PM10 PARTICULATE MATTER POLLUTION

6.1 Theory of Impact Pathway Methodology

Efficient management of the environment requires an assessment of the damage caused by pollution when they are emitted into the air, water or soil. Impact pathway methodology provides a means of analyzing environmental impacts since the pollution damage depends on the sites of emission and the receptors. The principal steps in the impact pathway methodology include:

(i) Characterization of a pollution source and its associated environmental problems (e.g. emission strength)

(ii) Calculation of pollutant concentrations in all affected areas using atmospheric dispersion models;

(iii) Determination of physical impacts due to PM10 particulate matter using the dose-response function;

(iv) Economic valuation of these impacts (optional).

This procedure can be represented as an equation for the incremental damage D due to an incremental quantity Q of a pollutant emitted by the plant (Curtis and Rabl, 1996) as

$$D = \sum f_{dr \to i}\left(f_{disp \to i}(Q)\right) \qquad 6.1$$

Where $f_{disp \to i}(Q)$ = C = increase in the pollutant concentration for receptor i, and $f_{dr \to i}$ is the dose–response function for receptor i. The summation index i runs over all receptors such as population, buildings, crops etc that may be affected by the

source.

The total damage D can also be written in terms of density of receptors $\rho(x)$ at point **x** = (x, y) as

$$D = \int dx \int dy \rho(x) f_{dr}(x, c(x)) \qquad 6.2$$

Using the approximation suggested by Curtiss and Rabl (1996)

$$f_{dr}(x, c(x)) = d(x)c(x) \qquad 6.3$$

Equation 6.2 can be written as

$$D = \int dx \int dy\, \rho(x)\, d(x)\, c(x) \qquad 6.4$$

c (x) = $f_{disp \rightarrow x}(Q)$ is the concentration increase at **x** due to emission Q.

Equation 6.4 can further be written in terms of the deposition flux

$$F(x) = c(x)k(x) \qquad 6.5$$

as

$$D = \int dx \int dy \rho(x) \frac{F(x)}{k(x)} \qquad 6.6$$

Since by conservation of matter the surface integral of the removal flux equals the emission. i.e.

$$Q = \int dx \int dy\, F(x) \qquad 6.7$$

Equation 6.5 reduces to

$$D = \rho(x)\, d(x) \frac{Q}{k(x)} \qquad 6.8$$

Assuming that the World were homogenous with uniform receptor density $\rho(x) = \rho_H$, uniform dose-response function $d(x) = d_H$, and uniform atmosphere $k(x) = K_H$,

equation 6.7 would be simplified as

$$D = D_H = d_H \rho_H \frac{Q}{k_H} \qquad 6.9$$

Equation (6.9) is called the Uniform World Model. It has also been derived by Trukenmuller and Krewit (1993), using a different approach.

If a point source is considered, the assumption of uniform atmosphere (i.e. $k=k_H$) may appear unrealistic, but this is not necessarily so. In fact, the sensitivity to deviations from uniformity is surprisingly small as demonstrated by Curtiss and Rabl (1996). For example, they found that, in France, the damage ranges from 0.35 to 2.6 times D_H if the pollution source is moved from a rural area to a metropolitan area. Thus the simple equation (6.9) above can be used as a good estimate to at least an order of magnitude for the impact assessment of a pollution source.

In the subsequent section, meteorological factors and the underlying theory of atmospheric dispersion will be discussed. In particular, the Gaussian plume model for dispersion studies (Dobbins, 1979) will be used along with the multi-sample data in Table 3.4 to determine the source strength for the mechanized quarry operations. This will be followed by the detailed discussion on the dose response function. The results of the dose response function determined from epidemiological study from the literature will be used along with the Gaussian model calculations to determine the damage to the environment.

6.2 Dispersion Theory

Pollutants emitted into the atmosphere from a source are dispersed by a variety of mixing mechanisms in the atmosphere, which dilute them and transport themaway from the source. Once in the atmosphere, the motion and concentration of air pollutants is governed by meteorological factors, the most important being the wind motion. The wind is responsible for dispersion of pollutants in both horizontal and vertical directions. In general, the greater the wind velocity the greater the rate of dilution.

Apart from wind motion, the dispersion of pollutants is also controlled by the extent of temperature inversion. Temperature inversion occurs when the temperature of the atmosphere which normally decreases with increasing height above the earth's surface, suddenly changes and begins to increase with height. If this layer is sufficiently thick, it can form a lid in the atmosphere, which will envelop many pollutants in this region. If this inversion layer is very low, pollutant level can build up in the lower atmosphere to dangerous levels. Also, pollutants emitted from an elevated source may possess enough momentum to be transferred through a narrow inversion layer into the next stratum. The pollution may then be trapped in the non-turbulent air above the inversion layer for several months and consequently resulting in long range transport of pollutants through hundreds of kilometers before deposition as demonstrated by Pacyna et al (1984).

The dispersion of a pollutant is also affected by the topography (such as hills, valleys and coastlines) of the region through which it passes. The extent of turbulence tends to be higher in the hilly terrain resulting in more rapid dispersion.

Many mathematical models have been developed to describe the dispersion of pollutants in the atmosphere from different types of sources and under different meteorological conditions. A simple procedure for determination of the concentration of pollutants at a given location, which relies on the knowledge of meteorological factors, is the Gaussian plume model. This model works on three main assumptions. These include quasi-steadiness of the boundary layer winds, chemical inertness of the pollutants and approximation of the boundary layer wind profile by a single vector whose magnitude u and direction are constant at all levels (Dobbins, 1979).

The Gaussian plume model is applicable to emissions from quarry industries in spite of the absence of tall chimneys, since it can be modified to describe pollution from ground level point sources. Also, pollutants collected from the quarry operations are limited to PM10 particulate matter, which can be carried over long distances. Furthermore, PM10 particulate matter can be regarded as inert because of their small sizes.

In the following subsection, meteorological factors will be discussed. This will be followed by discussion of the Gaussian plume model and its application to ground level point source. This will lead to calculation of source strengths for the various mechanized quarry operations and hence determination of concentrations of pollutants at various locations around the source.

6.2.1 Meteorological effects

The earth's weather condition is restricted to the troposphere which is about 10-20km from the ground. The region of the troposphere affected by the transport and dispersion of pollutants is the lowest 1000m called the atmospheric boundary layer, which represents the influence of the earth's surface on the wind structure in the atmosphere. Such effects on the wind structure include the prevailing high level flows and frictional drag force of the surface. This gives rise to variation of the wind speed and direction with altitude which in turn is a function of surface roughness and temperature profile. Meteorological factors such as wind, temperature, atmospheric stability, humidity and topography, which affects dispersion and transport of pollutants will be discussed shortly.

Winds

Winds are produced by pressure differences arising from circulating air masses due to differential heating of the earth's surface by the sun. In the areas where there is intense heating by the sun, the air there gets hot, expands, rises and later cools, resulting in loss in pressure. Naturally, the hot air is replaced by colder air at higher pressure from other areas. This movement of air, which is due to pressure differences produce winds. If ground friction is neglected, the circulating air masses will be balanced by Coriolis force due to earth's rotation. This balance determines the wind velocity and direction (geostrophic wind) (Henderson-Sellers, 1984).

On a meteorological map, the wind speed is determined from the spacing between lines of equal pressure represented by isobars. It is inversely proportional to the

spacing between the isobars. Also the wind direction (which is conventionally taken as the direction from which the wind is blowing) is parallel to the isobars. For dispersion studies, wind data over a period of time is best represented with the aid of wind rose (Smith, 1968). The wind rose is a pictorial display of wind data with lines whose lengths are proportional to the frequency of wind blowing along the cardinal directions converging at a center. The prevailing wind direction is represented by the longest line on the wind rose.

The wind velocity changes vertically and horizontally with distance. This may give rise to wind shear, the effect of which can be observed in cloud formations as they are subjected to shear stress. Friction has the effect of rotating the wind counterclockwise and reducing the velocity to approximately 60% of the geostrophic wind velocity over land.

Vertical variation of the wind speed may not be significant. It is represented by the logarithmic profile

$u = a \ln (z/z_0)$

Where u is the wind velocity at height z, a is the function of stability and z_0 is a constant depending upon the roughness characteristics of the underlying surface. The value of the roughness length is approximately 10% of physical obstruction size. Thus pollution may be dispersed differently according to position in the troposphere. In urban areas, wind produced by pressure differences may be considerably disturbed. This disturbance can be observed on a small scale such as eddying flows around entrances to tall buildings.

Temperature

Temperature is another meteorological factor affecting dispersal of pollutant from a source. In the case of a chimney the temperature will directly dictate the buoyancy of the flue gases and therefore the maximum height to which they might rise. However, it is the temperature at the chimney relative to atmospheric temperature that is of significance.

Since the pressure decreases with height, a rising parcel of air will expand and such expansion produces cooling. The rate of decrease of temperature with height is called the temperature lapse rate. If this decrease in temperature does not involve any heat loss, then it is called adiabatic lapse. Conversely if the parcel of gases is falling, the temperature will decrease, a process known as inversion. This has the effect of preventing upward dispersal of pollutants. If the temperature remains constant, then the process is known as isothermal.

The effect of temperature on the dispersal of a plume from a chimney has been classified into five groups. These include looping, coning, fanning, lofting and fumigation (Jackson, et al, 1989). Looping occurs when the lapse rate is adiabatic. Under this condition, the motion of a warm parcel of air is reinforced giving rise to unstable condition and thus causing rapid dispersal of pollutants with distance. Coning tends to occur when conditions are slightly adiabatic or isothermal. The air is less buoyant and so conditions are stable. They tend to be associated with moderate to strong winds and so pollution dispersal is less rapid. Fanning occurs when the lapse rate is negative or isothermal. It produces very stable conditions with very little mixing of the plume with surrounding layers. It is characterized with

slow dispersion since it spreads horizontally. Lofting occurs with the two conditions of inversion at the lower layer that prevents dispersion and adiabatic lapse rate at the upper layer that enhances dispersion. These conditions are transient and occur as adiabatic condition changes to inversion condition. Fumigation is the reverse of lofting and tends to occur in the early morning when the ground is warming. Concentration of pollutants can be high under such conditions.

Atmospheric stability

A rising parcel of air will generally expand. If this expansion occurs without exchange of heat between the parcel and the surroundings (adiabatic process) the temperature of the parcel will decrease. For a dry parcel of air, this decrease of temperature occurs at a constant rate known as dry adiabatic lapse rate. The actual rate at which the atmospheric temperature changes with height is the environmental lapse rate, which is not necessarily equal to dry adiabatic lapse rate. If however, the environmental lapse rate is equal to the dry adiabatic lapse rate the atmosphere is described as neutral or in neutral equilibrium. The stability of the atmosphere is generally described with reference to the neutral equilibrium (Hanna et al, 1977). If the environmental lapse rate has lower negative temperature gradient than the dry adiabatic lapse rate, the temperature of a parcel of air will be less than that of the surrounding air. Thus the density is greater and there is a net restoring force downwards until the parcel returns to its original position. The system is thus severely damped and the atmosphere is said to be stable. Conversely, if the environmental lapse rate is greater than the dry adiabatic lapse rate, a rising parcel of air will continue to rise so that only a small disturbance is necessary to initiate vertical motion. This condition gives rise to

unstable equilibrium. The stable equilibrium condition can be further classified into slightly and moderately stable conditions while the unstable equilibrium condition can be further classified into extremely, moderately and slightly unstable equilibrium. The key to the various stability categories based on Pasquill stability classes as presented by Turner (Turner, 1970) is shown in Table 6.1. Incoming solar radiation varies with the season and time of the day and appropriate choice must be made between strong, moderate and slight insolation Indicated in Table 6.1. Also, the neutral class D should be assumed for overcast conditions during day or night particularly within 1hr of sunset or sunrise.

Table 6.1 key to Pasquill stability categories (from Turner, 1970)

Surface Wind speed at 10m (m/s)	Daytime (1hr after sunrise and 1hr before sunset)				Night time			
	Incoming solar radiation ($mWcm^{-2}$)				Within 1hr of sunset or sunrise	Cloud cover		
	Strong ≥60	Moderate 30-60	Slight ≤30	Overcast		0-3	4.7	8
< 2	A	A-B	B	C	D	F or G	F	D
2.3	A-B	B	C	C	D	F	E	D
3.5	B	B-C	C	C	D	E	D	D
7.6	C	C-D	D	D	D	D	D	D
>6	C	D	D	D	D	D	D	D

Humidity

Humidity and its associated precipitation also affects dispersion of pollutants in the atmosphere. Under the condition of low humidity, water droplets may evaporate producing cooling and thus may affect the buoyancy of a parcel of air. Conversely, cooling of the parcel may cause condensation. If particulate matter is present in the atmosphere, they can stimulate such condensation by forming foci upon which

the water vapour condenses giving rise to fog or mist. Under such condition, solar radiation penetration to the ground is reduced, and thus normal heating is slowed down giving rise to inversion and hence the trapping of the pollutants which may persist over a long period. Sometimes, condensation can occur and later be deposited under gravity as rain. Under such condition, the pollutant will be removed from the atmosphere. Thus the presence of water vapour in the atmosphere may increase pollution or reduce them.

Topography

In a rural flat terrain environment, the lateral wind field is essentially uniform. This is however absent in an urban environment where many large obstacles such as buildings may produce interference in the laminar flow of air. From the continuity considerations, the deviated airflow adds to the total mass flow around the edges of the buildings. Since the mass flow rate must be unchanged, the velocity must increase. However, this increase is not uniform at all locations around the building. Particularly, stagnation points where there is no wind occurs at the leeward side. These stagnation points are located at the wake of the building such that the wind shear across its boundary creates circulating eddies within the wake resulting in flow reversal within this region. In such a situation, upward dispersal of pollutants trapped within the wake of the low-pressure cavity may be prevented, a phenomenon known as downdraught. In order to avoid downdraught, the chimney must discharge at a height of at least 2.5 times any nearby building which is likely to produce such disturbance in the air flow. In practice, there are often many buildings in the vicinity and the disturbance of air flow is complex, creating turbulence with multiple high and low pressure points. It is therefore essential for

the chimney stacks to terminate above the greatest height of the disturbed air flow produced by the buildings.

In a situation whereby the effluent is transported into the low pressure region in the lee of the chimney itself, a phenomenon known as downwash occurs. The occurrence of downwash is determined by the ratio of the effluent exit velocity to the wind speed at the stack top. Downwash is unavoidable if this ratio is less than 1.0 but can be avoided if this ratio is greater than 1.5.

The air moves over a building such that a positive pressure builds up on the windward side while negative pressure develops on the leeward side. In addition the disturbance of the laminar flow is noticeable for some distance above the building. Because a chimney imposes less resistance to air flow the same effects are much less noticeable, but if a building is in the vicinity of the chimney, the disturbed air flow may affect the plume from the chimney stack.

6.2.2 The Gaussian plume model.

Principles

A suitable model for studying atmospheric dispersion over a distance of the order of tens of km is the Gaussian plume model (Seinfield, 1986). This model is based on the approximation that the concentration downwind of a point source in the atmospheric boundary layer is described by the product of two unequal Gaussian distributions. One of these distributions represents the spread in the vertical direction while the other represents the spread in horizontal direction

perpendicular to the direction of the prevailing wind. This is schematically represented in Figure 6.1.

The concentration C (x, y, z) for a point source located at position (0, 0, H) is given by

$$C(x,y,z)=\frac{Q}{2\pi\sigma_y\sigma_z u}\exp\left[-\frac{1}{2}\left(\frac{y}{\sigma_y}\right)^2\right]\exp\left[-\frac{1}{2}\left(\frac{z-H}{\sigma_z}\right)^2\right] \qquad 6.10$$

Where:

Q = emission rate (g/s)

C (x,y,z) = Concentration at point (x, y, z)

u= average wind speed, in the x- direction

H = effective emission height (stack height + plume rise)

σ_y= plume width parameter (dispersion coefficient) in the y-direction

σ_z = plume width parameter (dispersion coefficient) in the z-direction

In order to take into consideration the fact that the plume may extend beyond the planetary boundary layer or below the ground, Equation 6.1 above needs to be modified to take into account reflection or absorption of the plume. With the assumption of total reflection both above and below, the second exponential in equation 6.1 is replaced by the reflection term R(z) given by

$$R(x,y,z)=\exp\left[-\frac{1}{2}\left(\frac{H-z_r}{\sigma_y}\right)^2\right]+r_g\exp\left[-\frac{1}{2}\left(\frac{H-z_r}{\sigma_z}\right)^2\right] \qquad 6.11$$

In order to account for the removal of pollutant, equation 6.9 is further multiplied by a decay factor of the form decay factor = exp (- βx), where β can be a function of x.

As first approximation β may be considered as constant of the form $\beta=\frac{k}{vH}$

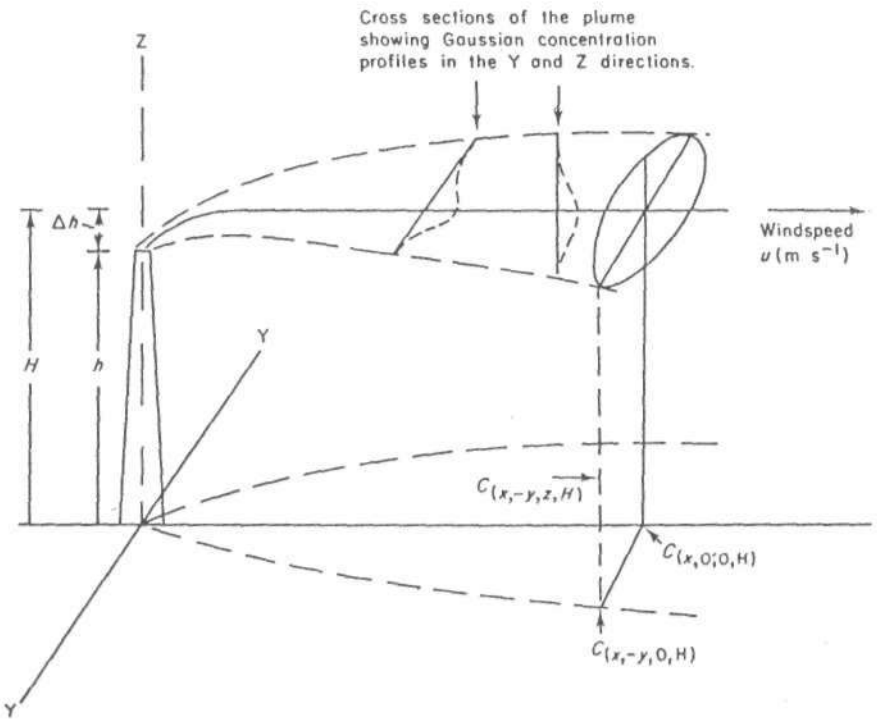


Fig. 6.1: Co-Ordinate Representation of the Gaussian Distribution as Applied to a Point Source.

Where k is defined by equation 6.5 above and assumed to be site independent.

For total reflection, ground level receptors and non-buoyant ground level sources,

the reflection coefficient $r_g = 1$, $z_r = 0$, and $H = 0$ respectively so that

$$R(0) = 2 \qquad 6.12$$

Thus equation 6.10 becomes

$$C(x,y,z) = \frac{Q}{\pi\sigma_y\sigma_z u}\exp\left[-\frac{1}{2}\left(\frac{y}{\sigma_y}\right)^2\right]\exp\left(\frac{-kx}{vH}\right) \qquad 6.13$$

If the receptor is located in the direction of the prevailing wind, the observed aerosol may be assumed to arrive along the centre line of the plume so that

$$y = 0 \qquad 6.14$$

Therefore, equation 6.13 reduces to

$$C(x,y,z) = \frac{Q}{\pi\sigma_y\sigma_z u}\exp\left(\frac{-kx}{vH}\right) \qquad 6.15$$

Dispersion coefficients

The plume width parameters σ_y and σ_z are based on empirical correlation and take into consideration the prevailing meteorological factors. There are many different models for the computation of the plume width parameters from the atmospheric stability classes and the downwind distance. The stability class can be determined using Pasquil or Turner methods as explained earlier.

Several formulae are available in the literature for calculation of the horizontal and vertical dispersion coefficients. These include:

(a) Pasquill-Gifford Sigmas (Pasquil, 1983).

The dispersion coefficients were derived from diffusion experiments in which a non-buoyant tracer gas was released near the surface, which is a flat terrain and measured downwind up to a distance of 800m from the source. The sigmas were presented in graphical form by Turner (Turner, 1970) for the various atmospheric stability classes. The graphical presentation was put in analytical form by Green et al. (Green et al., 1980) as

$$o_y(x) = \frac{k_1 x}{[1 + (x/k_2)]^{k_3}} \qquad 6.16$$

$$o_z(x) = \frac{k_4 x}{[1 + (x/k_2)]^{k_5}} \qquad 6.17$$

where the constants k_1, k_2, k_3, k_4, k_5 are given in Table 6.2.

Table 6.2: Values of constants in equation 6.16 and equation 6.16.

Stability classification	Stability class	k_1	k_2	k_3	K_4	k_5
Extremely unstable	A	0.250	927	0.189	0.1020	-1.918
Moderately unstable	B	0.202	370	0.162	0.0962	-0.101
Slightly unstable	C	0.134	283	0.134	0.0722	0.102
Neutral	D	0.0787	707	0.135	0.0475	0.465
Slightly stable	E	0.0566	1070	0.137	0.0335	0.624
Moderately stable	F	0.0370	1170	0.134	0.0220	0.700

(b) Brookhaven Sigmas (Smith, 1968)

The Brookhaven sigmas are derived from elevated releases over a rough surface. Also, the concentrations are measured up to a few kilometres downwind. The power law function is assumed in deriving expressions for the dispersion coefficients. Thus σ_y and σ_Z are expressed as

$$o = ax^b \qquad 6.18$$

The values of a and b for each "gustiness" category are provided in Table 6.3. Also Table 6.4 gives the relationship between each gustiness category and Pasquill classes.

Table 6.3. Coefficients a and b for equation 6.4

Gustiness Category	σ_y		σ_Z	
	a	B	a	b
B_2	0.40	0.91	0.41	0.91
B_1	0.36	0.86	0.33	0.86
C	0.32	0.78	0.22	0.78
D	0.31	0.71	0.06	0.71

Table 6.4: Relation between the gustiness category and the Pasquill class (Gifford, 1976)

Pasquill Class	A	B	C	D	E	F
Gustiness Category	B2 Very unstable	B1 Unstable	B1 Unstable	C Neutral	C/D Neutral/ Stable	D Stable

(c) Biggs Sigmas (Briggs, 1973)

There are two versions of Briggs sigmas: the rural and urban models. Both agrees with Pasquill-Gifford in the downwind distance of 100m to 10km, except that σ_z values for A and B stability classes approximate the B2 and B1 Brookhaven curves. The Briggs sigma are tabulated in Table 6.5. The urban sigmas called McElroy-Pooler sigmas, were derived from several urban dispersion experiments with low-level tracers. Several other parameterizations of σ_z and σ_y are provided in the literature, for example (Briggs, 1985).

Table 6.5: The Briggs sigma functions for urban conditions (Panosky and Dutton, 1984)

Urban Dispersion Parameters (for distances between 100 and 10,000m)		
Pasquill stability	σ_y(m)	σ_z(m)
A-B	$0.32 x (1+ 0.0004 x)^{-0.5}$	$0.24 x (1+ 0.001 x)^{-0.5}$
C	$0.22 x (1+ 0.0004 x)^{-0.5}$	$0.20 x$
D	$0.16 x (1+ 0.0004 x)^{-0.5}$	$0.14 x (1+ 0.0003 x)^{-0.5}$
E-F	$0.11 x (1+ 0.0004 x)^{-0.5}$	$0.08 x (1+ 0.00015 x)^{-0.5}$

6.3 Application of Gaussian Model to the Quarry Industry Emissions

The application of Gaussian dispersion model will be limited to ambient PM10 particulate matter from drilling, and mechanized quarry operations such as MECH1, MECH2 AND MECH3 crusher assembly. It should be noted that the Gaussian plume model for ground level point source applies in all the cases provided sampling was performed in the downwind direction.

\Table 6.6: The Briggs sigma functions for rural condition (Panosky and Dutton, 1984)

Rural Dispersion Parameters (for distances between 100 and 10,000m)		
Pasquill stability	σ_y(m)	σ_z(m)
A	$0.22 x (1+ 0.0001 x)^{-0.5}$	$0.20 x$
B	$0.16 x (1+ 0.0001 x)^{-0.5}$	$0.12 x$
C	$0.11 x (1+ 0.0001 x)^{-0.5}$	$0.08 x (1+ 0.0002 x)^{-0.5}$
D	$0.08 x (1+ 0.0001 x)^{-0.5}$	$0.06 x (1+ 0.0015 x)^{-0.5}$
E	$0.06 x (1+ 0.0001 x)^{-0.5}$	$0.03 x (1+ 0.0003 x)^{-1}$
F	$0.04 x (1+ 0.0001 x)^{-0.5}$	$0.016 x (1+ 0.0003 x)^{-1}$

Firstly, one needs to calculate the dispersion coefficients for the appropriate stability category from the knowledge of mean wind speed, and incoming solar radiation. For example, in the case of MECH3 quarry operation, the surface wind speed varies between 4 and 6m/s with the mean value of 2.48±0.41m/s. Temperature was constant within ±2°C with a mean value of 32°C during the day. Incoming solar radiation was generally slight (i.e. ≤30mWcm^{-2}). Under this meteorological condition, the atmospheric stability was classified under the D category during the day when the sampling was conducted. The atmospheric stability condition during collection of ambient PM10 particulate matter from other quarry industry operations is provided in Table 6.7. Table 6.8 shows the calculated horizontal and vertical dispersion parameters based on Brookhaven sigmas (Smith, 1968) for the appropriate gustiness category. The resulting source strength for PM10 particulate matter for DRILLING, MECH1, MECH2, MECH2.W and MECH3 quarry operations are presented in Table 6.8. These source strengths

are useful in estimating the actual impact of the quarry operation in the environment.

Table 6.7: Atmospheric Stability Conditions During Sampling from the Quarry Operations.

Quarry Operation	Sampling Dates	Mean Wind Speed (m/s)	Solar Radiation ($mWcm^{-2}$)	Mean temp. (°C)	Pasquill Stability class	Gustiness category
Drilling	17/2/96 - 23/2/96	2.18±0.67	20.30	32.80	C	B_1
MECH1	27/2/96 – 16/3/96	1.55±0.69	20.67	29.54	B	B_1
MECH2	27/3/96 - 6/4/96	1.94±0.71	21.24	37.20	B	B_1
MECH2-W	27/5/96- 20/6/96	2.76±0.65	17.59	27.25	C	B_1
MECH3	23/10/96- 26/10/96	2.48±0.41	20.10	32.75	C	B_1

Table 6.8: Vertical and Horizontal dispersion parameters for Quarry operations.

QUARRY OPERATION	GUSTINESS CATEGORY	DISTANCE FROM SOURCE (m)	a	b	σ_y	A	b	σ_z
DRILLING	B_1	100	0.36	0.86	18.89	0.33	0.86	17.32
MECH1	B_1	200	0.36	0.86	34.29	0.33	0.86	31.43
MECH2	B_1	200	0.36	0.86	34.29	0.33	0.86	31.43
MECH2-W	B_1	200	0.36	0.86	34.29	0.33	0.86	31.43
MECH3 (wet rocks)	B_1	200	0.36	0.86	34.29	0.33	0.86	31.43

Table 6.9: Calculated Source Strength for Various Quarry Operations.

QUARRY OPERATION	SOURCE STRENGTH gs^{-1}
DRILLING	0.052±0.016
MECH1	0.348±0.146
MECH2	0.983±0.400
MECH2-W	0.357±0.085
MECH3	1.753±0.290

6.4 Dose Response Functions

6.4.1 Introduction

The dose-response function relates the quantity X of a pollutant that affects a receptor to the physical impacts $Y= f_{dr}(X)$ on the receptor. In other words, dose response phenomenon involves estimating physical or medical relationships linking environmental variables such as ambient concentration of air pollutants to observable health effects. The fundamental statistical problem for such study is that health effects are potentially affected by other factors besides air pollution. Such factors include the effects of weather, changes in medical care, infectious disease epidemics, changes in lifestyles etc. A variety of regression analysis techniques are used in isolating the impact of air pollution by epidemiologists and in such study risk is dealt with in form of relative risk. The relative risk at some pollution level X is equal to the ratio of the expected health impact Y at the pollutant level X to the mean value of Y at pollutant level 0 (Calthrop and Maddison, 1996). Thus, a unit change in concentration of a pollutant results in a

certain percentage in the risk ratio. Alternatively, for study of population at risk, the effects of particulate matter could be expressed as the change in probability that an event such as death will occur when the concentration of particulate matter increases by one unit. Dose response functions can also be derived for lesser health impacts such as asthma attack, acute respiratory symptoms, bronchitis, eye irritation, and so on.

If one has the knowledge of the size of the population at risk, and the concentration of pollutants to which this population is exposed, the number of health events due to poor air quality predicted can be determined. Valuation is then conducted on the health events. This will require a separate application of stated preference techniques (Harrington, 1987) for valuing non-marketed goods such as health.

6.4.2 The nature of the dose-response function

In most cases, dose response function starts at the origin and increases monotonically with dose X as shown in Figure 6.2. However, very high doses are characterized by saturation. Dose response functions are determined from epidemiological studies or from laboratory studies. The problems arising from the application of dose response function determined from laboratory studies is that such studies are limited to animals and in trying to extrapolate to humans, large uncertainties may be introduced. Also, one requires very high doses in order to obtain observable responses in a sample under investigation in contrast with low doses usually encountered in environmental impact studies. Thus, there is a need to extrapolate the observed data towards low doses.

Figure 6.2 indicates several forms of the dose-response function. The simplest is the linear model consisting of a straight line from the origin through the observed data points. Health effects associated with exposure to fine particulate matter is an example of such linear DRF (Dockery et al, 1992).

In some cases, positive impact may be obtained at low doses in which some trace elements (N and S) cause increase in crop yield. In such cases the damage is negative and the dose-response function represented by the dashed lines in Figure 6.2 is termed fertilizer effect (Curtis and Rabl, 1996).

If nothing is known about a threshold, the dose response function can be anywhere between zero and the straight line through the origin as represented by the curved line in Figure 6.2.

6.4.3 Problems of the dose response function

Pollution data linking changes in PM10 concentrations to health effects in US cities are used to derive dose-response functions. In order to use such a dose-response functions to estimate deaths as a result of exposure to PM10 in urban areas of another city, some assumptions need to be made. Such assumptions relate the validity of the epidemiology underlying the dose-response function and the validity of transferring such results. The critical factors to be considered shortly include the assumption that there is some biological pathway by which particulate matter affects health. Also, to be considered is the argument that dose-response functions are generally linear and implications of the presence of threshold. Finally, the argument that conditions in US cities and measurements taken there

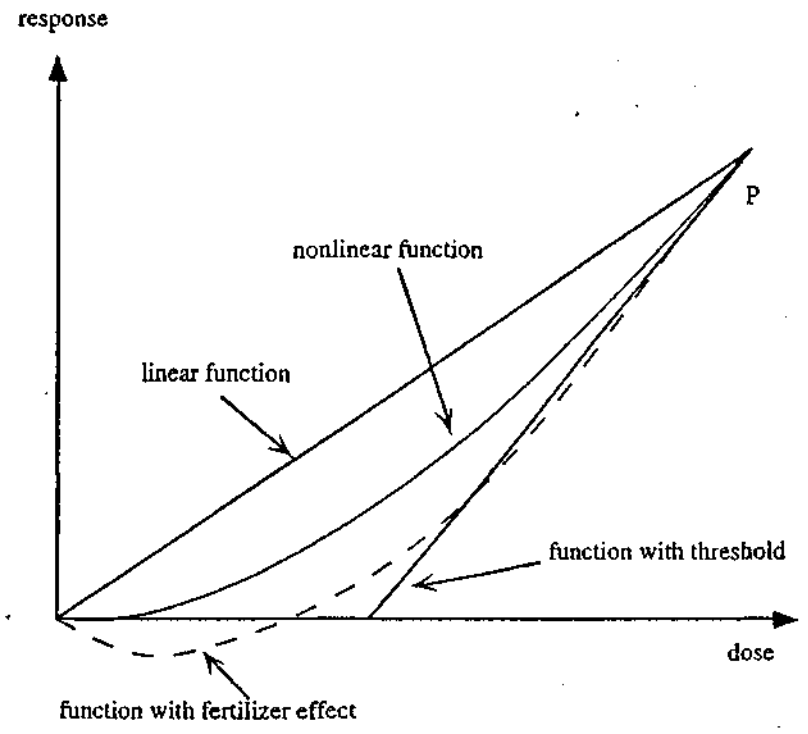


Fig. 6.2: Graphical Representation of the Dose-Response Function

are comparable to other cities and thus dose-response functions in US cities can be transferred to other cities need to be considered.

Some researchers had argued that the biological pathway by which particulate matter affects human health is uncertain. For example Utell and Samet (1993) reviewed various epidemiological studies and concluded that biological mechanism is unknown. Ostro (1995) suggested that pollution exposure represent additional burden of inflammation which may worsen the conditions of already affected persons. This is supported by earlier studies (Kalacic, 1973), which had shown that fine particles may cause alveolar inflammation which exacerbates lung disease when they are deposited in the lungs.

The form of the dose-response function has implication on the methodology of impact analysis. If the dose-response function were a straight-line graph through the origin (no threshold), any increase in pollution would cause an impact. Even if there is threshold the same situation exists provided the background concentration is above this threshold. In most industrialized countries, the background levels for some pollutants, (e.g. particulate matter), is above the level where effects are likely to occur (Dockery et al, 1992). Schwartz (1994) later observed that there is no evidence of threshold in his Philadelphia study. Thus, the precise form of dose-response function at low doses is unnecessary. If on the other hand, the dose-response function has a threshold that is above the background concentration of the pollutant and if emission from the source is not enough to cause increase in this background concentration above threshold, there is no impact. The analysis in this case is greatly simplified and only requires the verification that the resulting

KASSIM IB

concentration remains below the threshold. Such analysis can easily be handled by a short-range dispersion model.

In order to use the dose-response function in impact assessment study, the best approach is always to conduct dose-response modeling in situ thereby avoiding the inherent dangers in transferring estimates from another country. However, the cost of conducting such an exercise is enormous and thus one is compelled to make use of the dose-response estimates for other countries where such exercise had been carried out.

It should however be noted that when transferring dose-response function from another country one has to ensure that the important baseline factors in the various studies are controlled for. This can be done by using the 'benefit transfer function' used for modeling key parameters of the dose-response function as a function of baseline factors such as demographic composition and income levels before applying it. Unfortunately, what the important base-line factors are may not be known initially or they may be large in number in relation to the available number of studies.

In order to avoid consideration of baseline factors a method was developed for conducting meta-analysis by Calthrop and Maddison (1996). This approach involve the use of weighted least square regression analysis to perform meta-analysis and assumed that the parameters used in the estimation process are themselves deduced from a 'mother' distribution. Also, the estimation process involves conversion of all possible measures of risk to increase in relative risk and

also different measures of particulate matter were converted into their PM10 equivalents using a conversion factor. The results of the study which involves analysis of data from 15 different studies suggests that the increase in relative risk of death associated with 1μg/m^3 increase in PM10 particulate matter is 0.079%. This figure may be considered as the best estimate so far of the true impact of PM10 particulate matter because of the large number of constituent studies and the underlying theory of the weighting procedure. It therefore enables researchers to calculate the deaths attributable to PM10 particulate matter regardless of the baseline factors. However the accuracy of the assessment may be improved if adjustments are made for age and health profiles (which indicate predisposition to ill-health) of populations in the country where the dose-response function is being transferred.

6.5 Methodology for Estimating Impacts of PM10 Particulate Matter from Quarry Activities

The impact of PM10 particulate matter emission from the quarry industry can be estimated following the procedures explained above. In this case the source strength Q for various quarry operations for the various pollutant measured are provided in Table 6.8 above. Using the value of $\beta = 1.852km^{-1}$ deduced from the curve fit to the EMEP SO_2 data (Curtiss and Rabl, 1996), together with the mean wind speed, and mixing layer height H = 800m the removal velocity $k=vH\beta$ can be calculated. The relevant dose-response function for morbidity and mortality effects are provided by Rowe et al (1995) and Calthrop and Maddison (1996). The assumption is that such dose-response function can be transferred to Nigerian context. The central estimate of the dose-response function for various health

effects and mortality obtained from Rowe et al (1995) and Calthrop and Maddison (1996) are presented in Table 6.9.

In order to estimate the impact of PM10 particulate matter, one requires the knowledge of population at risk, which is not readily available, as the only official figures available are those compiled during 1991 census. However, to achieve our

Table 6.10: Morbidity and mortality dose-response functions for PM10 particulate matter (effect per 10µg/m^3 change in PM10) from Rowe et al (1995) and Calthrop and Maddison (1996)

Morbidity effect	Effect per 10ugm^3 change in PM10
RHA/100 000	12.0
ERV/100 000	237.0
RAD per person	0.58
LRI per child per asthmatic	0.017
Asthma attack per person	0.58
Respiratory symptoms per person	1.68
Chronic bronchitis/100 000 (risk of new case)	61.2
Increase in relative risk of Mortality per person (from Calthrop & Maddison (1996)	0.0079

RHA = respiratory hospital admissions; ERV= emergency room visits; RAD = restricted activity days;

LRI = lower respiratory illness (in children)

Source: Rowe et al (1995) ; Calthrop and Maddison (1996).

own purpose, we have decided to use these figures along with the average growth rate of 2.8% for the Country. This is not necessarily realistic especially for the Federal Capital Territory where the present population is more than twice the 1991 figures.

Nevertheless, the adjusted population density figures for FCT and Zaria of (53 and 91km^{-2}) respectively will be used in estimating the impact of PM10 particulate matter pollution from the Quarry industry.

For example, the damage for the Federal Capital Territory in terms of mortality can be estimated as follows:

Q = 1.753 g/s

$\rho_H = 60.4\ km^{-2} = 7.04 \times 10^{-5}\ m^{-2}$

$k_H = vH\beta = 2.48 \times 800 \times 1.852 \times 10^{-6} = 0.00367$

$d_H = 0.00079$ IRRDyr^{-1} (increase in relative risk of deaths yr^{-1} / ($\mu g/m^3$)

$$D = \frac{1.753 \times 10^6 \times 0.604 \times 10\text{-}4 \times 0.00079}{0.00367} = 23 \text{ IRRD/yr}$$

i.e there is increase in relative risk of 23 deaths per year.

Table 6.10 shows the estimated damage for various morbidity classes and mortality for various quarry operations in Abuja and Zaria. These estimates are based on the dose-response values obtained from Rowe et al (1995) and Calthrop and Maddison (1996) and 1991 population figures (National population Commission, 1991) and growth rate of 2.8% for Abuja and Zaria.

It should be noted that the estimated mortality and morbidity are for a single type of quarry operation. If all the quarry operations are to be taken into consideration then the mortality and morbidity values will change. For example, in the Federal capital territory, there are as many as 20 quarry operations using MECH3 crusher type and most of them do not even employ dust suppression mechanisms. Thus the estimated mortality and morbidity for FCT will be greater than 20 times the values quoted above if all the quarries were to be in operation simultaneously.

Table 6.11: Calculated Morbidity and Mortality Values for Various Quarry Operations

Morbidity effect	MECH1	MECH2	MECH2-W	MECH3
RHAs	188.8	425.9	108.6	345.7
ERVs	3729.0	8411.5	2145.5	6828.4
RADs	9.1	20.6	5.3	17.7
LRIs (asthmatic children)	0.3	0.6	0.2	0.5
Asthma attacks	9.1	20.6	5.3	17.7
Respiratory symptoms	27.4	59.6	15.2	48.4
Chronic bronchitis	962.9	2172.0	554.0	1770
Increase in relative risk of Mortality (from Calthrop & Maddison (1996)	12.4	28.0	7.2	22.8

It should be noted that there are some uncertainties associated with the above results. These include the uncertainty associated with the transferability and legitimacy of the underlying DRF, values used for population at risk taken into consideration the avertive behaviour of the public to pollutant intake and the absence of log-term pollution source. The first is not likely to be a major source of

uncertainty considering the basis of the meta-analysis and the number of constituent studies used in obtaining the DRF. The second could be a major source of uncertainty. It can however be addressed by conducting a survey into the extent and nature of avertive behaviour. The absence of DRF for long-term pollution source may result in underestimation of the true damage.

CHAPTER 7

CONCLUSIONS AND RECOMENDATIONS

The scope of this work is mainly the sampling and analysis of PM10 particulate matter for conducting impact assessment of pollution from the quarry industry. The sampling equipment developed in this work allows for collection of particles with sizes less than or equal to 10μm AED. Size fractionation of these PM10 particulate matter was further achieved by the inclusion of stacked filter cassette capable of separating the PM10 into coarse and fine fractions with diameter in the range 2-10μm an <2μm AED respectively. These PM10 particles do not only have health significance, they also have life-time of the order of weeks and thus can be transported from the source to relatively long distances and hence can cause significant increase in the existing PM10 concentration in air.

The impact assessment of pollution from quarry industry was carried out by firstly developing an accurate and efficient sampling protocol bearing in mind that considerable errors in air quality assessment often occur during the sampling process. To obtain an in depth understanding of accurate sampling methods in calm air, the aerodynamics concerning the capture of the suspended particles by aerosol sampler were briefly reviewed. This review showed that the most significant sources of error are associated with the settling velocity and the inertia of the particles to be sampled. The collection efficiency is therefore a function of the sampler orientation, the face velocity, the inlet geometry and the particle size. Since the existing criteria for accurate dust sampling in calm air are expressed in terms of these parameters, especially the inlet diameter and the particle size, a critical review of the existing criteria for accurate dust sampling in calm air in terms

of these parameters is also made. Due to the difficulties in simulating real particle motion, all criteria are based on some simplified flow patterns around an idealized sampling head (e.g. a long tube with a thin wall). The review of Davies criteria revealed that they are somewhat over restrictive as they require high flow rates and large inlets which are unsuitable for sampling in still air and at workplace. On the other hand, the Aggrawal and Liu criteria allows flexibility in the choice of sampling inlet for accurate non-biased sampling even for particles with aerodynamic equivalent diameter greater than 10μm. Fortunately, the Stacked Filter Unit aerosol sampler used in this work satisfied both criteria and hence made possible accurate sampling of PM10 particulate matter.

Size fractionated sampling is usually applied for the purpose of studying particle size-mass distribution pattern and for the assessment of dust fraction which possibly enters and deposits in the human respiratory system. The former requires a multistage size fractionating sampler such as a cascade impactor or multistage cyclone which should be characterized with sharp cut-off point and larger fractionating capacity for large particles. However, commonly used cascade impactors used for study of industrial particulate matter do not satisfactorily fulfill these requirements owing to their poor separation ability especially for particles larger than 10μm. The second purpose of size selective sampling is more often of concern to industrial hygienists. Normally, two stage samplers are preferred. The first stage is a pre-separation system followed by a collector for the fraction of the particles with hygienic significance. The separation function of the sampler should thus be similar to the deposition function of the particles in the human respiratory

system. The Stacked filter Unit aerosol sampler used in this work exhibits such similarity in performance.

Total reflection X-ray fluorescence was applied for the survey of the air quality within and in the vicinity of the quarry industry. This analytical procedure though commonly used for liquid samples was adapted to analysis of PM10 particulate matter collected on "Nuclepore" membrane filters. The technique was used to analyze up to 12 elements simultaneously in each of the 86 samples after a simple extraction procedure greatly aided by the surface deposition property of membrane filters. The accuracy of the technique which had been previously established by previous workers was re-checked through analysis of a multi-element standard with known concentration. There was good agreement between the two values. Low detection limits were achieved for all the elements measured in addition to reliable quantification through internal standardization. This work thus demonstrated the applicability of TXRF in environmental analysis since pollution and contamination can effectively be detected by the technique.

In spite of the applicability of TXRF in environmental analysis established in this work, the accuracy of the technique can still be improved by emphasizing accurate clean bench working as is common practice for micro and trace analysis. Further, in order to avoid systematic errors of extraction and dilution methods used in this work, direct analysis of air particulate matter collected on suitable substrate is recommended. This can be achieved by using TXRF sample carriers in cascade impactor of the Anderson and Battele types. However, proper choice of relatively pure sample carriers and the inherent impurities in these sample carriers should

be established prior to analysis. Also the troublesome particle bounce-off and blow-off effects on flat carriers should be avoided by coating with medical Vaseline which are known to be characterized with high purity.

The knowledge of elemental composition allows a crude assessment of impact of the PM10 constituent elements on human health through comparison with Threshold Limit Values promulgated for some pollutants. The assessment shows that even the workers at the MECH1 quarry operation located at the region of immense dust pollution are exposed to concentration levels lower than the TLV values for all the elements. It can however be argued that this does not necessarily imply that the workers are not in any danger as the TLV values are only based on concentration of total suspended particulate matter without size consideration. Recent studies have shown that it is the PM10 constituent of the TSP that actually predispose humans to health problems since only this fraction are capable of penetrating the human respiratory system. Since the emission of particles from the quarry industry are based on mechanical action which are normally dominated by coarse particles with aerodynamic equivalent diameter greater than 10μm AED, the TLV values cannot be used as a reliable yardstick of assessing the health impact of PM10 particulate matter. It is thus recommended that new TLV values should be promulgated for various elements based on their PM10 concentration levels.

Based on the above arguments, the health impact of PM10 particulate matter on workers at the quarry industry was further assessed by calculating the regional deposition of the measured constituent elements in the human respiratory tract

using established models. The results obtained suggest deposition fraction ranging from 0.37 to 0.68 for elements Pb, Zn, Cu, Fe, Ca, K, Si, Al. The results also indicate that the fractional deposition in the pulmonary compartment of the lung is nearly identical for these elements.

The level of air pollution in the neigbouring environment of the quarry industry was also investigated by setting up a local sampling station at specific distances from the quarry. The resulting particulate matter concentration was used along with meteorological factors to estimate the source strengths for PM10 particulate matter for the various quarry operations using the Gaussian plume dispersion model. The source strengths obtained for the three types of mechanized quarry i.e. MECH1, MECH2 and MECH3 showed that the source strengths increase as the crushing capacity of the crusher assembly increases. Results obtained also showed that application of wetting agents greatly reduces the source strength and hence the dust output. This is evident in the result for MECH2 crusher where the ambient dust output during the wet season was reduced to about 50% and less than 20% for fine and coarse fraction respectively of the dust in its dry form. This is also confirmed by the calculated 36% reduction in source strength for the same crusher during the dry season as compared to wet season. The calculation of source strength using Gaussian plume model as demonstrated in this work is particularly useful for monitoring plant's environment where the concentration levels of dusts is bound to be relatively high. The technique is not restricted to the quarry industry alone but can also be applied to the cement industry and any other industry using ores and minerals. Since the emissions are fugitive, the method

may prove useful for studying local emissions or for short range transported pollutants.

The above conclusion therefore suggests that the easiest way to reduce dust output from the quarry industry is the use of wet dust suppression technique, which involves utilization of a liquid for the control, reduction or suppression of airborne dust at its source. Effective control of dust output involves the confinement of the dust within the dust producing area by a curtain of moisture, the wetting of the dust by direct contact between the particles and the droplets of moisture and the formation of agglomerates too heavy to become airborne or too heavy to remain airborne by combining dust particles with each other and with the droplets of liquid. Water appears to be the ideal fluid from the standpoint of availability and economy. However, from the standpoint of effectiveness it is not. As a result there is need to blend the water with specially formulated dust control compounds consisting of special surface active agents to enhance its dust suppression qualities. The effects of application of dust suppression fluid produce carryover dust control effect to other points beyond the actual application location. Application should be made at all crushers where new dry surfaces are created and where it is possible to utilize the action of the crusher in mixing the moisture into new dry surfaces of the rocks. Application therefore should be made at the primary, secondary and tertiary crushers. Since the rock has been previously properly conditioned, it can be handled at the coveyors, transfers, screen units and stockpiles with negligible emission of dust. This dust suppression mechanism can be used on a wide variety of stone and ore such as limestone, granite, shale, copper ore, iron ore, sand, gravel etc.

This work also reviewed the structure of the impact pathway methodology and showed that simple equations can be derived for calculating the expectation value of marginal damage due to emission of PM10 particulate matter from a point source using the uniform world model. The relevance of this simple formula had also been tested by some Authors where it was concluded that there is a remarkably small sensitivity to geographical detail. Thus by combining atmospheric dispersion and dose response functions, it is possible to analyze the general features of air pollution damage. The simple formula for Uniform damage is correct within an order of magnitude for real situations as demonstrated by some Authors. However, tolerance to errors in receptor distributions may be high. Thus the various source strengths calculated were used in conjunction with the dose response values from the literature to determine the impact of dust emissions on the environment by estimating the resulting mortality and morbidity estimates for PM10 particulate matter. The results show that PM10 particulate matter is still a significant cause of mortality and morbidity. However there are presently some objections to this and other existing evidences on the ground of statistical competence and the question of avertive behaviour. A useful starting point will therefore be a survey into the extent and nature of avertive behaviour. Such survey should naturally proceed in parallel with more elaborate study of the dispersal patterns of pollutants from the quarry and related industry and hence to confirm that these industries significantly contribute to the dose of air pollutants inhaled by the general public.

REFERENCES

ACGII(1971). Documentation of the Threshold Limit Values for Substances in the Workroom Air. Proceeding, American Conference of Governmental Industrial Hygienists, Cincinnati, Ohio.

Agarwal, J. K. and Liu, B. Y. H. (1980). A Criterion for Accurate Aerosol Sampling in Calm Air. *Am. Ind. Hyg. Assoc.,* J. 41:191-197.

Arinc, F., Wielopolski, L. and Gardner, R. P.(1977). The Linear Least Squares Analysis of X-ray Fluorescence Spectra of Aerosol Samples Using Pure Element Library Standards and Photon Excitation, In: Dzubay, T. G. (Ed), X-ray Fluorescence Analysis of Environmental Samples. Ann Arbor Science, Michigan, p227-240.

Bambynek, W., Craseman, B., Fink, R. W., Frehund, H. U., Mark, H., Swift, C. D. and Price, R. E. (1972). Coster-Kronig Transition Probabilities, *Rev. Mod. Phys.,* 44(4):716.

Bamford, S., Dangie, M.,Greaves, E., Holynska, B., Markowitcz, A.,Van Grieken, R., Vis, R. D. and Walsh, R. L. (1997). Sampling, Storage and Sample Preparation Procedures for X-ray Fluorescence Analysis of Environmental Materials, ECDOC-950. IAEA, Vienna.

Barret, C. F., Carroll, J. D. and Irwin, J. G. (1982), A Field Comparison of Belgian, French and United Kingdom Particle Samplers. Warren Spring Laboratory Venage, Report No CR2315 (AP).

Bauman, S., Houmere, P. O. And Nelson, J. W.(1981). Cascade Impactor Aerosol Samples for PIXE and PESA Analyses. *Nucl. Instr. Methods*, 181:499-502. Bown, W. (1994). Dying from Too Much Dust. *New Scientist,* 12 March, 12-13. Briggs, G. A. (1985). Analytical Parameterization Of Diffusion: TheConvective Boundary Layer. *J. Climate and Appl. Meteor.*, 24:1167.

Butler, J. D. (1979). Air Pollution Chemistry, Academic Press, London.

Cahill, T.A., Ashbaugh, L.L., Borone J. B., Eldred R. A., Feeney, P.J., Flocchini, R. G., Goodact, C., Shadoan, D. J., and Wolfe G. W. (1977). Analysis of Respirable Fractions in Atmospheric Particulates via Sequential Filtration. *J. Air Pollut. Contr. Assoc.,* 27:675-678.

Calthrop, E. And Maddison, D. (1996). The Dose-Response Function Approach to Modeling the Health Effects of Air Pollution. *Energy Policy,* 24(7):599-607.

Campbell, J. L., Maenhaut, W., Bombelka, E., Clayton, E., Malmqvist, K., Maxwell, J. A., Pallon, J., and Vandenhaute, J.(1986). An Intercomparisonof Spectra Data Processing Techniques in PIXE. *Nucl. Instrum. Methods*, B14:204-220. Chameides, W. L. and Davis, D. D. (1982). The Free Radical Chemistry of Cloud Droplets and Its Impact upon the Composition of Rain. *J. Geophys. Res.*, 87:4863-4877.

Chan, T. L. and Lippmann, M. (1980). Experimental Measurements and Empirical Modeling of The Regional Deposition of Inhaled Particles in Humans. Am. Ind. Hyg. Assoc., 41:385-391

Curtiss, P. S and Rabl, A. (1996). Impacts of Air Pollution: General Relationships and Site Dependence, *Atmos Environ.,* 30(19):3331-3347.

Davies, C. N. (1968). The Entry Of Aerosols into Sampling Tubes and Heads. *Brit. J. Appl .Phys.,* 2(1):921-932.

Derbertin, K and Helmer, R. G. (1988). Gamma and X-ray Spectrometry with Semiconductor Detectors. North-Holland .

Dockery, D. W., Schwartz, J and Spengler, J. (1992). Air Pollution and Daily Mortality: Association with Particulates And Acid Aerosols. *Environ. Res.,* 59(4):362-373.

Dzubay T. G. (Ed) (1977). X-ray Fluorescence Analysis of Environmental Samples. Ann Arbor Science, Michigan.

Dzubay, T.G. and Stevens, R. K. (1975). Ambient Air Analysis with Dichotomous Sampler and X-ray Fluorescence Spectrometer. *Environ. Sci. Technol.*, 9:663-668

F&J SPECIALTY PRODUCTS (1987). Technical Manual for Low Volume Air Sampler. F&J SPECIALTY PRODUCTS Inc., Miami Springs, Florida.

Fleischer, R. L., Price, P. B. and Walker, R. M. (1965). Tracks of Charged Particles in Solids. *Science,* 149:383-393.

Friedlander, S. K. (1977). Smoke, Dust and Haze. Fundamentals of Aerosol Behaviour, John Wiley and Sons, New York.

Fucks, N.A. (1964). The Mechanics of Aerosols, Pergamon Press, Inc., New York.

Galloway, J. N., Thornton, J. D., Norton, S. A., Volchok, H. I. and Mclean, R. A. (1982). Trace Metals in Atmospheric Deposition: A Review and Assessment. *Atmos. Environ.,* 16:1677-1686.

Gifford, F. A. (1961). Use of Routine Meteorological Observations for Estimating Atmospheric Dispersion. *Nucl. Safety,* 2:47-51.

Gifford, F. A. (1976). Turbulent Diffusion Typing Schemes: A Review. *Nucl. Safety,* 17: 68-86.

Gilfrich, J., V., Skeltom, E. F., Qadri, S. B., Kirkland, J. P. and Nagel, D. J. (1983). Synchrotron Radiation X-ray Fluorescence Analysis. *Anal. Chem.,* 55:187-190.

Gordon, B. M. (1982). Sensitivity Calculations for Multi-Element Trace Analysis by Synchrotron Radiation Induced X-ray Fluorescence. *Nucl. Instrum. Methods*, 204:223-229.

Goulding, F. S., Jaklevic, J. M., Jarret, B. V. and Landis, D. A. (1972). Detector Background and Sensitivity of X-ray Fluorescence Spectrometers. *Adv. X-ray Anal.* 15:470.

Green, A. E. (1980). Analytical Extensions of the Gaussian Model. *JAPCA*, 30(7):773-776.

Hanna, S. R., Briggs, G. A., Deadorff, J., Egan, B. A., Gifford, F. A. and Pasquill, F. (1977). AMS Workshop on Stability Classification Schemes and Sigma Curves- Summary of Recommendations. *J. Climate and Appl. Meteor.*, 58(12):1305-1309.

Harrington, W. and Portney, P. (1987). Valuing the Benefits of Health and Safety Regulations, *J. Urban Economics*, 22(1):135-140.

Heidam, N. Z. (1981): Review: Aerosol Fractionation by Sequential Filtration with Nuclepore Filters. *Atmos. Environ.*, 15: 891-904.

Henderson-Sellers, B. (1984). Pollution of Our Atmosphere, Adam Hitger Ltd, Bristol.

Hesketh, H. E. (1977). Fine Particles In Gaseous Media, Ann Arbor Science Publishers, Inc. Michigan.

Hinds, W. C. (1982). Aerosol Technology, John Wiley and Sons, New York.

Hubbel, J. H., Veigele, W. J., Briggs, E. A., Brown, R. T., Cromer, D. T. and Howerton, R. J. (1975). Atomic Form Factors, Incoherent Scattering Functions and Photon Scattering Cross Sections. *J. Phys.Chem.*, Ref. Data 4, 471.

International Atomic Energy Agency (1978). Particle Size Analysis in Estimating the Significance of Airborne Contamination. IAEA, Vienna.

International Atomic Energy Agency (1995). Quantitative X-ray Analysis System, Documentation Version 1.2, IAEA, Vienna.

Jackson, M.H., Morris G.P., Smith P.G. and Crawford, J. F. (1989) Environmental Health Reference Book, Alden Press.

Jaklevic, J. M., Landis, D. A. and Goulding, F. S., (1976). Energy Dispersive X-Ray Fluorescence Spectrometry Using Pulsed X-ray Excitation, Adv.X-ray Anal., 19:253.

Jaklevic, J. M. and Giauque, R. D. (1993). Energy Dispersive X-ray Fluorescence Analysis Using X-ray Tube Excitation. In: M. E. Van Grieken And A. A. Markowitcz (Ed), Handbook Of X-ray Spectrometry, Marcel Dekker Inc.New York. Pp151-180.

Jenkins, R., Gould, R. W. and Gedcke, D. (1981). Quantitative X-ray Spectrometry.Marcel Decker, Inc. New York.

Junge, C. E. (1970). Air Chemistry and Radioactivity. Int. Geophysics Series, Vol. 4, Academic Press, New York

Kalacic I. (1973). Chronic Nonspecific Lung Disease in Cement Workers. *Arch. Envir. Health,* 26:76-83.

Klockenkamper, R. and Von Bolen, A. (1996). Elemental Analysis of Environmental Samples by Total Reflection X-ray Fluorescence: AReview. *X-ray Spectrometry*, 25:156-162.

Krause, M. O. (1979). Atomic Radiative and Radiationless Yields For The K And L Shells. *J. Phys.Chem.,* Ref. Data 8, 307.

Kregsamer, P. (1991). Fundamentals of Total Reflection X-ray Fluorescence *Spectrochim. Acta.*, 46b(10):1333-1340.

Kump, P., Nacemer, M. and Snajder, J. (1996). Determination of Trace Elements in Bee Honey, Pollen and Tissue by Total Reflection X-ray Fluorescence. *Spectrochim. Acta.*, 51b:499-507.

Larsen, R.I. (1969). A New Mathematical Model of Air Pollutant Concentrations of Atmospheric Pollutant Averaging Time. *J. Air Pollut. Contr. Assoc.*, 19:24-30.

Liu, B. Y. H. and Pui, D. Y. H.(1981). Aerosol Sampling Inlets and Inhalable Particles. *Atmos. Environ.,* 15:589-600.

Maenhaut, W. (1989). Analytical Techniques for Atmospheric Trace Elements. In J. M. Pacyna And B. Ottar (Eds), Control and Fate of Atmospheric Trace Elements, Kluwer Academic Publishers, 259-301.

Maenhaut, W., Francois, F., Cafmeyer, J. and Okunade, O. (1995). Atmospheric Aerosol Studies Using the "Gent" Stacked Filter Unit Aerosol Sampler, with Multi-Elemental Analysis of The Samples By Nuclear-Related Analytical Techniques. NAHRES-19, IAEA, Vienna, 4:1-19

Maenhaut, W., Francois, F., Cafmeyer, J. and Okunade, O. (1996). Size-fractionated Aerosol Composition at Gent, Belgium. Results from a One-year Study. *Nuclear Instr. Methods In Physics Research B*, 109/110:476-481.

Maenhaut, W. and Raemdonck, H. (1984). Accurate Calibration of a Si(Li) Detector for PIXE Analysis. *Nucl. Instrum. Methods*, B1:123-126.Markowicz, A. A. (1993). X-ray Physics. In R. E. van Grieken and A. A. Markowicz (Eds), Handbook of X-ray Spectrometry, Marcel Dekker inc., New York. pp 1-72.

Mcguire, E. J. (1971). Atomic L-Shell Coster-Kronig Auger And Radiative Rates and Fluorescence Yields for Na-Th. *Phys. Rev.*, A3:587.

Milford, J. B. and Davidson, C.I. (1985). The Sizes of Particulate Trace Elements in the Atmosphere: A Review. *J. Air Pollut. Contr. Assoc.*, 35(12): 1249-1260.

Mitchell, R. I. and Pilcher, J.M.(1959). Improved Cascade Impactor for Measuring Aerosol Particle Sizes. *Ind. Eng. Chem.*, 51:1039-1042.

Murozumi M., Chow, T. J. and Patterson, C. (1969). Chemical Concentrations of Pollutant Lead Aerosols, Terrestrial Dusts, and Sea Salts in Greenland and Anarctic Snow Strata. *Geochem. Cosmochem. Acta.*, 33:1247-1294.

National Population Commission (1991). 1991 Population Figures for the Federal Republic of Nigeria. National Population Commission, Abuja, Nigeria.

Natusch, D. F. S. and Wallace, J. R.(1974). Urban Aerosol Toxicity: The Influence of Particle Size. *Science* 186:695.

Nullens, H., Van Espen, P and Adams, F. (1979). Linear and Non-Linear Peak Fitting in Energy-Dispersive X-ray Fluorescence. *X-ray Spectrometry* 8(3):104-109

Oleru, U.G. (1984). Pulmonary Function and Symptoms of Nigerian Workers Exposed to Cement Dusts. *Environ. Res.*, 33:379-385.

Pacyna, J. M., Semb, A. and Hanssen, J. E. (1984). Emission and Long Range Transport of Trace Elements in Europe. *Tellus* 36B(3):163-178

Panosky, H. A. and Dutton, J. A. (1984). Atmospheric Turbulence. John Wiley and Sons, New York.

Pasquill, F. and Smith, F. B. (1983). Atmospheric Diffusion: Study of the Dispersion of Wind Borne Material from Industrial and other sources. Ellis Horwood, London.

Pearce, D. and Crowards, T. (1996). Particulate Matter and Human Health in the United Kingdom. *Energy Policy,* 24(7):609-619.

Pierson, W. R., Brachaczek, W. W., Korniski, T. J., Truex, T.J. and Butler, J. W. (1980). Artifact Formation of Sulfate, Nitrate and Hydrogen Ion on Backup Filters: Allegheny Mountain Experiment. *J. Air Pollut. Contr. Assoc.*, 30: 30-34.

Pope III, C. A., Schwartz, Z. J. and Ransom, M. (1992). Daily Mortality and PM10 Pollution in Utah Valley. *Arch. of Environ. Health*, 47(3):211-217.

Prange, A. (1989). Total Reflection X-ray Spectrometry: Method and Applications. *Spectrochim. Acta,* 44b:437-443.

Rhodes, J. R., Pradzynski, A. H., Hunter, C.B., Payne J.S. and Lindgren, J. L. (1972). Energy Dispersive X-ray Fluorescence Analysis of Air Particulates in Texas. *Environ. Sci. Technol.,* 6: 922-927.

Rowe, R. Chestnut, L., Lang, C., Bernow, S and White, D. (1995). The New York Environmental Externalities Cost Study: Summary of Approach and Results. Proceedings of European Commission, International Energy Agency and Organization for Economic Co-Operation and Development Workshop on External Cost of Energy, Brussels, 30-31 Jan., 1995.

Schwartz, J. (1994). Air Pollution and Daily Mortality: A Review and Meta-Analysis. *Environ. Res.*, 64:36-52.

Sehmel, G. A. (1980). Particle and Gas Dry Deposition: A Review. *Atmos. Environ.*, 14:983-1011.

Seinfield, J. H., (1986). Atmospheric Chemistry and Physics of Air Pollution. John Wiley and Sons, New York, Pp 23-26.

Smith, M. E. (1968): Recommended Guide for the Prediction of the Dispersion of Airborne Effluents. American Society of Mech. Engineers, New York.

Spurny, K. R., Lodge J. P., Frank, E. R., and Sheesley, D. C. (1969). Aerosol Filtration by Means of Nuclepore Filters: Structural and Filtration Properties. *Environ. Sci. Technol.*, 3:453-468

Task Group On Lung Dynamics (1966). Deposition and Retention Models For Internal Dosimetry Of the Human Respiratory Tract. *Health Physics*, 12:173-207

Tertian, R. and Claisse, F. (1982). Principles of Quantitative X-ray Fluorescence Analysis. Heyden and Sons Ltd. London.

Tolgyessy, J. and Klehr, E. H. (1987). Nuclear Environmental Chemical Analysis, Ellis Harwood Series in Analytical Chemistry. John Wiley and Sons, New York.

Trukenmuller A. and Krewit, W. (1993). Some Reflections on the Problem of System Boundaries for a Regional-Range Analysis of Human Impacts. IER, Universitat Stuttgart.

Turner, D. B. (1970). Workbook of Atmospheric Dispersion Estimates. EPA, Research Triangle Park, North Carolina.Urone, P. and R. C. Ross (1979). Pressure Charge Effects on Rotometer and Flow Rates. *Environ. Sci. Technol.*, 13:732-734.

US Environmental Protection Agency Report (1982). Air Quality Criteria for Particulate Matter and Sulphur Oxide. EPA600/8-82-029A, US Environmental Protection Agency.

Urone, P. and Ross, R. C. (1979). Pressure change effects on rotometer and flow rates. *Environ. Sci. Technol.* 13:732-734.

Utell, S. and samet, J. (1993). Particulate Air Pollution and Health: New Evidence of an Old Problem. *Am. Rev. Resp. Disease*, 147:1334-1335.

Vanoeteren, C., Cornelis, R. and Sabbioni, E. (1986). Critical Evaluation of Normal Levels of Major and Trace Elements in Human Lung Tissue. Commission of European Communities, Luxembourg.

Wedding, J. B., Mcfarland, A. R. and Cermark, J. E. (1977). Large Particle Collection Characteristics of Ambient Aerosol Samplers. *Environ. Sci. Technol.*, 11:387-390.

Wedding, J. B. and Weigand, M. A. (1985). The Wedding Ambient Aerosol Sampling Inlet (D50 = 10μM) For the High Volume Sampler. *Atmos. Environ.*, 19: 535-538.

Went, F. W. (1964). The Nature of Aitken Condensation Nuclei In The Atmosphere, Proc. U. S. Nat. Acad. Sci 51:1229-1267.

Whitby, K. T. (1977). The Physical Characteristics of Sulphur Aerosols,Proceeding of international symposium on sulphur in the atmosphere, sept. 7-14, Dubrovinik, Yugoslavia.

Wobarauschek, P. (1989). Adjustment and Working Instructions For The Total Reflection Attachment Module. IAEA, Vienna.

Zannetti, P. (1990). Air Pollution Modeling: Theories, Computational Methods and Available Software. Van Nostrand Reinhold, New York.

Zhang, J. (1983). Sampling and Analysis of Particulate Matter Suspended in the Workplace of an Iron foundry. Ph. D thesis, University of Gent, Unpublished Results.

APPENDIX 1

SUMMARY OF ANALYTICAL PROCEDURES FOR PM10 PARTICULATE MATTER (COARSE FRACTION)

'SAMPLE 'LABEL	PM CONC µg/m^3	MASS OF PM ANALYZED µg	VOL.OF SOLVENT ml	CONC. OF PM IN SOLVENT µg/ml	CONVERSION FACTOR TO AIR CONC
QC01	234.57	1196.30	5	239.3	0.98
QC02	240.74	778.57	5	155.7	1.55
QC03	234.57	996.72	5	199.3	1.18
QC04	222.22	1114.29	5	222.9	1.00
QC05	259.26	782.80	5	156.6	1.66
QC06	50.93	612.50	5	122.5	0.42
QC07	55.56	590.37	5	118.1	0.47
QC08	66.67	747.47	5	149.5	0.45
QC09	61.11	617.28	5	123.5	0.50
QC10	46.30	556.18	5	111.2	0.42
QC11	2888.89	1333.33	5	266.7	10.83
QC12	101.85	1100.00	5	220.0	0.46
QC13	2777.78	1224.49	5	244.9	11.34
QC14	97.22	942.86	5	188.6	0.52
QC15	2888.89	1422.89	5	284.6	10.15
QC16	92.59	948.45	5	189.7	0.49
QC17	3000.00	1213.64	5	242.7	12.36
QC18	92.59	1010.53	5	202.1	0.46
QC19	2888.89	1293.40	5	258.7	11.17
QC20	101.85	1237.50	5	247.5	0.41
QC21	1777.78	727.27	5	145.5	12.22
QC22	1666.67	754.05	5	150.8	11.05
QC23	1888.89	818.18	5	163.6	11.54
QC24	1777.78	936.17	5	187.2	9.49
QC25	148.15	800.00	5	160.0	0.93
QC26	138.89	706.81	5	141.4	0.98
QC27	157.41	1085.11	5	217.0	0.73
QC28	175.93	876.92	5	175.4	1.00
QC29	166.67	904.76	5	181.0	0.92
QC30	37.04	406.63	5	81.3	0.46
QC31	18.52	200.00	5	40.0	0.46
QC32	22.22	277.46	5	55.5	0.40
QC33	18.52	231.95	5	46.4	0.40
QC34	19.32	205.78	5	41.2	0.47
QC35	259.26	359.89	5	72.0	3.60
QC36	197.53	946.24	5	189.2	1.04
QC37	296.30	451.40	5	90.3	3.28
QC38	209.88	927.27	5	185.5	1.13
QC39	46.30	274.57	5	54.9	0.84
QC40	259.26	342.13	5	68.4	3.79
QC41	246.91	1031.25	5	206.3	1.20
QC42	266.67	349.15	5	69.8	3.82
QC43	208.33	858.29	5	171.7	1.21

APPENDIX 2

SUMMARY OF ANALYTICAL PROCEDURES FOR PM10 PARTICULATE MATTER (FINE FRACTION)

'SAMPLE 'LABEL	PM CONC µg/m^3	MASS OF PM ANALYZED µg	VOL.OF SOLVENT ml	CONC. OF PM IN SOLVENT µg/ml	CONVERSION FACTOR TO AIR CONC
QF01	74.07	282.80	5.0	56.6	1.31
QF02	92.59	279.22	5.0	55.8	1.66
QF03	74.07	292.31	5.0	58.5	1.27
QF04	74.07	303.80	5.0	60.8	1.22
QF05	92.59	274.51	5.0	54.9	1.69
QF06	27.78	321.02	5.0	64.2	0.43
QF07	33.33	321.29	5.0	64.3	0.52
QF08	38.89	383.44	5.0	76.7	0.51
QF09	33.33	317.20	5.0	63.4	0.53
QF10	27.78	321.29	5.0	64.3	0.43
QF11	555.56	262.82	5.0	52.6	10.57
QF12	41.67	475.47	6.2	76.7	0.54
QF13	555.56	217.95	6.2	35.2	15.80
QF14	41.67	374.53	6.2	60.4	0.69
QF15	555.56	210.19	6.2	33.9	16.39
QF16	41.67	464.15	6.2	74.9	0.56
QF17	555.56	237.18	7.4	32.1	17.33
QF18	41.67	472.50	7.4	63.9	0.65
QF19	555.56	267.97	7.4	36.2	15.34
QF20	41.67	483.75	7.4	65.4	0.64
QF21	33.33	165.79	7.4	22.4	14.88
QF22	44.44	185.81	5.0	37.2	11.96
QF23	44.44	181.58	5.0	36.3	12.24
QF24	44.44	212.99	5.0	42.6	10.43
QF25	64.82	332.28	5.0	66.5	0.98
QF26	64.82	303.18	5.0	60.6	1.07
QF27	64.82	327.85	5.0	65.6	0.99
QF28	64.82	378.98	5.0	75.8	0.86
QF29	64.82	428.03	5.0	85.6	0.76
QF30	27.78	267.52	5.0	53.5	0.52
QF31	18.52	188.39	5.0	37.7	0.49
QF32	17.78	192.21	5.0	38.4	0.46
QF33	18.52	207.79	5.0	41.6	0.45
QF34	19.32	227.10	5.0	45.4	0.43
QF35	111.11	173.38	5.0	34.7	3.20
QF36	74.07	258.23	5.0	51.6	1.43
QF37	111.11	158.71	5.0	31.7	3.50
QF38	74.07	292.31	5.0	58.5	1.27
QF39	37.04	216.77	5.0	43.4	0.85
QF40	111.11	150.98	5.0	30.2	3.68
QF41	74.07	298.09	5.0	59.6	1.24
QF42	133.33	157.79	5.0	31.6	4.22
QF43	83.33	273.08	5.0	54.6	1.53